Numerical Studies of Disordered Tight-Binding Hamiltonians

Outline

Acknowledgements: It is a pleasure to acknowledge the collaborators together with whom I have learned much of the physics and numerics presented in these notes: Zhaojun Bai, Andrew Baldwin, George Batrouni, Karim Bouadim, Wenbin Chen, Peter Denteneer, Fred Hébert, Norman Paris, Nandini Trivedi, Martin Ulmke, Ichitaro Yamazaki and Gergely Zimanyi. This work was supported by the National Science Foundation (NSF-DMR-0312261 and NSF–ITR–0313390), and China Special Funds for Major State Basic Research Projects under contract 2005CB321700.

I. INTRODUCTION

A. Contents of these notes

In these notes we will discuss the physics of electrons which move in a disordered potential and which also interact with each other. This is an enormous field, one of the most interesting in condensed matter physics, both for theory and experiment. In order to make it tractable, we will consider a specific model- the Hubbard Hamiltonian with random bond and site energies, although we will also take a brief foray into an interesting case when the hopping is non-Hermitian. We will also focus on a particular computational method, "determinant Quantum Monte Carlo"[1].

We begin, in Section II., by examining the physics of the Hubbard Hamiltonian in the limit of no disorder, and present its strong, weak, and mean field treatments. Appendix 1 briefly reviews the formalism of second quantization, for those students for whom it is not so familiar. We will also describe the exact diagonalization method. In Section III., we will summarize some of the central features of the Anderson localization transition, that is, the case when we have disorder and no interactions. We will also discuss a generalization, the Hatano-Nelson model, in which the left and right hopping amplitudes are unequal, and hence the Hamiltonian is not Hermitian. In doing so, we will discuss a relatively new mathematical tool, the 'pseudospectrum'. Section IV. outlines the determinant Quantum Monte Carlo (DQMC) method. Our emphasis will be on presenting the 'pseudocode' for DQMC, relegating a more complete derivation to Appendix 3. Quantum Monte Carlo involves an understanding of classical monte carlo, which is summarized in Appendix 2.

Then, after having considered the effects of randomness and interactions separately, and introduced DQMC, Section V. puts the phenomena of randomness and interactions together. We show results of simulations of the "Anderson-Hubbard Hamiltonian", including evidence that, in two dimensions, interactions can drive a state that is localized by randomness into a metallic phase. A Zeeman field, which spin polarizes the electrons and thereby reduces their effective interaction, can return the system to insulating behavior. We present evidence that particle-hole symmetry, and whether the disorder directly competes with the formation of magnetic moments, plays a crucial role in these transitions. Appendix 4 contains a review of aspects of this particle-hole mapping. We conclude section V. with a discussion of the band insulator to metal transition. We show that an insulating phase caused by a periodic potential which doubles the unit cell can, like a disorder-induced Anderson insulator, also be made metallic by interactions.

I have interspersed these notes with exercises. Some are rather simple- a few lines of analytic derivation might serve to complete them. Others might go down the road to being small research topics, and could involve trying to write a nontrivial program. The lecture notes contain substantially more material than we will be able to cover in a week, especially when the Exercises are attempted. I hope they will provide additional avenues for exploration after this summer school is completed, or topics for the more advanced student who wishes to proceed a bit further or more rapidly.

We close this introduction with a (very!) brief review of the history of some of these problems. For details concerning the two dimensional MIT and the Anderson-Hubbard Hamiltonian, the student is encouraged to look at the various reviews of the field[2,3]. A nice introduction to the Hubbard model, both its motivation and properties is contained in[4]. Further summaries of DQMC may be found in a variety of articles and summer school notes, including[5–8].

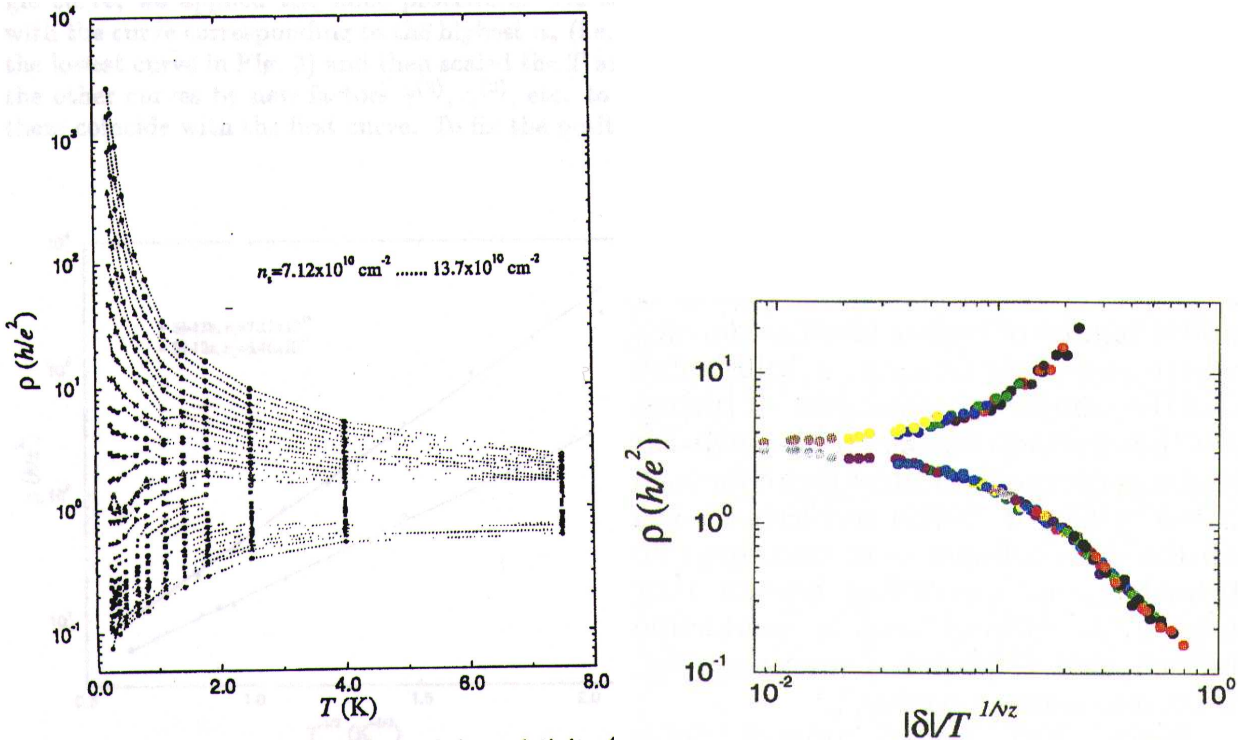

FIG. 1: Left: Resistivity ρ versus temperature T for samples with a varying density of electrons n. As the density increases, the system undergoes a transition from insulating to metallic. Right: Similar data for a transition tuned by disorder strength δ. Horizontal axis is an appropriately scaled form. A large family of curves collapses to two curves, one for metallic disorder strengths, and one for insulating ones. Plots from: ****

B. Brief Overview of Physics

When electrons are confined to two dimensions in a disordered environment, common understanding until relatively recently was that the electronic states would always be localized and the system would therefore be an insulator. This idea is based on the scaling theory of localization[9] for non-interacting electrons and corroborated by subsequent studies using renormalization group (RG) methods[10,11]. The scaling theory highlights the importance of the number of spatial dimensions and demonstrates that while in three dimensions for non-interacting electrons there exists a transition from a metal to an Anderson insulator upon increasing the amount of disorder, a similar metal–insulator transition (MIT) is not possible in two dimensions.

The inclusion of interactions into the theory has been problematic, certainly when both disorder and interactions are strong and perturbative approaches break down. Following the scaling theory the effect of weak interactions in the presence of weak disorder was studied by diagrammatic techniques and found to increase the tendency to localize[12]. Subsequent perturbative RG calculations, including both interactions and disorder, found indications of metallic behavior, but also, for the case without a magnetic field or magnetic impurities, found runaway flows to strong coupling outside the controlled perturbative regime, and hence were not conclusive[13–15]. The results of such approaches therefore did not change the widely held opinion that, in the absence of a magnetic field coupling to orbital motion, or magnetic impurities, the MIT does not occur in two dimensions.

The situation changed dramatically with the recent transport experiments on effectively

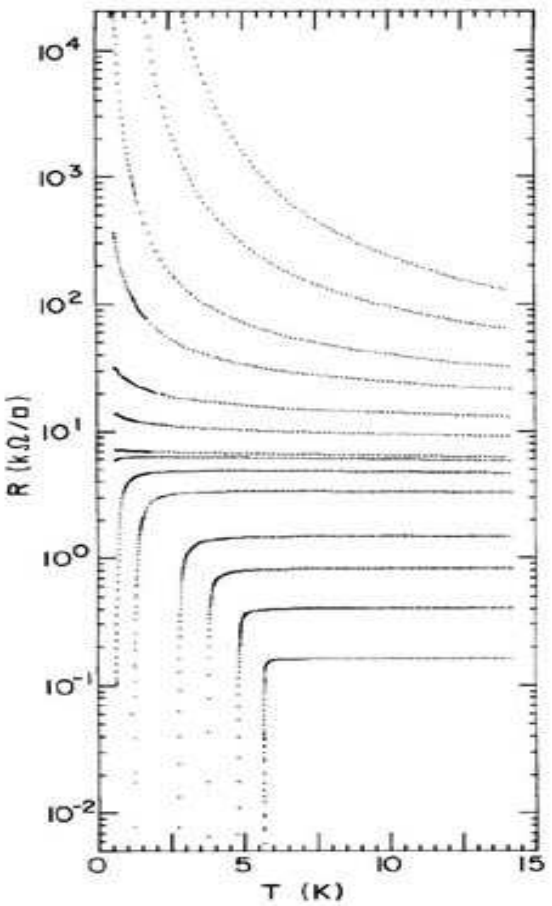

FIG. 2: A superconductor to insulator transition is well established in two dimensional thin films. Here results for the resistance $R(T)$ of Pb films of varying thickness are shown. The transition can also be controlled with degree of disorder, and magnetic field. Figure from: *****

2D electron systems in silicon MOSFETs which have provided surprising evidence that a MIT can occur in 2D[16–18]. In these experiments the temperature dependence of the resistivity ρ changes from that typical of an insulator (increase of ρ upon lowering T) at lower density to that typical of a conductor (decrease of ρ upon lowering T) as the density is increased above a critical value. (See Fig. 1, left panel.) The fact that the data can be scaled onto two curves (one for the metal, one for the insulator) is seen as evidence for a quantum phase transition with carrier density n as the tuning parameter. (See Fig. 1, right panel.) The possibility of such a transition has stimulated a large number of further experimental[19–22] and also theoretical investigations[23–26], including proposals that a superconducting state is involved[27,28]. Explanations in terms of trapping of electrons at impurities, i.e. not requiring a quantum phase transition have also been put forward[29,30]. While there is no definitive explanation of the phenomena yet, it is likely that electron-electron interactions play an important role.

One central question motivated by the experiments is: Can electron-electron interactions enhance the conductivity of a 2D disordered electron system, and possibly lead to a conducting phase and a MIT[31,32]? In order to address this issue theoretically, we of course need to identify an appropriate model and, then, work out its properties.

As mentioned above, these lectures will begin by providing some background on the "Anderson-Hubbard" Hamiltonian, which is one of the most simple models that incorporate

both disorder and interactions. We will discuss several methods to develop an initial insight into the physics of this Hamiltonian, but our focus will be on Determinant Quantum Monte Carlo (DQMC). We will conclude with a detailed description of the MIT studied with this model and method. DQMC has previously been applied extensively to the Hubbard model without disorder.[1,6,33–36] While the strengths of DQMC in addressing this problem are considerable: disorder and interaction can be varied in a controlled (ie exact) way and strong interaction is treatable, it is important also to acknowledge its serious limitations: the size of the lattice is finite (a few hundred sites) and low temperatures are often not accessible due to the sign problem.

There are many analogies between the MIT and the superconducting-insulator transition (SIT). As for the MIT, one of the most interesting issues again focuses on the behavior in two dimensions. A transition from superconductor to insulator is observed as the degree of disorder or the magnetic field is changed, but the fundamental question is not whether a superconducting phase can exist (it surely can!), but rather why the value of resistance at the transition appears to take on a universal value. Interestingly, the connection between the MIT and SIT can be brought out in the context of the Hubbard Hamiltonian through a particle-hole transformation which changes the sign of the interaction between the electrons from repulsive to attractive, since the latter case allows for superconducting phases. We will not discuss this problem, but the interested reader can begin with reviews such as[37–42] or, for applications of DQMC, to[43,44].

C. Guide to Exercises

I hope these notes will provide interesting problems for students of different levels of familiarity with numerical work and with the Hubbard model. The most advanced/ambitious students might wish to construct a determinant Quantum Monte Carlo code. Though not phrased in the form of exercises, Section IV. writes down all the required equations and shows some simple results. Appendix 3 provides a derivation. It is, however, unlikely such a task could be fully accomplished in only the several hours a day we have here. A more realistic objective for a student who wants a 'research' code is to try a mean field or exact diagonalization program. These are discussed in Section II., and also in the material presented by other lecturers. Perhaps most straightforward, though, would be to attempt the exercises. Many are, I hope, suitable for time frames such as our evening 'Training Sessions.' Here are some of the options.

Section II: Exercises extending aspects of the weak ($U = 0$) and strong ($t = 0$) coupling limits of the Hubbard Hamiltonian, for example, determining the tight binding dispersion relations and density of states of the periodic Anderson model, the three band Emery model, or the Hubbard model on triangular and honeycomb lattices.

Section III: Execrcises involving the Hatano-Nelson model.

Appendix 1: Exercises involving the manipulation of creation and destruction operators and the Hubbard Hamiltonian.

Appendix 2: Exercises involving the formal foundations of *classical* monte carlo (detailed balance, the Metropolis algorithm, the relation of monte carlo to molecular dynamics and the Langevin equation, etc).

Appendix 4: Exercises involving particle-hole symmetry and the relation between the attractive and repulsive Hubbard Hamiltonians.

II. THE TRANSLATIONALLY INVARIANT HUBBARD MODEL

The Hubbard Hamiltonian, in the absence of disorder, is,

$$H = -t \sum_{\langle \mathbf{j},\mathbf{l}\rangle \sigma} c^\dagger_{\mathbf{j}\sigma} c_{\mathbf{l}\sigma} + U \sum_{\mathbf{j}} n_{\mathbf{j}\uparrow} n_{\mathbf{j}\downarrow} - \mu \sum_{\mathbf{j}} (n_{\mathbf{j}\uparrow} + n_{\mathbf{j}\downarrow}). \tag{1}$$

Here $c^\dagger_{\mathbf{j}\sigma}(c_{\mathbf{j}\sigma})$ are creation(destruction) operators for electrons on site $\mathbf{j}$ with spin σ. (Their properties are reviewed in Appendix 1.) The first term of H is the kinetic energy since it describes the destruction of an electron of spin σ on site $\mathbf{l}$ and its creation on site $\mathbf{j}$ (or *vice-versa*). The symbol $\langle \mathbf{j}, \mathbf{l}\rangle$ indicates that hopping is allowed only between specified pairs of sites (usually the near neighbors). We will mostly consider square lattices in two dimensions. The second term is the interaction energy: a doubly occupied site ($n_{\mathbf{j}\uparrow} = n_{\mathbf{j}\downarrow} = 1$) adds an energy U to the state. The final term is a chemical potential which controls the filling. The situation where the filling is one electron per site is referred to as as 'half-filling,' since the lattice contains half as many electrons as the maximum number (two per site). The value $\mu = U/2$ results in half-filling for any choice of hopping t or temperature T, if the lattice is bipartite and the hopping only connects sites on the two independent sublattices. Studies of the Hubbard model often focus on the half-filled case because it exhibits a lot of interesting phenomena (Mott insulating behavior, anti-ferromagnetic order, etc.)

As we shall see, the Hubbard Hamiltonian offers a way to get qualitative insight into how the interactions between electrons can give rise to insulating, magnetic, and even novel superconducting effects in a solid. It was written down in the early 1960's and initially applied to understanding the behavior of the transition metal monoxides like FeO, NiO, CoO. These compounds are antiferromagnetic insulators, but are predicted to be metallic by "electronic structure" methods which treat strong interactions less carefully.

Over the intervening years, the Hubbard model has been applied to the understanding of many systems, from 'heavy fermion' systems in the 1980's, to high temperature superconductors in the 1990's. In the last several years the 'boson-Hubbard' model has been invoked to study the physics of untra-cold atoms. Indeed, it is an amazing feature of the Hamiltonian that, despite its simplicity, its exhibits behavior relevant to many of the most subtle and beautiful properties of solid state (and now atomic) systems.

A. Analytic Treatments

The Hubbard model has been studied by the full range of analytic techniques developed by condensed matter theorists, from simple mean field approaches to field theoretic methods employing Feynman diagrams, expansions in the degeneracy of the number of 'flavors' (spin, orbital angular momentum), the Bethe Ansatz, etc. It has also been extensively attacked with numerical methods like diagonalization and Quantum Monte Carlo (QMC). In these lectures, our main tool will be QMC, but first we will discuss the non-interacting and zero hopping limits, and static mean field theory, to develop some simple pictures of the physics.

1. Noninteracting Limit ($U = 0$):

In Appendix 1, we present two, equivalent, ways to solve the Hubbard Hamiltonian at $U = 0$. The first is based on explicitly constructing the matrix for $\hat{H}$ in the single particle

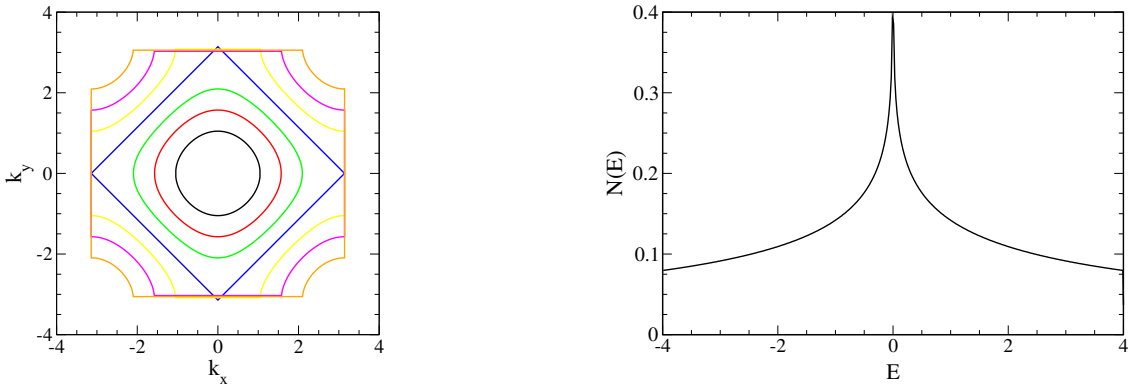

FIG. 3: Left: Surfaces of constant energy E for the square lattice dispersion relation. Note that for $E = 0$ the topology is a rotated square and that $\epsilon_{\mathbf{k}+(\pi,\pi)} = \epsilon_{\mathbf{k}}$ for points $\mathbf{k}$ on the surface. Right: The density of states. Note the divergence ('van Hove singularity') at $E = 0$.

sector. The second considers a change to momentum creation and destruction operators,

$$c^{\dagger}_{\mathbf{k}\sigma} = \frac{1}{\sqrt{N}} \sum_{\mathbf{l}} e^{i\mathbf{k}\cdot\mathbf{l}} c^{\dagger}_{\mathbf{l}\sigma}. \tag{2}$$

The key result is that the kinetic energy term in the Hamiltonian can be rewritten as

$$H = \sum_{\mathbf{k}\sigma} (\epsilon_{\mathbf{k}} - \mu) c^{\dagger}_{\mathbf{k}\sigma} c_{\mathbf{k}\sigma} \tag{3}$$

where $\epsilon_{\mathbf{k}}$ depends on the specific lattice geometry, as do the discrete allowed values of the momentum $\mathbf{k}$. For a one dimensional lattice of length N with near neighbor hopping, $\epsilon_k = -2t\,\mathrm{cos}k$ and $k = k_n = 2\pi n/N$ with $n = 1, 2, 3, ..., N$. This is much more simple than the original expression in terms of spatial creation and destruction operators, because it is diagonal. That is, the Hamiltonian only counts the number of electrons in each momentum state without converting electrons from one momentum to another. A useful analogy is of course with normal modes in classical physics which can be excited without setting other modes into motion. Just as the normal mode construction in classical physics is possible only for quadratic potential energies, the diagonalization of a tight binding Hamiltonian can be done only when it is quadratice in the fermion creation and destruction operators.

Because the case of the two dimensional square lattice is of interest physically for the cuprate superconductors, and because it forms the bulk of the applications we will discuss in Section V., we will review a few of its properties. The dispersion relation is $\epsilon_{\mathbf{k}} = -2t\,(\mathrm{cos}k_x + \mathrm{cos}k_y)$. This dispersion relation has a number of interesting and important features. First, its Fermi surface, ie the contours of constant energy, is 'nested' at half-filling. That is, a particular wave-vector, $\mathbf{k} = (\pi, \pi)$ connects extended lengths of the Fermi surface.

Second, its density of states,

$$N(E) = \frac{1}{N} \sum_{\mathbf{k}} \delta(E - \epsilon_{\mathbf{k}}). \tag{4}$$

is singular at half-filling, $E = 0$. Regarding the former, a number of response functions, for example the magnetic susceptibility $\chi(\mathbf{q})$, involve energy denominators of the form $\epsilon_{\mathbf{k}+\mathbf{q}} -$

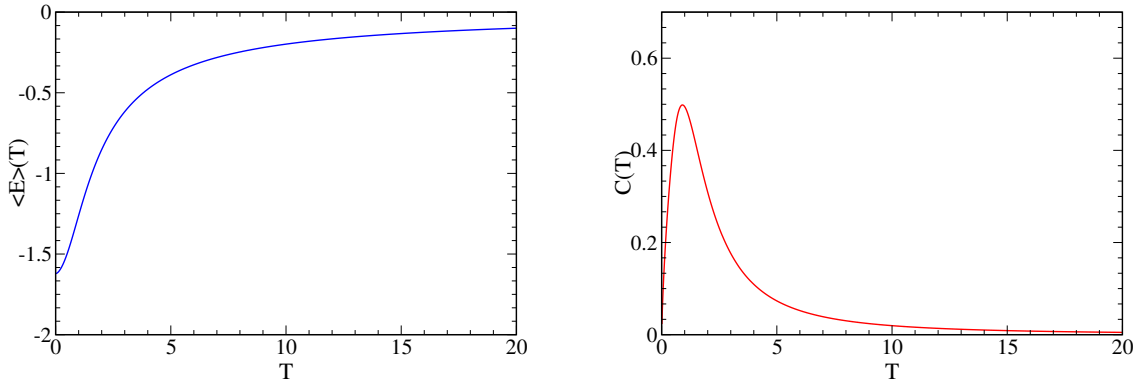

FIG. 4: Left: Energy $\langle E(T)\rangle$ of the square lattice Hubbard Hamiltonian with $t = 1$, $U = 0$, and density $\rho = 1$ (half-filling). Right: Specific heat $C(T)$.

$\epsilon_{\mathbf{k}}$ and hence become large when nesting occurs. Possible implications of both of these features have been discussed in the context of theories of high temperature superconductivity. Regarding the latter, there are a number of physical responses of a system which have a temperature scale $T_* = V_1 e^{-1/(N(E_F)V_2)}$ where V_1 and V_2 are some energy scales in the problem and E_F is the Fermi energy. (An example is the form of the energy gap in the BCS theory of superconductivity.) If $N(E_F)$ diverges, T_* can be large.

The average energy of the $U = 0$ Hubbard model it is,

$$\langle E(T)\rangle = \frac{1}{N}\sum_{\mathbf{k}} \epsilon_{\mathbf{k}}(1 + e^{+\beta(\epsilon_{\mathbf{k}}-\mu)})^{-1}. \tag{5}$$

In Fig. 4 we show the energy and specific heat, $E(T)$ and $C(T) = dE/dT$, as functions of temperature. As expected, $C(T)$ has a peak at a temperature T set by the hopping t.

This treatment of the $U = 0$ Hubbard Hamiltonian is perhaps well known to you all. We now turn, mainly as exercises, to several refinements which are interesting, and perhaps less familiar.

Exercise 1: In Section V.D. we will consider the one-dimensional Hubbard Hamiltonian with a staggered site energy $V = A\sum_l (-1)^l\, n_l$. Solve the $U = 0$ limit by going to momentum space. Show that you get two energy bands separated by a gap.

Exercise 2: Compute (numerically) the density of states $N(E)$ of the Hubbard model on a two dimensional honeycomb lattice. You will need to determine the dispersion relation and how the periodic boundary conditions restrict the allowed $\mathbf{k}$ values. You should find that $N(E)$ vanishes linearly at $E = 0$. The system is said to be a *semi-metal* there.

Exercise 3: Compute (numerically) the density of states $N(E)$ of the Hubbard model on a two dimensional triangular lattice. Again, you will need to determine the dispersion relation and how the periodic boundary conditions restrict the allowed $\mathbf{k}$ values. Unlike the preceding cases, you will find that $N(E) \neq N(-E)$. This is a consequence of the fact that the model is not "particle-hole" symmetric on a triangular lattice. This will be discussed further in Sections V.C. and Appendix 4 below.

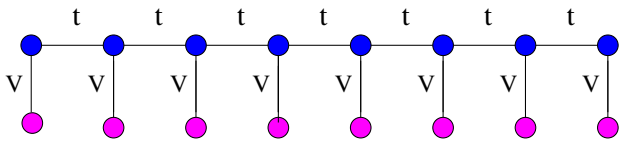

FIG. 5: Lattice connections of a one-dimensional periodic Anderson model. Sites of the top ('conduction') chain are connected to one another by hopping parameter t. Sites of the lower ('localized') chain are not connected to each other, but hybridize with a hopping parameter V with the sites in the top chain.

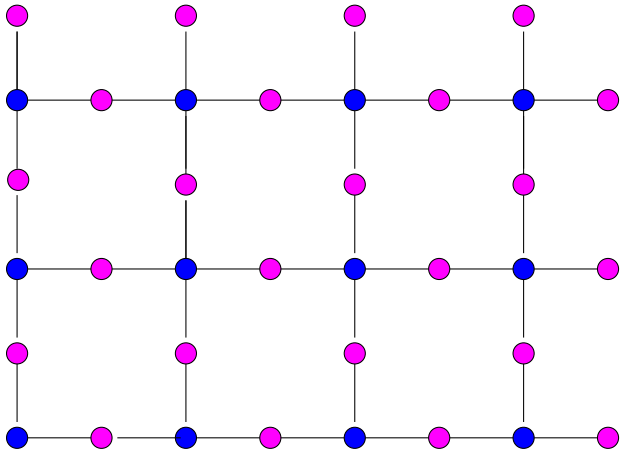

FIG. 6: Lattice connections of a three band Emery model of the CuO_2 sheets of the cuprate superconductors. The Cu atoms lie in a square array with intervening O atoms. Pairs of Cu and O atoms are connected by hopping t. Sometimes an additional hopping t' between oxygen atoms is also included. The O sites are also given a site energy ϵ_{pd} relative to the Cu sites.

These last two exercises pertain to the single band Hubbard model on non-square geometries in two dimensions. Some model Hamiltonians contain more than one orbital and hence several energy bands. Constructing the non-interacting dispersion relations are a first step in elucidating their physics.

Exercise 4: Almost as widely studied as the Hubbard Hamiltonian is the 'Periodic Anderson Model' (PAM). It consists first of a set of sites whose near neighbors are connected with hopping 't'. These might be in a one-d chain, or a two-d square lattice arrangement for example. Then there is a second set of localized sites which are disconnected from each other. However, they hybridize with their partners in the first set with amplitude 'V', as illustrated in Fig. 3. Compute $E(k)$ and $N(E)$ for this model, in $d = 1$. Show there is a band gap when $V \neq 0$. If one adds a Hubbard U on the localized orbitals one gets the Periodic Anderson model.

Exercise 5: A three-band Hubbard model introduced by Emery and widely studied for high temperature superconductivity has the geometry shown in Fig. 4. Compute $E(k)$ and $N(E)$. Does one of your bands have a very simple form? This geometry can be viewed as a square array of sites with additional sites sitting on the links between them. The copper atoms in high-T_c materials form just such a planar square arrays, whilst the oxygen atoms bridge them.

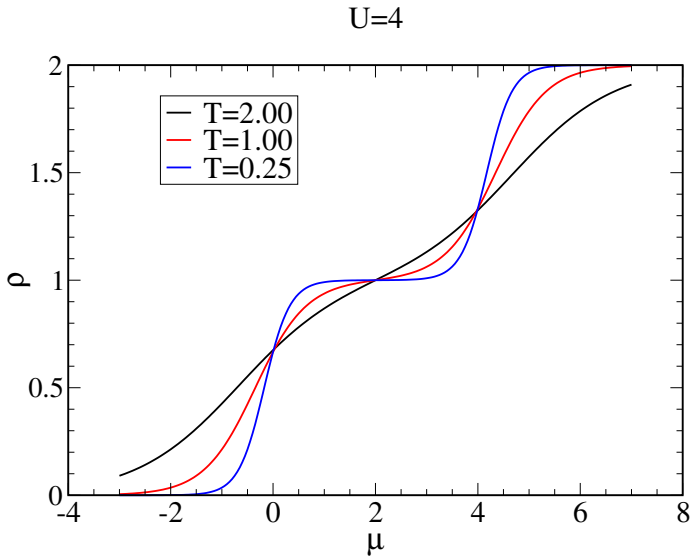

FIG. 7: Density $\langle\rho\rangle$ as a function of chemical potential for the single site ($t = 0$) Hubbard model at $U = 4$ for three different temperatures. At low T a 'Mott plateau' develops.

2. Extreme Strong Coupling Limit (t=0):

Having looked at some of features of the noninteracting Hubbard Hamiltonian (in various geometries), we now get a first insight into the role of interactions by considering a single site. Alternately phrased, we can set $t = 0$ in the Hamiltonian. In this case we have a collection of independent sites. The one site model is easily solved. We have four possibilities corresponding to the site being empty, having a single electron (either spin up or spin down) or being doubly occupied. Each of the states $|0\rangle, |\uparrow\rangle, |\downarrow\rangle, |\uparrow\downarrow\rangle$ is an eigenstate of H with eigenvalues $0, -\mu, -\mu, U - 2\mu$ respectively. The partition function is

$$Z = \sum_{\alpha} \langle\alpha|e^{-\beta H}|\alpha\rangle = 1 + 2e^{\beta\mu} + e^{2\beta\mu-\beta U}, \tag{6}$$

and the energy is,

$$E = \langle H + \mu n\rangle = Z^{-1} \sum_{\alpha} \langle\alpha|He^{-\beta H}|\alpha\rangle = (1 + 2e^{\beta\mu} + e^{2\beta\mu-\beta U})^{-1}\, U\, e^{2\beta\mu-\beta U}. \tag{7}$$

The occupation is given by,

$$\rho = \langle n\rangle \quad = 2(1 + 2e^{\beta\mu} + e^{2\beta\mu-\beta U})^{-1}(e^{\beta\mu} + e^{2\beta\mu-\beta U}) \tag{8}$$

In Fig. 7 we plot ρ vs. μ for $U = 4$ and $T = 2$ and $T = 0.5$ to exhibit one of the fundamental features of the Hubbard model, namely the "Mott insulating gap". At low temperature ($T = 0.5$) μ jumps to a higher value when the filling crosses through $\rho = 1$. This is the most simple indication of a 'Mott' insulating phase in the half-filled Hubbard model.

We will discuss this phenomenon in much more detail, but it is clear that, since the chemical potential $\mu = \partial E/\partial\rho$ it measures how much the energy changes when you change

the density of the system, ie. the cost to add a particle to the system. If you have a noninteracting system described by a set of energy levels, and you have filled the levels up to some 'Fermi energy' E_F the cost to add a particle is the next energy level just above the last level you filled, that is, $\mu = E_F$.

That a jump in μ should occur is easy to imagine: Consider a nearly empty lattice and ask what the energy cost is to add an electron. This cost need not involve U because it is easy to find a site which is empty. When one gets to half-filling, however, suddenly the cost to add an electron jumps by U since inevitably an added electron must sit on top of an electron which is already there. This sudden jump in the cost to add a particle is referred to as the "Mott gap."

Returning to thinking about the gap in terms of energy levels, if there is a region of energy where there are no levels to be filled, then μ has to take a jump from the energy at the top of the band which has just been filled to the energy at the bottom of the next band. Thus a jump in μ reflects the existence of a gap (and hence that your system is insulating). Even when interactions are turned on, and you cannot describe the system in terms of a bunch of energy levels, a jump in μ still indicates the existence of a gapped, insulating phase. While band and Mott insulators are characterized by gaps at the Fermi level, 'Anderson insulators', arising from disorder, can have a finite $N(E_F)$, as we shall discuss in the next section.

Half-filling $\rho = 1$ occurs when $\mu = U/2$. Because half-filling is so often studied, it is convenient to write the Hubbard Hamiltonian as,

$$H = -t \sum_{\langle \mathbf{j},\mathbf{l}\rangle \sigma} c^\dagger_{\mathbf{j}\sigma} c_{\mathbf{l}\sigma} + U \sum_{\mathbf{j}} (n_{\mathbf{j}\uparrow} - \frac{1}{2})(n_{\mathbf{j}\downarrow} - \frac{1}{2}) - \mu \sum_{\mathbf{j}} (n_{\mathbf{j}\uparrow} + n_{\mathbf{j}\downarrow}) \tag{9}$$

This just corresponds to a shift in the chemical potential μ by $U/2$. When this is done, half-filling conveniently occurs always at $\mu = 0$ for any value of t, T, U on a bipartite lattice. To emphasize, the properties of this 'new' model are identical to the old one, if one compares them at the same density. It's just that the chemical potentials used to get those densities are offset.

Exercise 7: Write expressions for Z, E and ρ at $t = 0$ with this new convention for the interaction term in the Hubbard model. You should notice that they are a bit more symmetric looking at $\mu = 0$.

A fundamental physical quantity in the Hubbard model is the 'local moment'. Formally, this quantity is defined by,

$$\langle m^2_{\mathbf{j}} \rangle = \langle (n_{\mathbf{j}\uparrow} - n_{\mathbf{j}\downarrow})^2 \rangle. \tag{10}$$

The local moment is zero if the site is either empty, $|0\rangle$, or has two oppositely pointed spins, $|\uparrow\downarrow\rangle$, but takes the value one if the site has a single electron, $|\uparrow\rangle$ or $|\downarrow\rangle$.

In Fig. XX, we plot the local moment as a function of U at half-filling for fixed $T = 0.5$. As U increases, the local moment rises from its uncorrelated value $\langle m^2_{\mathbf{j}} \rangle = 0.5$ which reflects a uniform mixture of empty, singly occupied, and doubly occupied sites, to the value $\langle m^2_{\mathbf{j}} \rangle = 1.0$ which reflects the presence only of singly occupied sites. This is a first indication of the tendency towards magnetism in the Hubbard model. An obvious question is whether, when these moments form on individual sites, there is a mechanism for developing correlations between them.

In Fig. XX we show the energy $E = \langle H \rangle$ and the specific heat $C = dE/dT$ for the half-filled $t = 0$ Hubbard Hamiltonian, as a function of T for $U = 8$. $C(T)$ has a peak at $T \sim U/3$ associated with the suppression of double occupation.

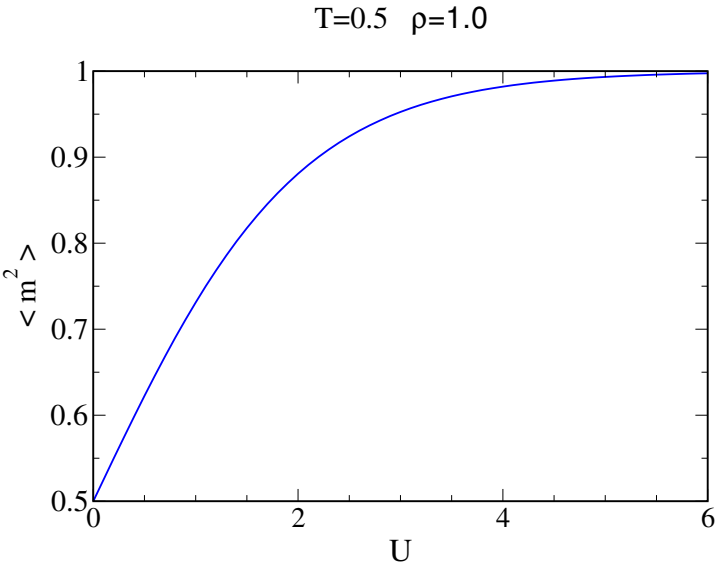

FIG. 8: Local moment $\langle m^2 \rangle$ as a function of U for the single site ($t = 0$) Hubbard model at half-filling $\rho = 1$ and temperature $T = 0.5$. As U increases, a perfect moment develops.

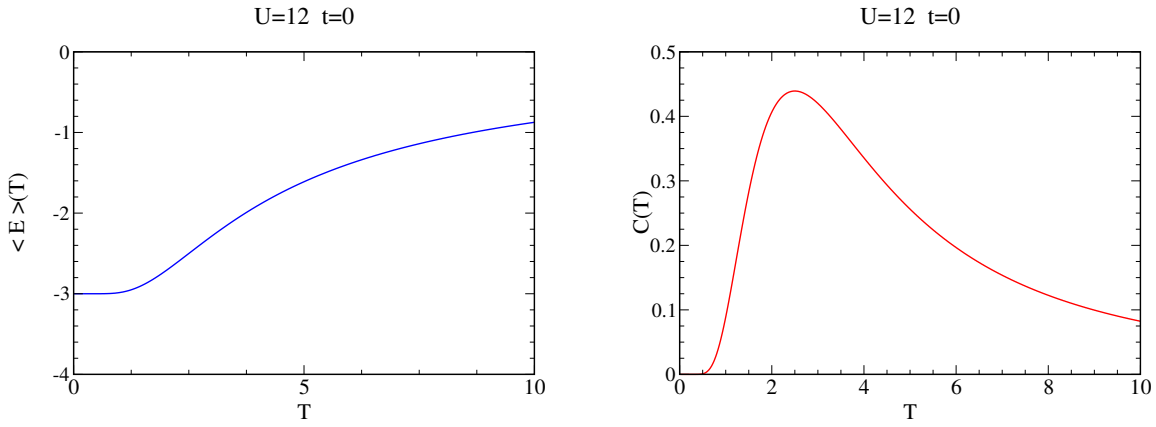

FIG. 9: Energy (left) and specific heat (right) as functions of temperature T for the single site Hubbard model with $U = 12$.

Exercise 8: Show the local moment is related to the 'double occupancy' $d_{\mathbf{j}} = \langle n_{\mathbf{j}\uparrow} n_{\mathbf{j}\downarrow} \rangle$ by,

$$\langle m_{\mathbf{j}}^2 \rangle = \langle n_{\mathbf{j}\uparrow} + n_{\mathbf{j}\downarrow} \rangle - 2d_{\mathbf{j}}. \tag{11}$$

At half-filling, the relation between the moment and the double occupancy becomes $\langle m_{\mathbf{j}}^2 \rangle = 1 - 2d_{\mathbf{j}}$. In this case, interpret the evolution of the local moment between the two limits $\langle m_{\mathbf{j}}^2 \rangle = \frac{1}{2}$ and $\langle m_{\mathbf{j}}^2 \rangle = 1$ in terms of what the double occupancy $d_{\mathbf{j}}$ is doing.

Having understood the limit of strictly zero hopping, $t = 0$, it is natural to consider perturbation theory in t. Indeed, this is a very fruitful approach and connects the half-filled Hubbard Hamiltonian with the spin-$\frac{1}{2}$ Heisenberg model. We will defer a discussion of this until Section IIB where we consider exact diagonalization where the solution of the two site

Hubbard Hamiltonian, presented there, can be examined in the limit of small, but nonzero, t/U.

3. Green's Functions for the Hubbard Hamiltonian

As we mentioned, the Hubbard Hamiltonian has been extensively studied via Green's function methods. While we will not say anything about that method, let us at least compute the Green's function in our weak and strong coupling limits.

The one particle Greens function,

$$\begin{aligned} G_{\mathbf{jn}}(\tau) &= \langle c_{\mathbf{j}}(\tau) c^{\dagger}_{\mathbf{n}}(0) \rangle \\ c_{\mathbf{l}}(\tau) &= e^{H\tau} c_{\mathbf{l}}(0) e^{-H\tau}, \end{aligned} \tag{12}$$

is a fundamental quantity in understanding the many body physics of interacting electron systems. Its momentum space and frequency transform, the spectral function $A(\omega)$, yields the photoemission spectrum, and from it two particle Greens functions which yield the charge and spin susceptibilities can be obtained.

In the limit of no interactions, $G_{\mathbf{jn}}(\tau)$ can be computed analytically.

Exercise 9: Show that at $U = 0$,

$$c_{\mathbf{k}}(\tau) = e^{H\tau} c_{\mathbf{k}}(0) e^{-H\tau} = e^{-\epsilon_{\mathbf{k}}\tau} c_{\mathbf{k}}(0) \tag{13}$$

You should do this two ways: First show that both expressions give the same result on the two states $|0\rangle$ and $|1\rangle$. Next, prove the result using the general theorem that $\partial A(\tau)\partial\tau = [H, A(\tau)]$. This result immediately follows from the definition $A(\tau) = e^{H\tau} A(0) e^{-H\tau}$.

Exercise 10: Show that at $U = 0$,

$$G_{\mathbf{jn}}(\tau) = \frac{1}{N} \sum_{\mathbf{k}} e^{i\mathbf{k}\cdot(\mathbf{n}-\mathbf{j})} (1 - f_{\mathbf{k}}) e^{-\epsilon_{\mathbf{k}}\tau}. \tag{14}$$

Notice that G is just a function of the difference $\mathbf{n} - \mathbf{j}$, as you would expect for a translationally invariant Hamiltonian.

Exercise 11: Write a program to evaluate $G_{\mathbf{jn}}(\tau)$ numerically at $U = 0$ for a $d = 1$ chain and a $d = 2$ square lattice. This is a useful calculation to have in checking a DQMC code.

Actually, we have been a little bit sloppy in defining G. Usually in many-body theory one defines the so-called 'time ordered' Green's function, $G_{\mathbf{k}}(\tau) = -\langle \mathcal{T} c_{\mathbf{k}}(\tau) c_{\mathbf{k}}(0) \rangle$ where the time ordering operator T is defined by

$$\begin{aligned} \mathcal{T} c_{\mathbf{k}}(\tau) c_{\mathbf{k}}(0) &= c_{\mathbf{k}}(\tau) c_{\mathbf{k}}(0) \qquad && \tau > 0 \\ \mathcal{T} c_{\mathbf{k}}(\tau) c_{\mathbf{k}}(0) &= -c_{\mathbf{k}}(0) c_{\mathbf{k}}(\tau) \qquad && \tau < 0 \end{aligned} \tag{15}$$

This definition of G and associated formalism opens the door into the huge world of diagrammatic perturbation theory and its application to the Hubbard model. However, the next few Exercises take you down the road just a little way.

Exercise 12: Prove that $G(\tau + \beta) = -G(\tau)$ for $-\beta < \tau < 0$.

Exercise 13: Prove that the result of Ex. 27, that $G(\tau)$ is antiperiodic with β requires that the Fourier transform of G given by

$$G(\tau) = \sum_n G(i\,\omega_n) e^{-i\omega_n \tau} \tag{16}$$

involves the 'Matsubara frequencies' $\omega_n = \pi(2n+1)/\beta$.

Exercise 14: Prove the inversion relation

$$G(i\,\omega_n) = \int_0^\beta \frac{d\tau}{\beta} G(\tau) e^{i\,\omega_n \tau} \tag{17}$$

Exercise 15: In Ex. 24 we solved for the time evolution of the fermion operator for $H = \epsilon_{\mathbf{k}} c_{\mathbf{k}}^\dagger c_{\mathbf{k}}$. Show that the Greens function is given by

$$\begin{aligned} G_{\mathbf{k}}(\tau) &= -e^{-\epsilon_{\mathbf{k}}\tau}(1 - f_{\mathbf{k}}) \qquad\qquad 0 < \tau < \beta \\ G_{\mathbf{k}}(\tau) &= e^{-\epsilon_{\mathbf{k}}\tau} f_{\mathbf{k}} \qquad\qquad -\beta < \tau < 0 \end{aligned} \tag{18}$$

Exercise 16: Using the result of Ex. 30 and the transformation rule of Ex. 29 show that

$$G_{\mathbf{k}}(i\,\omega_n) = \frac{1}{i\,\omega_n - \epsilon_{\mathbf{k}}}. \tag{19}$$

Exercise 17: Another way to get the result of Ex. 31 is to take $\partial/\partial\tau$ of the definition of the time ordered Greens function written in the form

$$G_{\mathbf{k}}(\tau) = \langle c_{\mathbf{k}}(\tau) c_{\mathbf{k}}(0) \rangle\, \theta(\tau) - \langle c_{\mathbf{k}}(0) c_{\mathbf{k}}(\tau) \rangle\, \theta(-\tau). \tag{20}$$

Be careful to take the appropriate derivatives of the step functions! Then Fourier transform both sides and solve for $G_{\mathbf{k}}(i\,\omega_n)$.

The approach used in Ex. 32 is the basis of the 'equation of motion' method for computing G. One starts with the definition of G, takes a time derivative, evaluates the resulting commutators of H with $c_{\mathbf{k}}$ and then Fourier transforms. If the Hamiltonian is quadratic in the fermion operators, then the set of equations closes, even if the different fermion operators mix. Otherwise, when can introduce an approximate truncation to terminate the hierarchy.

Exercise 18: The ambitious student should use the above procedure to evaluate $G_{\mathbf{k}}(i\,\omega_n)$ and $G_d(i\,\omega_n)$ for

$$H = \sum_{\mathbf{k}} \epsilon_{\mathbf{k}} c_{\mathbf{k}}^\dagger c_{\mathbf{k}} + V \sum_{\mathbf{k}} (c_{\mathbf{k}}^\dagger d + d^\dagger c_{\mathbf{k}}) + \epsilon_d d^\dagger d \tag{21}$$

which describes the mixing of a *single* impurity orbital (labeled by 'd') with a band of conduction electrons (labeled by '$\mathbf{k}$'). This is a model akin to the PAM mentioned earlier. You will need to write the two definitions of $G_{\mathbf{k}}(\tau)$ and $G_d(\tau)$, take their τ derivatives,

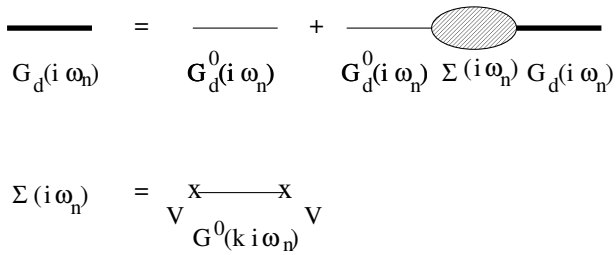

FIG. 10: Dyson equation and self-energy for the localized (d) electron for the Anderson impurity model.

and Fourier transform. You'll end up with two equations in two unknowns (the two Greens functions). Solving, your result for G_d should be

$$G_d(i\,\omega_n) = -\frac{1}{i\,\omega_n - \epsilon_d - V^2 \sum_{\mathbf{k}} \frac{1}{i\,\omega_n - \epsilon_{\mathbf{k}}}} \tag{22}$$

Exercise 20: In section II.A1 we analyzed the *zero* coupling limit of the Hubbard Hamiltonian. The Greens function for this $U = 0$ problem, which we have described in section IIA3, offers the jumping-off place for perturbative studies of the Hubbard, and related, Hamiltonians which allow us to build up solutions for finite U. If you have some familiarity with those approaches, you can attempt to rederive the result of Ex. 34 by evaluating the diagrammatic form of the self-energy, pictured below, by inserting the forms of the $U = 0$ Greens function and performing the necessary summations. Plugging into the Dyson Equation

$$\begin{aligned} G(k, i\omega_n) &= G_0(k, i\omega_n) + G_0(k, i\omega_n)\Sigma(k, i\omega_n)G(k, i\omega_n) \\ G^{-1}(k, i\omega_n) &= G_0^{-1}(k, i\omega_n) + \Sigma(k, i\omega_n) \end{aligned} \tag{23}$$

should reproduce the Greens function of Ex. 33. In this case, the perturbative Feynman diagram method, like the equation of motion method, provides an exact expression (ie correct to all orders in V). This provides a simple illustration of the method, but it should be kept in mind that this simple result is highly atypical.

It is also instructive to look at the Green's function for a single site, that is, the $t = 0$ Hubbard model. We have previously written down the Hilbert space for this problem and obtained the partition function and various equal time quantities. Now consider the calculation of

$$G_\uparrow(\tau) = \langle c_\uparrow(\tau) c_\uparrow^\dagger(0) \rangle. \tag{24}$$

Only the states $|\,0\,0\,\rangle$ and $|\,0\,1\,\rangle$ contribute to the expectation value since the creation operator for up electrons needs to see an empty up state. We can easily compute the action of the sequence of operators on $|\,0\,0\,\rangle$:

$$\begin{aligned} c_\uparrow(\tau)c_\uparrow^\dagger(0)\,|\,0\,0\,\rangle &= e^{H\tau}c_\uparrow(0)e^{-H\tau}c_\uparrow^\dagger(0)\,|\,0\,0\,\rangle = e^{H\tau}c_\uparrow(0)e^{-H\tau}\,|\,1\,0\,\rangle \\ &= e^{H\tau}c_\uparrow(0)e^{+U\tau/4}\,|\,1\,0\,\rangle = e^{H\tau}e^{+U\tau/4}\,|\,0\,0\,\rangle = e^{+U\tau/2}\,|\,0\,0\,\rangle \end{aligned} \tag{25}$$

and similarly for $|\,0\,1\,\rangle$.

Exercise 21: Complete the calculation begun above to show that,

$$G_\uparrow(\tau) = \frac{e^{+\beta U/4}e^{-\tau U/2} + e^{-\beta U/4}e^{\tau U/2}}{2\,e^{\beta U/4} + 2\,e^{-\beta U/4}}. \tag{26}$$

Exercise 22: The Green's function is related to the spectral density $A(\omega)$ by the relation,

$$G(\tau) = \int_{-\infty}^{+\infty} A(\omega)\frac{e^{-\omega\tau}}{e^{-\beta\omega}+1}\,d\omega. \tag{27}$$

Show that if you plug in

$$A(\omega) = \frac{1}{2}\,(\,\delta(\omega - U/2) + \delta(\omega + U/2)\,) \tag{28}$$

and do the integral you get precisely the $G(\tau)$ we computed.

The spectral function of the single site Hubbard model consists of two delta function peaks separated by U (the Mott gap).

We have discussed the Mott transition from the viewpoint of the development of a plateau in ρ vs μ at $\rho = 1$. The connection to insulating behavior was simple: In a dilute lattice electrons can move without double occupation. However, for an electron to move in a half-filled lattice in which each site is singly occupied, double occupation must occur. This costs an energy U. It is plausible to imagine that if U is very large, the electrons will not want to move at all, and one will have an "Mott" insulator.

The structure of $A(\omega)$, evaluated in the $t = 0$ limit above, which consistes of two delta functions separated by U, provides another illustration of the opening of a gap and Mott insulating phenomenon. Though the Mott gap is similar to the way that the cost to add an electron jumps if there is a gap separating single particle energy bands, it is worth noting that this analogy goes only so far, and the Mott gap differs in very fundamental ways from band gaps.

Exercise 23: It is also interesting to compute G and A when there is a local site energy or chemical potential present. Work with the Hamiltonian $H = U(n_\uparrow - \frac{1}{2})(n_\downarrow - \frac{1}{2}) - \mu(n_\uparrow + n_\downarrow)$. Show that,

$$\begin{aligned} A(\omega) &= a_+\ \delta(\omega - U/2 + \mu) + a_-\ \delta(\omega + U/2 + \mu). \\ a_+ &= (\ e^{\beta U/2}e^{\beta\mu} + e^{2\beta\mu}\ )/(\ 1 + 2\,e^{\beta U/2}e^{\beta\mu} + e^{2\beta\mu}) \\ a_- &= (\ 1 + e^{\beta U/2}e^{\beta\mu}\ )/(\ 1 + 2\,e^{\beta U/2}e^{\beta\mu} + e^{2\beta\mu}\ ) \end{aligned}$$

by evaluating $G(\tau)$ explicitly from its definition. μ now enters both the partition function Z and the imaginary time propagation. The coefficients a_+ and a_- are obtained by equating this expression for $G(\tau)$ with what you get from plugging $A(\omega)$ into the formula relating G and A. Notice that at $\mu = 0$ we recover $a_+ = a_- = \frac{1}{2}$, and that, regardless of what μ, β and μ are, we always have $a_+ + a_- = 1$. Interestingly, the spectral function is not just shifted by μ as one might have expected. The peak heights are also changed.

Exercise 24: We conclude this section by noting the form of the interaction term in momentum space. Substitute the equation which relates real and momentum space operators for each of the four real space creation operators in the interaction term of the Hubbard model.

As with the hopping term, the sum over sites leads to momentum conservation and reduces the four momentum sums to three. Show that the result is

$$\frac{U}{N}\sum_{\mathbf{k}_1,\mathbf{k}_2,\mathbf{k}_3} c^\dagger_{\mathbf{k}_1+\mathbf{k}_2-\mathbf{k}_3\uparrow} c^\dagger_{\mathbf{k}_3\downarrow} c_{\mathbf{k}_2\uparrow} c_{\mathbf{k}_1\downarrow}.$$

The physical content of this form is that an up and down electron of momentum $\mathbf{k}_2$ and $\mathbf{k}_1$ scatter and emerge with momenta $\mathbf{k}_3$ and $\mathbf{k}_1 + \mathbf{k}_2 - \mathbf{k}_3$, the same total momentum as initially. One can rewrite the sum over the three momentum variables as,

$$\frac{U}{N}\sum_{\mathbf{k}_1,\mathbf{k}_2,\mathbf{q}} c^\dagger_{\mathbf{k_2}+\mathbf{q}\uparrow} c^\dagger_{\mathbf{k}_1-\mathbf{q}\downarrow} c_{\mathbf{k}_2\uparrow} c_{\mathbf{k}_1\downarrow}.$$

Here $\mathbf{q}$ is seen to be the momentum exchanged in the collision of the two electrons of initial momenta $\mathbf{k}_1$ and $\mathbf{k}_2$.

B. Exact Diagonalization

We have considered the limits $t = 0$ and $U = 0$. The Hubbard model cannot be solved exactly when both terms are non-zero. Our next approach is to consider a small cluster of sites. Let's start with two sites. The Hilbert space has 16 states, since each site can have four possibilities: no electrons, an up electron, a down electron, or both. However, since H commutes with $N_\uparrow$ and $N_\downarrow$ we actually have to consider only much smaller matrices.

Exercise 28: Show that the sixteen dimensional Hilbert space of the two site Hubbard model factorizes into four spaces of dimension one, four spaces of dimension two, and one space of dimension four. Construct the matrices by applying H to each of the vectors.

Exercise 29: Diagonalize the matrices of the preceding Exercise. Even the four dimensional matrix can be done by hand. Compute the partition function and the energy.

Earlier, when we studied the one site Hubbard model, we learned that magnetic moments form when the ratio U/T is large. Put another way, thermal fluctuations can destroy magnetic moments, while interactions cause them to form. This was at $t = 0$. We will now see that 'quantum fluctuations'- the motion of the electrons which occurs when the hopping t is made nonzero, also competes with moment formation.

Exercise 30: Compute the local moment $\langle m^2 \rangle$ in the sector with one up and one down electron for low temperature. Plot $\langle m^2 \rangle$ as a function of U/t. Interpret your result in terms of the effect of U and t on moment formation.

We have now learned that U drives the formation of moments on the sites of our lattice and that thermal fluctuations (T) and quantum fluctuations (t) both try to inhibit moments. We conclude this discussion of the two site case by pointing out something about the order of magnetic moments between sites in the Hubbard model.

Exercise 31: Compute the energy difference between the two states $|\uparrow\ \uparrow\rangle$ and $|\downarrow\ \downarrow\rangle$ (which have the same energy) and the lowest energy state of the sector which connects the states

$|\uparrow\ \downarrow\rangle$, $|\downarrow\ \uparrow\rangle$, $|\uparrow\downarrow\ \ 0\rangle$, and $|\downarrow\uparrow\ \ 0\rangle$. Show that the lowest energy state in this $N_\uparrow = N_\downarrow = 1$ sector is lower in energy by an amount proportional to $J = t^2/U$.

The result of the preceding Exercise tells us something about magnetic order in the Hubbard model. In the half-filled sector, one elctron per site, the states with antiferromagnetic order (neighboring sites have electrons with opposite spins) are lower in energy than ferromagnetic ones (neighboring sites have parallel spins). Although this has come out of consideration of only two sites, it is a general feature: The Hubbard model has antiferromagnetic order at half-filling. Indeed, the antiferromagnetic 'exchange' energy scale $J = t^2/U$ that we found is precisely the energy scale for this order even in the thermodynamic limit.

In addition to antiferromagnetism, one can see the Mott gap in this little two site model by looking at the eigenvalues of the sector with one up and one down electron. As you found in Exercise x, there are two eigenvalues close to $-U/2$ and two close to $+U/2$. More precisely, the eigenvalues are shifted by values involving the hopping t away from $\pm U/2$. The separation U between $\pm U/2$ is the Mott gap, and, as one increases t the separation becomes less and less clear. This puts a very simple quantitative face on the statement that when U is large one has an insulator (a Mott gap) but when U is small, the electrons can still move around.

This analysis of the two site model can be extended quite easily to somewhat larger lattices by writing a program which generates the matrix elements of H and diagonalizes the resulting matrices. In fact, this is one important way that information has been gained concerning the Hubbard model. Although it is limited to 10-20 sites (depending on how much computational effort one is willing to put up with) the results obtained are exact and any possible quantity, including time dependent ones, can be computed.

Exercise 36: Write a program to diagonalize the four site Hubbard model. Compute E and $\langle m^2 \rangle$.

In these notes, the idea of diagonalization has arisen twice. First, we pointed out that in the absence of interactions, the Hamiltonian is quadratic in the fermion creation and destruction operators, $H = \sum_{\mathbf{i},\mathbf{j}} c^\dagger_{\mathbf{i}} h_{\mathbf{i},\mathbf{j}} c_{\mathbf{j}}$, and we can solve the Hubbard model by diagonalizing the matrix h. Second, in the discussion immediately above, we talked about constructing the matrix for H when the interactions are nonzero. However, there is a very important difference in the two usages of the term "diagonalization." This is emphasized in the Exercise which follows.

Exercise 37: Compare the computational cost of the diagonalizations in each of the two cases, $U = 0$ and $U \neq 0$. How big are the matrices involved for N sites? How large a system could you study in both cases?

We took the first steps towards an exact diagonalization solution of the Hubbard model when we discussed the extreme strong coupling limit, $t = 0$, which divided the lattice into a collection of single sites.

The following routine

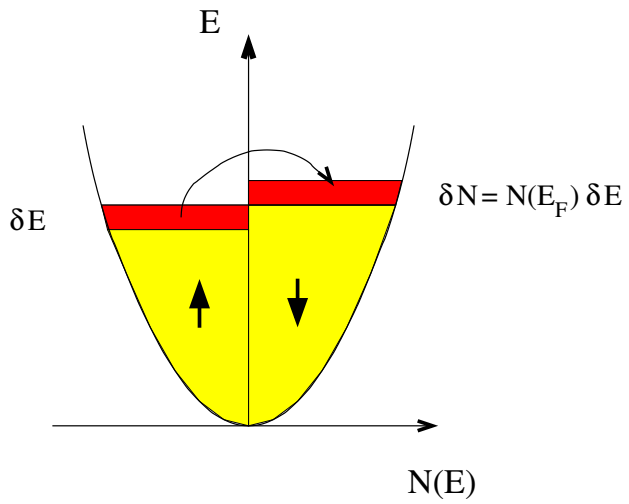

FIG. 11: Qualitative picture of Stoner construction. δN down spin electrons are converted to up spin electrons, at a cost in kinetic energy $\delta K = +\delta n \delta E$. If this is less than the potential energy lowering, a ferromagnetic state is favored.

C. Mean Field Theory

Stoner's Picture: Stoner developed a very simple picture of ferromagnetism based on the competition between the kinetic energy cost of making the up and down spin electron numbers different and the associated potential energy gain. The basic idea is the following: Because of the Pauli principle the way to occupy a given set of energy levels with the lowest energy is to start filling from the bottom and put two electrons, one of each spin, in each level. Otherwise, if you make the numbers of up and down electrons unequal, and don't fill each level with two electrons, you have to occupy higher energies.

However, if you make the number of up and down electrons unequal, you can reduce the potential energy: Consider the limit of complete spin polarization where there are no electrons of one spin species. Then, obviously, the potential energy is zero.

Perhaps this competition can lead to non-trivial effects. Consider a system with density of states $N(E)$ and both up and down spin electrons filling the energy levels up to the same maximum called the 'Fermi level' E_F. The density of up and down electrons is equal. We'll call it n. Let's compute the change in energy which results from a reduction in the density of down spin electrons by δn and at the same time an increase the number of up spin electrons by δn. The potential energy changes by,

$$\delta P = U(n + \delta n)(n - \delta n) - Un^2 = -U(\delta n)^2.$$

If we shift an extra δn electrons into the up group, we will occupy energy levels above the original E_F. Recalling the definition of the density of states as the number of levels at an energy E we see that $N(E) = dN/dE$ whence $\delta n = N(E_F)\delta E$. This tells us how big the range of energies is above E_F we are filling in terms of δn. Likewise, we are emptying levels below E_F that used to be occupied by down spin electrons. The net result of this process is to shift δn electrons up in energy by an amount δE. The change in the kinetic energy is then,

$$\delta K = +\delta n \delta E = +\frac{1}{N(E_F)}(\delta n)^2.$$

Putting these two expressions together,

$$\delta E = \delta P + \delta K = (-U + \frac{1}{N(E_F)})(\delta n)^2 = (-UN(E_F) + 1)\frac{(\delta n)^2}{N(E_F)}.$$

We see that if $UN(E_F) > 1$ the total energy change $\delta E < 0$, so it is favorable to have the up and down electron densities different and hence favorable to have ferromagntism. This is called the Stoner criterion. It tells us that magnetism is favored by large electron interactions. As we shall see, this simple calculation yields results in precise agreement with mean field theory.

Mean Field Theory: Ferromagnetism: We have considered the Hubbard model in the simple limits of no hopping ($t = 0$), no interactions ($U = 0$), very small system sizes (one and two sites), and using Stoner's approach. We now turn to our first 'serious' calculation of the Hubbard model- mean field theory. Our goal is to study ferromagnetism.

What is mean field theory? We commented in an earlier section that a Hamiltonian which is quadratic in the fermion creation and destruction operators, $H = \sum_{\mathbf{i},\mathbf{j}} c^\dagger_{\mathbf{i}} h_{\mathbf{i},\mathbf{j}} c_{\mathbf{j}}$, can be solved by diagonalizing the matrix h. Mean field theory is a method which produces such a quadratic Hamiltonian from a model like the Hubbard model which has quartic terms $U c^\dagger_\uparrow c_\uparrow c^\dagger_\downarrow c_\downarrow$ involving four fermion creation and destruction operators. The approach begins by expressing the number operators as an average value plus a deviation from the average:

$$\begin{aligned} n_{\mathbf{i}\uparrow} &= \langle n_{\mathbf{i}\uparrow}\rangle + (n_{\mathbf{i}\uparrow} - \langle n_{\mathbf{i}\uparrow}\rangle) \\ n_{\mathbf{i}\downarrow} &= \langle n_{\mathbf{i}\downarrow}\rangle + (n_{\mathbf{i}\downarrow} - \langle n_{\mathbf{i}\downarrow}\rangle). \end{aligned} \tag{29}$$

Substituting these expressions into the Hubbard interaction term, and dropping the 'small' term which is the product of the two deviations from the average yields,

$$\begin{aligned} n_{\mathbf{i}\uparrow} n_{\mathbf{i}\downarrow} &= [\langle n_{\mathbf{i}\uparrow}\rangle + (n_{\mathbf{i}\uparrow} - \langle n_{\mathbf{i}\uparrow}\rangle)][\langle n_{\mathbf{i}\downarrow}\rangle + (n_{\mathbf{i}\downarrow} - \langle n_{\mathbf{i}\downarrow}\rangle)] \\ &\approx \langle n_{\mathbf{i}\uparrow}\rangle\langle n_{\mathbf{i}\downarrow}\rangle + \langle n_{\mathbf{i}\downarrow}\rangle(n_{\mathbf{i}\uparrow} - \langle n_{\mathbf{i}\uparrow}\rangle) + \langle n_{\mathbf{i}\uparrow}\rangle(n_{\mathbf{i}\downarrow} - \langle n_{\mathbf{i}\downarrow}\rangle)] \\ &= n_{\mathbf{i}\uparrow}\langle n_{\mathbf{i}\downarrow}\rangle + n_{\mathbf{i}\downarrow}\langle n_{\mathbf{i}\uparrow}\rangle) - \langle n_{\mathbf{i}\uparrow}\rangle\langle n_{\mathbf{i}\downarrow}\rangle. \end{aligned} \tag{30}$$

The interpretation of this expression is simple. The up spin electrons interact with the average density of down spin electrons, and similarly the down spin electrons interact with the average density of up spin electrons. These two terms overcount the original single interaction term, so the product of the average densities is subtracted off.

Within this mean field replacement, the Hubbard Hamiltonian is now quadratic, and takes the form (in one dimension)

$$H = -t\sum_{l\sigma}(c^\dagger_{l\sigma}c_{l+1\sigma} + c^\dagger_{l+1\sigma}c_{l\sigma}) + n_{\mathbf{i}\uparrow}\langle n_{\mathbf{i}\downarrow}\rangle + n_{\mathbf{i}\downarrow}\langle n_{\mathbf{i}\uparrow}\rangle) - \langle n_{\mathbf{i}\uparrow}\rangle\langle n_{\mathbf{i}\downarrow}\rangle. \tag{31}$$

Since H is quadratic, its solution is a matter of diagonalizing an appropriate matrix. Specifically, for the case of ferromagnetism, one imagines that the average occupation is independent of spatial site $\mathbf{i}$ but allowed to be different for the two spin species. That is, $\langle n_{\mathbf{i}\uparrow}\rangle = n+m$ and $\langle n_{\mathbf{i}\downarrow}\rangle = n - m$. Our goal is to calculate the energy E for fixed n as a function of m and see whether the minimum is at $m = 0$ (paramagnetic state, no ferromagnetism) or $m \neq 0$ (ferromagnetism). Because the expectation values $\langle n_{\mathbf{i}\uparrow}\rangle$ and $\langle n_{\mathbf{i}\downarrow}\rangle$ have such a simple, site independent form, the energy levels can easily be written down. (See Exercise 23.) They are,

$$\begin{aligned} \epsilon_{\uparrow k} &= U(n - m) - 2t\cos k \\ \epsilon_{\downarrow k} &= U(n + m) - 2t\cos k. \end{aligned} \tag{32}$$

Again, I have assumed we are in one dimension.

One merely has to take the various possible fillings of the lattice with up and down electrons and add these levels up. That is, we proceed as follows:

(1) Fix the lattice size, N, to some fairly large value, for example $N = 128$ or greater.

(2) Choose a total particle number $N_{\rm tot}$ and on-site repulsion U.

(3) Loop over $N_\uparrow = 0, 1, 2, \ldots . N_{\rm tot}$. For each choice, set $N_\downarrow = N_{\rm tot} - N_\uparrow$. (Actually, your answers should be symmetric on interchange of $N_\uparrow$ and $N_\downarrow$, so you really only need do half the values $N_\uparrow = 0, 1, 2, \ldots . N_{\rm tot}/2$.) Define the densities, $n_\uparrow = N_\uparrow/N$ and $n_\downarrow = N_\downarrow/N$.

(4) Loop over the N allowed momentum values $k = 2\pi/N\{-N/2+1, -N/2+2, \ldots N/2\}$. Fill up the lowest $N_\uparrow$ and $N_\downarrow$ of the energy levels. That is, add the associated energy values to some accumulator which stores the total energy. Recall that the levels are given by $\epsilon_\uparrow(k) = -2\,t\,{\rm cos}k + U\langle n_\downarrow\rangle$ and $\epsilon_\downarrow(k) = -2\,t\,{\rm cos}k + U\langle n_\uparrow\rangle$.

(5) Finally, normalize your energy accumulator to the number of sites (divide by N) and add in the term $-U\langle n_\uparrow\rangle\langle n_\downarrow\rangle$. This gives the energy for the given $N_\uparrow$ and $N_\downarrow = N_{\rm tot} - N_\uparrow$. Make a list of them and see which is lowest.

(6) Repeat the calculation for different U and $N_{\rm tot}$ to get the phase diagram.

I will now show some real code for this problem and also a few results from running it.

The code

```
implicit none
integer i,N,Nup,Ndn,Ntot
real*8 t,U,tpin,k,ekup,ekdn,denup,dendn
real*8 efup,efdn,eftot

write (6,*) 'N,Ntot,t,U'
read  (5,*)  N,Ntot,t,U
tpin=8.d0*datan(1.d0)/dfloat(N)
do 1000 Nup=0,Ntot,2

Ndn=Ntot-Nup
denup=dfloat(Nup)/dfloat(N)
dendn=dfloat(Ndn)/dfloat(N)

efup=0.d0
efdn=0.d0
do 200 i=-N/2+1,N/2
    k=tpin*dfloat(i)
    if (i.ge.-Nup/2+1.and.i.le.Nup/2) then
       ekup=-2.d0*t*dcos(k)+U*dendn
       efup=efup+ekup
    endif
    if (i.ge.-Ndn/2+1.and.i.le.Ndn/2) then
       ekdn=-2.d0*t*dcos(k)+U*denup
       efdn=efdn+ekdn
    endif
200 continue
eftot=(efup+efdn)/dfloat(N)-U*denup*dendn

write (36,990) Nup,Ndn,eftot
990 format(2i6,f16.6)

1000 continue

end
```

Results for $\rho = 1/2$

Ferromagnetism vs. Paramagnetism: Here are results for one quarter filling, that is, a density $\rho = \rho_\uparrow + \rho_\downarrow = \frac{1}{2}$ electrons per site. (This is one quarter of the maximal density of two electrons per site.) The magnetization m is defined such that $m = (\rho_\uparrow - \rho_\downarrow)/(\rho_\uparrow + \rho_\downarrow)$.

You see that at $U/t = 2$ the optimal energy is paramagnetic: the energy E is minimized at $m = 0$. This is still the case at $U/t = 4$ (see next page), but the energy of the spin polarized solutions (m nonzero) are getting much closer to $m = 0$. (Note the energy scale.) When $U/t = 4.2$ the energies for large $|m|$ have started to turn down and are lower than intermediate m, though $E(m = 0)$ is still lowest. $U/t = 4.4$ has just gone ferromagnetic.

Notice that the transition is *first order*. That is, as U/t increases we jump suddenly from a minimum at $m = 0$ to a minimum at $m = \pm 1$. Another possibility would have

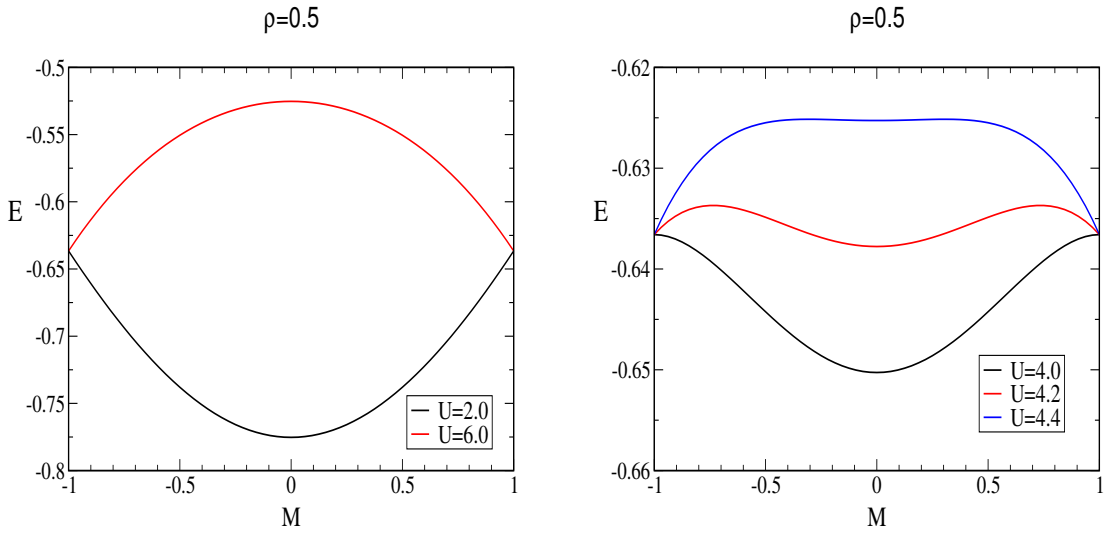

FIG. 12: Left: Energy versus magnetization of $d = 1$ Hubbard model at quarter filling, $\rho = \frac{1}{2}$ (128 electrons on an $N = 256$ site lattice). A paramagnetic state, $M = 0$, is favored at $U = 2.0t$, and a ferromagnetic one, with full spin polarization $M = 1$, at $U = 6.0\,t$. Right: Same as left panel, except in the transition region $U \approx 4.0\,t$. The Stoner critierion gives $U_{\rm crit} = \sqrt{2}\,\pi\,t \approx 4.44\,t$.

been a second order transition in which the minimum at $m = 0$ gradually shifts to larger m and partially polarized solutions are best for a range of U/t. Without examining other MF solutions (like antiferromagnetic ones) we cannot tell if this first order transition is 'real' or simply occurs because we have restricted to ferromagnetic solutions and something even lower in energy is actually winning.

Consistency with Stoner Criterion: We derived the Stoner Criterion for Ferromagnetism $UN(E_{\rm F}) > 1$. For the d=1 Hubbard model we can compute,

$$N(E) = 2\sum_k \delta(E - \epsilon_k) = 2\int \frac{dk}{2\pi}\delta(E - \epsilon_k) \tag{33}$$

with $\epsilon_k = -2t\cos(k)$. A simple calculation gives

$$N(E) = \frac{1}{\pi\sqrt{4t^2 - E^2}}. \tag{34}$$

(You also did this in Exercise x.) This is the density of states for a single spin species, which is what was used in the Stoner criterion.

We also need the relation between the density ρ and the Fermi energy $E_{\rm F}$:

$$\rho = 2\int_{-2t}^{E_{\rm F}} dE\ N(E). \tag{35}$$

I put in the factor of two for spin here, so that when I plug in ρ I use the total density (including both spin species). This yields,

$$\rho = \frac{2}{\pi}\cos^{-1}(-\frac{E}{2t}). \tag{36}$$

You can check this latter relation obeys the expected limits: $\rho = 0$ when $E_{\rm F} = -2t$, $\rho = 1$ when $E_{\rm F} = 0$, and $\rho = 2$ when $E_{\rm F} = +2t$.

Putting these equations together, we can get the density of states at $E_{\rm F}$ for a given filling:

$$N(\rho) = \frac{1}{2\pi t} \frac{1}{\sin(\pi\rho/2)} \tag{37}$$

For half-filling, $\rho = 1$ we see that $N(\rho = 1) = \frac{1}{2\pi t}$ and hence $U_{\rm crit} = 2\pi t$. For quarter-filling, $\rho = \frac{1}{2}$ we see that $N(\rho = 1) = \frac{1}{\sqrt{2}\pi t}$ and hence $U_{\rm crit} = \sqrt{2}\pi t = 4.44t$. This is in pretty good agreement with Figures 1–5 which showed us that $U_{\rm crit}$ was around $4.4t$. I suspect that the slight disagreement (Figure 4 suggests $U_{\rm crit}$ a bit less than $4.4t$ while Stoner gives $U_{\rm crit}$ a bit more than $4.4t$) is due to the fact that Figures 1-5 were run on $N = 256$ site lattices. That is, I believe the small difference is likely a finite size effect.

Exercise 25: Write a code to do mean field theory for the $d = 1$ Hubbard model as described above. Compute the critical U above which the ferromagnetic state is lower in energy than the paramagnetic one for $N_{tot} = 3N/4$.

Exercise 26: Verify that the critical U you obtained for ferromagnetism precisely agrees with the Stoner criterion. You will need to use the value for the density of state obtained in Exercise x.

There is another way to write the code, which you might find easier. Work in the grand-canonical ensemble. That is, provide a chemical potential μ and then *compute* $N_\downarrow$ and $N_\uparrow$ by filling those levels which are below μ. The density then comes out of the choice of μ, and, indeed, you will need to tune μ to get the density you desire. (This process is a bit annoying.)

One advantage of this method is that one can let the code find the lowest energy configuration, instead of searching through all the possible choices of magnetization. This is done in the usual way: Start at some densities $n_\uparrow, n_\downarrow$, compute $E(n_\uparrow, n_\downarrow)$, and then alter $n_\uparrow, n_\downarrow$, to reduce E (using your favorite gradient descent algorithm or whatever). Continue iterating until you reach the minimum.

Another reason this second, 'grand canonical', approach is more convenient is that it is easy to do things at finite temperature. One simply replaces the process where one accumulates the energies of all levels $\epsilon_\sigma(k) < \mu$ with accumulating $\epsilon_\sigma(k)$ times the Fermi function $1/[1 + e^{\beta(\epsilon_\sigma(k)-\mu)}]$. (Likewise, one puts this Fermi function in the computation of the density). Another reason the grand canonical approach is sometimes preferable is that it also generalizes better to states where the lowest energy is more complex, 'striped phases' etc, where the density of electrons is allowed to depend in a completely general way on the lattice site and spin species. In that situation, though, there is usually no longer an analytic form for the energy levels and one has to diagonalize a matrix to get them.

Exercise 27: Write your own code to do mean field theory for the $d = 1$ Hubbard model in the grand canonical ensemble as described above. Again compute the critical U above which the ferromagnetic state is lower in energy than the paramagnetic one for $N_{tot} = 3N/4$.

Before concluding with the discussion of mean field theory, it should be emphasized that this mean field approach, while very useful in yielding insight into the possible phases of the system, is a completely uncontrolled approximation. Mean field theory overestimates the tendency for ordered phases, and can (and does) predict magnetic order where none occurs.

Even if a particular phase transition is correctly predicted by mean field theory, the details of the transition (critical temperature, critical exponents, etc) are usually incorrect.
Mean Field Theory: AntiFerromagnetism: The basic idea to look for antiferromagnetism in the Hubbard model within mean field theory is the same as for ferromagnetism. The thing that is just slightly more difficult is to figure out the energy levels.

First, let's define precisely what an antiferromagnetic configuration is. Recall that a paramagnetic configuration has the same exact density $n_{l\sigma} = n$ regardless of site l or spin σ, and that a ferromagnetic configuration allows the density to depend on σ but not l: $n_{l\uparrow} = n_\uparrow$, and $n_{l\downarrow} = n_\downarrow$ (see above).

An antiferromagnetic configuration allows a simple *spatial* dependence in which the densities alternate: $n_{l\uparrow} = n + (-1)^l m$, $n_{l\downarrow} = n - (-1)^l m$. That is, the even sites have a surplus of up spin electron density: $n_{\mathrm{even}\,\uparrow} = n + m$, $n_{\mathrm{even}\,\downarrow} = n - m$. The odd sites have a surplus of down spin electron density: $n_{\mathrm{odd}\,\uparrow} = n - m$, $n_{\mathrm{odd}\,\downarrow} = n + m$. Note that the total number of up and down electrons in the whole system is the same, nN, and that each site has the same density $2n$, once the densities of the individual spin species are summed. More generally one might have some sort of mixed ferromagnetic and antiferromagnetic configuration.

The form of the Hamiltonian in mean field theory is, $H = \sum_{j,l} c^\dagger_{j\sigma} M_\sigma(j,l) c_{l\sigma}$, where $M_\sigma(j,l)$ has $-t$ just above and below the main diagonal, with $M_\uparrow(l,l) = U(n - (-1)^l m)$, or $M_\downarrow(l,l) = U(n + (-1)^l m)$ along the diagonal. The eigenvalues for this sort of tridiagonal matrix when the diagonal is constant ($m = 0$). When m is nonzero, the eigenvectors of momentum k and $k + \pi$ are mixed (see below for further discussion) and the eigenvalues become: $E(k) = \pm\sqrt{(-2\,t\cos k)^2 + (Um)^2} + Un$. Here k is now defined in a 'reduced zone', $k = 2\pi/N\{-N/4 + 1, -N/4 + 2, \ldots, +N/4\}$, so that there are still N eigenvalues as there should be for this N dimensional matrix (two eigenvalues for each k, but only half as many k. The eigenvalues are the same for $\sigma =\uparrow$ and $\sigma =\uparrow$.) You might want to check that these eigenvalues reduce to the old ones when $m = 0$. Can you also check the eigenvalues make sense when $t = 0$? (Check that all the counting (degeneracies) are correct!)

The process for computing the energy of an antiferromagnetic configuration is the same as the steps (1–5) above, with the replacement of the ferromagnetic eigenvalues by the antiferromagnetic ones. Since we are assuming the total up and down densities over the whole lattice are identical, one no longer loops over different $N_\uparrow$. However, one does have to loop over different m. More precisely, one fixes $n = N_{\mathrm{tot}}/2$ and then tries $m = 1/N, 2/N \ldots,$.

One reason this problem is worth doing is because of its formal connections to so many other problems in solid state physics. The most obvious is the opening of a gap in an energy band by a periodic potential $V(G)$ with wavevector G (e.g. see Ashcroft and Mermin). In our problem we can think of the up spin electrons as moving in a periodic potential which has period π resulting from the oscillating down spin density (and vice-versa). A gap is opened at $k = \pm\pi/2$. There is also a connection to simple phonon problems where one makes the masses or spring constants vary: $m_1, m_2, m_1, m_2, \ldots$ or $k_1, k_2, k_1, k_2, \ldots$. Again, the single phonon dispersion curve for uniform masses and springs breaks into two branches, optic and acoustic. Some of you are presently doing this problem in Physics 240B. There are many other examples.
Sample Code:

```
implicit none
integer i,N,Ntot,istag
real*8 t,U,tpin,k,ek,mstag
real*8 rho,Umstag,Urho
real*8 eaf,eaftot,lambdaminus

write (6,*) 'N,Ntot,t,U'
```

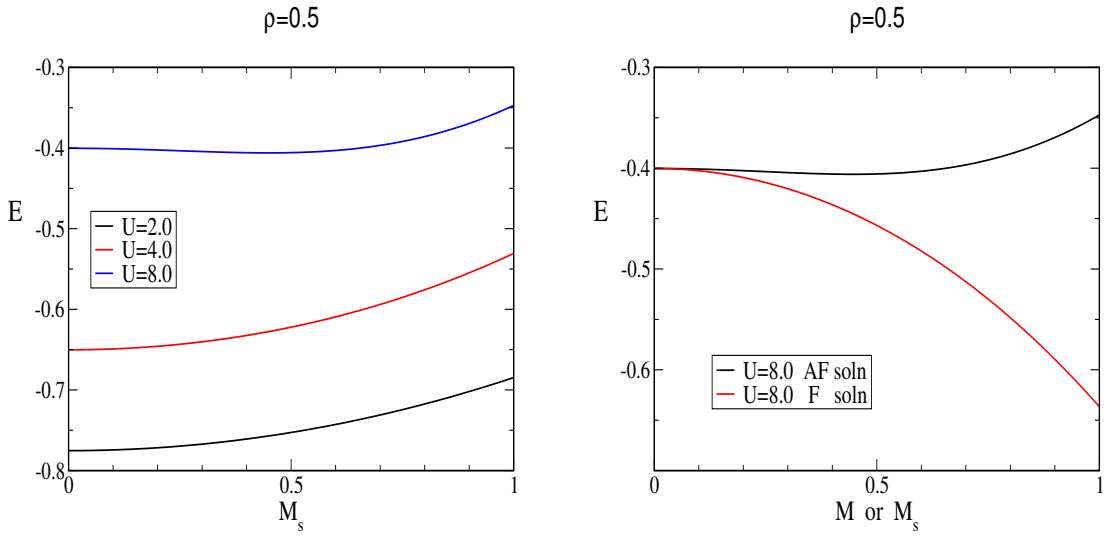

FIG. 13: Left: Energy versus staggered magnetization of $d = 1$ Hubbard model at quarter filling, $\rho = \frac{1}{2}$ (128 electrons on an $N = 256$ site lattice). A paramagnetic state, $M_s = 0$, is favored at $U = 2.0\,t$ and $U = 4.0\,t$. Nonzero staggered magnetization with partial staggered spin polarization, $M_s = 21/48$, has lower energy than $M_s = 0$ at $U = 8.0\,t$. Right: However, the ferromagnetic solution has yet lower energy for this filling and interaction strength.

```
      read  (5,*)  N,Ntot,t,U
      write (36,*) Ntot/2+1

      tpin=8.d0*datan(1.d0)/dfloat(N)
      rho=dfloat(Ntot)/dfloat(N)
      Urho=U*rho/2.d0

      do 1000 istag=0,Ntot,2

      mstag=dfloat(istag)/dfloat(N)
      Umstag=U*mstag/2.d0

      eaftot=0.d0
      do 200 i=-Ntot/4+1,Ntot/4
          k=tpin*dfloat(i)
          ek = -2.d0*t*dcos(k)
          lambdaminus=-dsqrt(ek*ek+Umstag*Umstag)
          lambdaminus=lambdaminus+Urho
          eaftot=eaftot+lambdaminus
200    continue
       eaftot=2.d0*eaftot/dfloat(N)-U*(rho*rho-mstag*mstag)/4.d0

      write (36,990) istag,eaftot
990   format(i6,f16.6)

1000  continue

      end
```

AntiFerromagnetism vs. Paramagnetism: Let's consider again the case of one quarter filling, that is, a density $n = n_\uparrow + n_\downarrow = \frac{1}{2}$ electrons per site. However now we will look for

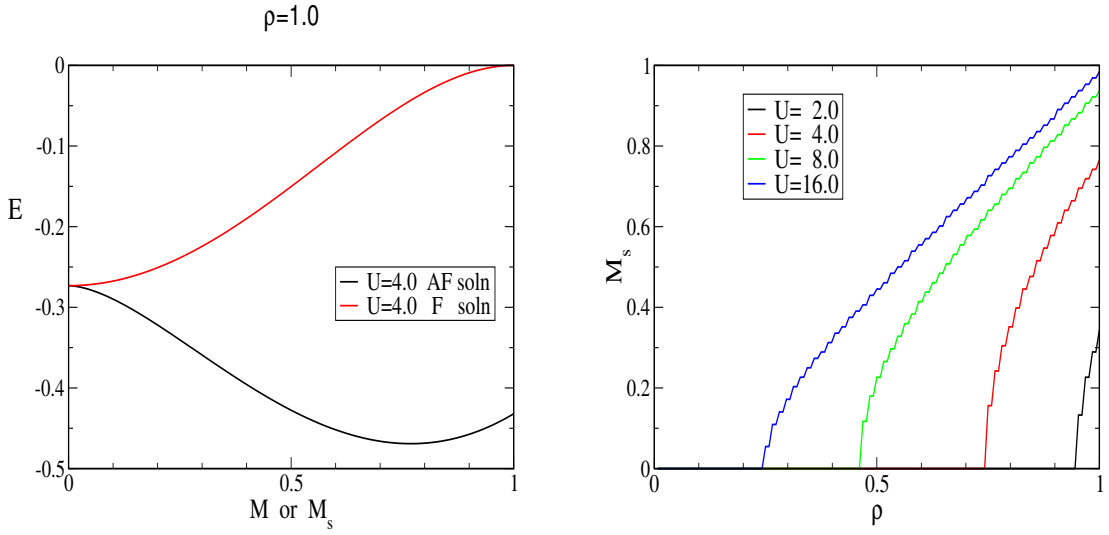

FIG. 14: Left: Energy versus magnetisation and staggered magnetization of $d = 1$ Hubbard model with $U = 4.0t$ and at half filling, $\rho = 1$ (256 electrons on an $N = 256$ site lattice). Nonzero staggered magnetization with partial staggered spin polarization, $M_s = 21/48$, has lower energy than $M_s = 0$. Unlike the quarter filled case of the right panel of Fig. 8 this antiferromagnetic solution is lower in energy than ferromagnetic ones. Right: Staggered magnetization which minimizes the energy, when restricted to the antiferromagnetic sector, as a function of filling, for different interaction strengths. In all cases, we need to check to see whether ferromagnetic solutions might be yet lower. Steps in the curves are a result of the finite lattice size.

antiferromagnetic behavior. The staggered magnetization m_s is defined such that the up and down spin densities are $n_\uparrow = n + (-1)^i m_s$ and $n_\downarrow = n - (-1)^i m_s$.

For $U = 2$ the paramagnetic solution m_s=0 has lowest energy. We know too from the preceding note that $m = 0$ is the lowest of the ferromagnetic energies. Notice as a check on the codes that one can compare with Figure 1 and see that $E(m_s = 0) = E(m = 0)$.

As before, we now start cranking up U. Figures 2 and 3 show the energy for $U = 4$ and $U = 8$ respectively. We see at $U = 8$ that a nonzero m_s is better than zero m_s. However, the state is not actually antiferromagnetic because (Figure 4) the ferromagnetic energy is yet lower. (Again, check the fact that $E(m_s = 0) = E(m = 0)$. Really I should plot the ferromagnetic and antiferromagnetic data, Figures 3 and 4, on the same graph to make comparisons nicer.)

Results for $n = 1$

The preceding results suggest that at quarter filling, $\rho = \frac{1}{2}$, the $d = 1$ Hubbard model is more prone to ferromagnetism than antiferromagnetism. Let's look at half-filling, $\rho = 1$, where antiferromagnetism tends to be most stable. Sure enough, Figures 5 and 6 show the antiferromagnetism is optimal (for $U = 4$). In fact, here, the best m_s is the biggest it can be.

Phase boundary: Our ultimate objective could be to analyze a bunch of energy curves, both ferro- and antiferromagnetic, for different densities ρ and couplings U and figure out the whole phase diagram in the $\rho - U$ plane. As a first step in this direction, Figure 7 shows the value of the staggered magnetization which minimizes the energy, as a function of density for different values of U. For small $U = 2$, the energy is minimized in the paramagnetic phase $m_s = 0$ until close to half filling ($\rho = 1$). As U increases, so does the regime of antiferromagnetism. For $U = 16$ the optimal staggered magnetization becomes nonzero

around $\rho = 0.24$. So looking at the five points where m_s becomes nonzero begins to give us a sense of the antiferromagnetic phase boundary. We have to do similar analysis for the ferromagnetic case (and compare energies) to complete the picture.

III. DISORDER IN THE ABSENCE OF INTERACTIONS

A. The Anderson Transition

The development of insulating behavior of noninteracting electrons in a random potential is called 'Anderson localization.' For concreteness, let's consider the Hubbard Hamiltonian at $U = 0$ but with a spatially varying (random) chemical potential $-\mu \sum_{\mathbf{j}\sigma} n_{\mathbf{j}\sigma} \rightarrow -\sum_{\mathbf{j}\sigma} \mu_{\mathbf{j}} n_{\mathbf{j}\sigma}$

As for phase transitions in general dimensionality plays a key role in whether the insulator-metal transition occurs. In one dimension, it is fairly easy to see that all states are localized by an arbitrarily small amount of randomness. Only the situation where there is zero disorder is metallic.

The celebrated 'gang-of-four' paper[9] showed the much less trivial result that the same applies in two dimensions. As discussed previously, this was the basis for the conjecture that, perhaps, even when interactions are included, there is no metallic phase in two dimensions.

So, it really only in three dimensions that the generic picture of the coexistence of localized and delocalized states, separated by a mobility edge, is really the case.

B. A Digression into Non-Hermiticity: The Hatano-Nelson Model

The Anderson transition, in which the eigenstates of of noninteracting electrons are localized by disorder, has been the subject of considerable theoretical and numerical work over the last thirty years[45]. By now it is well-understood that in one and two dimensions, any amount of randomness will localize all the eigenstates, while in three dimensions, a 'mobility edge' whose position depends on the disorder strength, separates localized eigenvectors whose eigenvalues lie at the edges of the eigenvalue distribution from extended eigenvectors whose eigenvalues lie near the center[9].

Various refinements of this problem have also garnered considerable attention. Perhaps the most famous is the question of the influence of many-body correlations on Anderson localization and, in particular, the possibility of a metallic phase in a disordered, interacting two dimensional system[2]. This is a very difficult problem whose resolution is still under debate[3].

However, another important line of work has retained the non-interacting character of the particles, and instead focused on a non-Hermitian generalization of the Anderson Hamiltonian, the Hatano-Nelson model[46]. In one dimension,

$$H = -\frac{t}{2}\sum_{l=1}^{N}(e^{h}c_{l+1}^{\dagger}c_{l} + e^{-h}c_{l}^{\dagger}c_{l+1}) + \sum_{l}\mu_{l}c_{l}^{\dagger}c_{l} \ .$$

Here $c_l^\dagger(c_l)$ are the usual fermion creation(destruction) operators. The parameter h controls the asymmetry between the hopping amplitudes in the $+x$ and $-x$ directions, while μ_l are a collection of random site energies which we will choose here to have a uniform distribution on $[-\Delta/2, +\Delta/2]$. N is the number of lattice sites. It is important to note that the periodic boundary conditions which connect the two ends of the lattice have a fundamental influence on localization, as we shall discuss further below. To set the scale of energy, we will choose the hopping parameter $t = 1$ throughout this paper,

Such non-Hermitian Hamiltonians have been used to describe a number of phenomena, including the motion of flux lines in disordered type-II superconductors[46] and nuclear decay,

dissipative systems, and quantum chromodynamics[47–55]. They have also provided useful insight into the Anderson localization transition[46,56].

A final line of inquiry which motivates the present work concerns tight-binding lattice models with a 'superlattice potential'

$$H \to H + \Delta H \qquad \Delta H = V \sum_l \cos(\frac{2\pi\omega}{N} l)\ c_l^\dagger c_l.$$

Here recent interest has arisen from experimental studies of optically trapped atoms in which a periodic potential is applied in addition to the optical lattice itself, creating a regular array of trapping potentials for the atoms[57–60]. We note that the relation between random potentials and problems with several periodic potentials of incommensurate frequency has also been examined[61–63].

In this paper we bring together the two issues of non-symmetric hopping and a superlattice potential. Specifically, we study the eigenvalues and eigenvectors of a one-dimensional Hatano-Nelson model with an additional periodic potential V. We first review some of the properties of the original, separate, models, before turning to our new results whch combine the two.

We begin with Hatano-Nelson Hamiltonian ($V = 0$). When $\Delta = 0$, the eigenvalues are easily obtained,

$$\lambda(k) = \frac{1}{2}(e^h e^{ik} + e^{-h} e^{-ik})\ .$$

Here $0 < k < 2\pi$. The eigenvalues lie on an ellipse in the complex plane, centered at the origin, with a semimajor axis of length $2\cosh h$ aligned with the real axis, and a semiminor axis of length $2\sinh h$ aligned with the imaginary axis. When disorder is turned on, $\Delta \neq 0$, lines of real eigenvalues extend outward from this ellipse. Fig. 1 shows the eigenspectrum for $h = 0.2$ and $\Delta = 2$.

While the present paper concerns one dimension only, we note that in higher dimension, the central eigenvalues become space filling and spread into a continuous eigenvalue 'blob'. Wings of real eigenvalues extend from the blob, just as in the one dimensional case.

The crucial observation to make is the relationship between the location of the eigenvalue, on the ellipse (complex) or the wings (real), and the nature of the associated eigenvector. Consider the eigenvalue problem in component form,

$$-\frac{t}{2}e^h\,\psi_{l+1} + \mu_l\,\psi_l - \frac{t}{2}e^{-h}\,\psi_{l-1} = \lambda\,\psi_l\ .$$

Performing the 'gauge transformation' $\psi_l = e^{-hl}\tilde{\psi}_l$ yields

$$-\frac{t}{2}\tilde{\psi}_{l+1} + \mu_l\,\tilde{\psi}_l - \frac{t}{2}\tilde{\psi}_{l-1} = \lambda\,\tilde{\psi}_l\ .$$

h has vanished from our equation and we precisely recover the eigenproblem of the (Hermitian) Anderson problem! However, this argument *fails* when the periodic boundary conditions are included. We see that, perhaps not surprisingly for a problem concerning localization and transport, that boundaries are crucial to the physics. The eigenvalues of the non-Hermitian matrix of the Hatano-Nelson Hamiltonian are *real* and identical to those of the Anderson Hamiltonian, when open boundary conditions are used, but differ dramatically otherwise. (Interestingly, even in the case when periodic boundary conditions are included, the gauge transformation allows us to accumulate all the factors of h in a single link, if we so desire.)

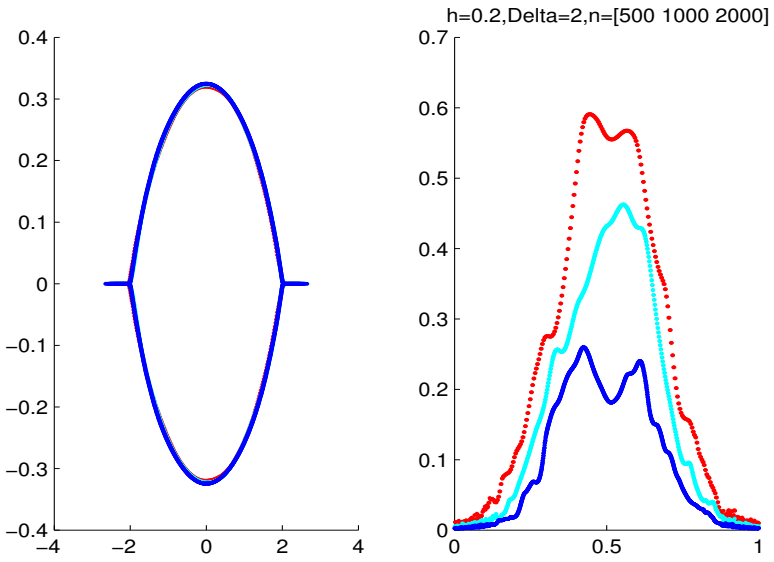

FIG. 15: Left: Eigenspectrum of the Hatano-Nelson Hamiltonian with $h = 0.2$ and $\Delta = 2$. The eigenvalues are located on a ellipse centered at the origin, with two 'wings' extending out along the real axis. Right: Corresponding (normalized) participation ratios: $\mathcal{P}_n/N$. Numerical results were obtained for $N = 500, 1000, 2000$ sites, averaging over ten disorder realizations.

Actually, this statement concerning the role of boundary conditions may be a bit too strong. If one looks at the 'pseudospectrum' of the Hatano-Nelson model in the open boundary condition case, one observes clear indications of the physics of the periodic case in the form of values of λ for which $det(H - \lambda I)$ becomes arbitrarily small and which lie on an ellipse in the complex plane[64]. [Bai- Is this statement correct?]

Let us now suppose that we have a localized eigenvector (and periodic boundary conditions). We can perform a gauge transformation which moves all the h factors away from the region of the lattice where the eigenvector is non-zero. It is then plausible that the eigenvector will be described by the same properties as the Anderson Hamiltonian. Hence its eigenvalue will be real. We thus conclude that the eigenvectors whose eigenvalues lie on the real wings are localized, while those on the ellipse, with complex eigenvalues, are delocalized. Fig. 1(right) shows the participation ratio,

$$\mathcal{P}_n = (\sum_{l=1}^{N} |\psi_l^n|^4)^{-1}$$

a measure of the number of components which are 'large' for the eigenvector ψ^n with components ψ_l^n. Parameters are the same as Fig. 1.

We turn now to the superlattice model. The eigenspectrum of the Hermitian ($h = 0$) Hamiltonian of tight-binding electrons in an additional periodic potential is again easily determined in the absence of randomness $\Delta = 0$. For the highest frequency potential, $\omega = N/2$, in which the periodic potential alternates positive and negative on the odd and even sites respectively, we have the familiar result,

$$E(k) = \pm\sqrt{\cos^2 k + V^2}$$

in which the eigenspectrum has a gap $2V$ at half-filling. Here k is in the reduced Brillouin zone $-\pi/2 < k < +\pi/2$.

The case of lower frequencies ω is less commonly quoted, but almost equally easy to write down[65]. Instead of the periodic potential mixing two momentum values k and $k+\pi$, it mixes a larger number N/ω. That is, in momentum space, the Hamiltonian breaks into ω blocks, each of size N/ω, with matrix elements

$$\begin{aligned} \mathcal{H}^k_{l,l'} &= \langle\, k + lQ \,|\, \hat{\mathcal{H}} \,|\, k + l'Q \,\rangle \\ &= -t\cos(k + lQ)\, \delta^\omega_{l,l'} + V\, \delta^\omega_{|l-l'|,1} \ , \end{aligned}$$

where $Q = 2\pi\omega/N$ and $\delta^\omega_{l,l'} = \delta_{l,l' \bmod N/\omega}$. The eigenvalues of $\mathcal{H}$ give the energy bands.

C. Pseudospectra

IV. PRESCRIPTION FOR DETERMINANT QUANTUM MONTE CARLO

A. Basic Formalism

The bulk of the physics I will discuss in these lectures is obtained with DQMC. I hope to convince you it is, within its limitations, a very powerful approach to the physics of the Hubbard Hamiltonian. This suggests that a possible goal for students here might be to write, or at least begin to write, a DQMC code. To be honest, this is a very ambitious goal, but to have any chance for it to be realistic, I would like to begin with the prescription for writing a DQMC program, literally by writing down some 'pseudo-code' for it in the same way we did for diagonalization. Appendix 3 covers some of the background derivations.

Besides the parameters t, U, μ in the Hubbard Hamiltonian $\hat{H}$, the physics is of course also determined by the inverse temperature $\beta = 1/T$. For reasons made clear in Appendix 3, in DQMC it is necessary to divide β into L 'imaginary time intervals', $\beta = L\,\Delta\tau$. The length of each interval $\Delta\tau$ should be chosen such that $t\,U\,(\Delta\tau)^2 < 1/10$.

1. Matrices Determining the Boltzmann Weight

We first consider the part of $\hat{H}$ which includes the terms which are quadratic in the fermion creation and destruction operators, eg the hopping and site energies,

$$\hat{K} = \sum_{\sigma} \begin{pmatrix} c_{1\sigma}^{\dagger} & c_{2\sigma}^{\dagger} & \cdots \end{pmatrix} \begin{pmatrix} k_{11} & k_{12} & \cdots \\ k_{21} & k_{22} & \cdots \\ \vdots & \vdots & \ddots \end{pmatrix} \begin{pmatrix} c_{1\sigma} \\ c_{2\sigma} \\ \vdots \end{pmatrix} \tag{38}$$

k is defined to be the NxN matrix with elements $\Delta\tau\, k_{ij}$.

As an example, for a one dimensional Hubbard model with $N = 6$ sites, nearest neighbor hopping, no disorder, and periodic boundary conditions,

$$k = \Delta\tau \begin{pmatrix} -\mu & -t & 0 & 0 & 0 & -t \\ -t & -\mu & -t & 0 & 0 & 0 \\ 0 & -t & -\mu & -t & 0 & 0 \\ 0 & 0 & -t & -\mu & -t & 0 \\ 0 & 0 & 0 & -t & -\mu & -t \\ -t & 0 & 0 & 0 & -t & -\mu \end{pmatrix} \tag{39}$$

Fill an array $s(i, l)$ (the 'Hubbard-Stratonovich field') randomly with values ± 1. The first index i goes from 1 to N, and the second index l goes from 1 to L. Define a set of L

diagonal matrices, each of dimension N,

$$v_\uparrow(l) = \lambda \begin{pmatrix} s(1,l) & 0 & 0 & 0 & \cdots \\ 0 & s(2,l) & 0 & 0 & \cdots \\ 0 & 0 & s(3,l) & 0 & \cdots \\ 0 & 0 & 0 & s(4,l) & \cdots \\ \vdots & \vdots & \vdots & \vdots & \ddots \end{pmatrix} \tag{40}$$

Here the parameter λ is given by $\cosh \lambda = e^{U\Delta\tau/2}$. The matrices for the down spin electrons differ only by a sign: $v_\downarrow(l) = -v_\uparrow(l)$.

2. Initializing The Greens Function

Compute the up and down Green's functions,

$$G_\sigma = [\ I + e^k\, e^{v_\sigma(1)}\, e^k\, e^{v_\sigma(2)}\, e^k\, e^{v_\sigma(3)} \cdots e^k\, e^{v_\sigma(L)}\ ]^{-1} \tag{41}$$

Here I is the N dimensional identity matrix.

Updating the Hubbard-Stratonovich Field

Suggest a change in the Hubbard Stratonovich field on site $i = 1$ of imaginary time slice $l = L$ by computing the quantity,

$$\begin{aligned} d_\uparrow &= 1 + (\,1 - [G_\uparrow]_{ii}\,)\,(\,e^{-2\lambda\, s(i,l)} - 1\,) \\ d_\downarrow &= 1 + (\,1 - [G_\downarrow]_{ii}\,)\,(\,e^{+2\lambda\, s(i,l)} - 1\,) \\ d &= d_\uparrow d_\downarrow \end{aligned} \tag{42}$$

Throw a uniformly distributed random number, $0 < r < 1$. If $r < d$, update the Hubbard Stratonovich field on site i of imaginary time slice l via $s(i,l) = -s(i,l)$.

3. Updating the Greens Function

If the move was accepted, the Green's functions, which depend on s (see Eq. 5 and remember $v_\sigma(l)$ are functions of s) will now be different. You could recompute G_σ from Eq. 5, using the new s. This will take a time which goes as N^3, since it involves a matrix inversion. There's a faster (order N^2) trick to get the new G_σ, which takes advantage of the fact that only one element in one of the $v_\sigma(l)$ has changed. Compute the vectors,

$$\begin{aligned} c_{j\uparrow} &= -(\,e^{-2\lambda\, s(i,l)} - 1\,)\,[G_\uparrow]_{ij} + \delta_{ji}\,(\,e^{-2\lambda\, s(i,l)} - 1\,) \\ c_{j\downarrow} &= -(\,e^{+2\lambda\, s(i,l)} - 1\,)\,[G_\downarrow]_{ij} + \delta_{ji}\,(\,e^{+2\lambda\, s(i,l)} - 1\,) \\ b_{k\uparrow} &= [G_\uparrow]_{ki}\ /\ (\,1 + c_{i\uparrow}\,) \\ b_{k\downarrow} &= [G_\downarrow]_{ki}\ /\ (\,1 + c_{i\downarrow}\,) \end{aligned} \tag{43}$$

Here δ_{ij} is the usual Kronecker δ. Remember that i is the fixed site whose Hubbard-Stratonovich field is being updated. The free indices j, k run from 1 to N. Then the new G_σ are given by

$$[G_\sigma]_{jk} = [G_\sigma]_{jk} - b_{j\sigma}\, c_{k\sigma}. \tag{44}$$

Don't forget to update your interaction energy matrix if you accept the move (Eq. 4). After the new G_σ are computed, go to Hubbard-Statonovich field on the second spatial site on imaginary time slice $l = L$ and suggest a change to it, and follow the procedure of Eqs. 6-8 again, with $i = 2$. Continue this until all spatial sites of time slice $l = L$ are updated.

4. Wrapping the Greens Function

After all spatial sites i of imaginary time slice $l = L$ have been updated, change the Green's functions via,

$$G_\sigma = [\, e^{k}\, e^{v_\sigma(l)}\,]\; G_\sigma\; [\, e^{k}\, e^{v_\sigma(l)}\,]^{-1} \tag{45}$$

Now update all the Hubbard-Stratonovich variables on imaginary time slice $l = L - 1$ following the procedures of Eqs. 6-8. When all spatial sites of imaginary time slice are finished, wrap the Greens functions using Eq. 9 again.

Continue the process of Eqs. 6-9 until all imaginary time slices are updated.

5. Measurements

After completing an entire set of updates to all the space-time points of the lattice. make measurements. For example, the density of electrons of spin σ on site i is given by,

$$\langle n_{i\sigma} \rangle = 1 - [G_\sigma]_{ii}. \tag{46}$$

The double occupancy rate on site i is

$$\langle n_{i\uparrow} n_{i\downarrow} \rangle = (\, 1 - [G_\uparrow]_{ii}\,)\; (\, 1 - [G_\downarrow]_{ii}\,) \tag{47}$$

The local moment on site i is,

$$\langle (n_{i\uparrow} - n_{i\downarrow})^2 \rangle = \langle n_{i\uparrow} + n_{i\downarrow} \rangle - 2\langle n_{i\uparrow} n_{i\downarrow} \rangle. \tag{48}$$

The correlation between moments on sites i and j, for $i \neq j$, is given by,

$$\begin{aligned} S_{+i} &= c^\dagger_{i\uparrow} c_{i\downarrow} \\ S_{-j} &= c^\dagger_{j\downarrow} c_{j\uparrow} \\ \langle S_{+i} S_{-j} \rangle &= -[G_\uparrow]_{ji}\; [G_\downarrow]_{ij} \end{aligned} \tag{49}$$

You can also measure pairing correlations, charge density wave correlations, etc.

6. Full Monte Carlo

Begin by initializing the Hubbard-Stratonovich field and computing the Kinetic and Interaction matrices (Eqs. 3,4), and finally the Green's function (Eq. 5). Do a few hundred 'equilibration' sweeps of the lattice (Eqs. 6-9) *without* making any measurements. Follow this by a few thousand 'measurement' sweeps in which you perform the operations of Eqs. 6-9 and also Eqs. 10-12. Normalize your measurements to the number of measurement sweeps performed.

7. Congratulations, you're done!

We conclude this section by mentioning that there are a number of alternate Quantum Monte Carlo approaches to the Hubbard Hamiltonian closely related to that discussed here. These include a ground state projection method[34,35], and approximate techniques which deal with the sign problem[66]. Dynamical mean field theory[67–69], especially when it employs the Hirsch-Fye QMC method[70] as its impurity solver, is a method of particular appeal since it not only provides a solution to tight-binding models (with the limit where the mometum dependence of the self-energy is neglected) but also offers a powerful methodology with which to put together electronic stucture and many body physics.

B. Results: Local Moment, Spin Correlation, and Specific Heat

The evolution of the local moment (Eq. 12) at half-filling as the temperature is decreased is shown in Fig. 1 on a 6x6 lattice for different interaction strengths U. We see the local moment begin to develop from its uncorrelated value $\frac{1}{2}$ at a temperature set by U, and then saturate at low T. The local moment does not reach 1 at $T = 0$ because significant quantum fluctuations allow doubly occupied and empty sites to occur even in the ground state. However, as U increases, these fluctuations are suppressed and the moment becomes better and better formed. The local moment also makes a further small adjustment at low T, which is due to the onset of long range magnetic order.

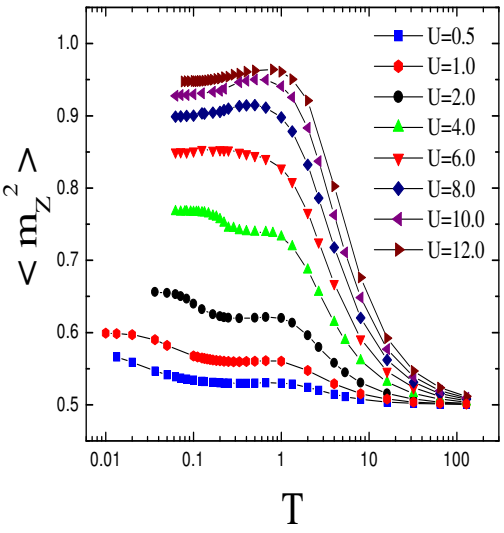

FIG. 16: The local moment $\langle m_z^2 \rangle$ as a function of temperature for different interaction strengths U and lattice size 6x6. The lattice is half-filled.

From the energy we can get the specific heat (Fig. 2). It shows an interesting two peak strudture. The high temperature peak is associated with the formation of local moments, and the low temperature peak with their ordering. The Hubbard model maps onto the Heisenberg model at large U. This connection is emphasized in Fig. 2 which shows that the low temperature peak in the specific heat of the Hubbard model can be mapped onto that of the Heisenberg model with $J = 4t^2/U$.

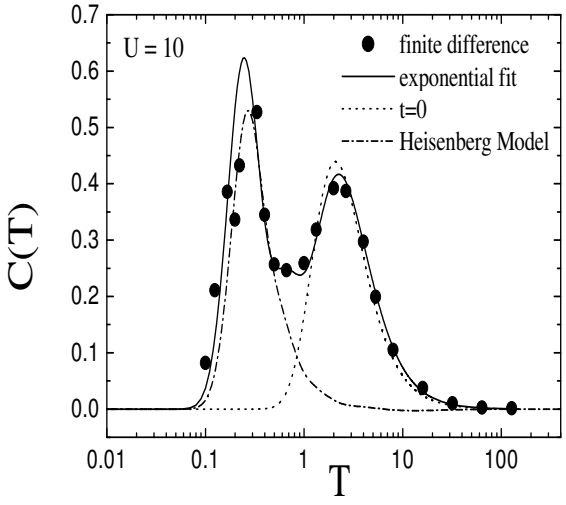

FIG. 17: The specific heat of the Hubbard model for $U = 10t$. There is a high temperature peak which is fit well by considering a single site Hubbard model ($t = 0$) and a low temperature peak which agrees well with the Heisenberg model with $J = 4t^2/U = 0.4$.

The near-neighbor spin correlation are shown in Fig. 3. The magnetic structure factor $S(\pi, \pi) = \frac{1}{N} \sum_{ij} \langle S_{z,i} S_{z,j} \rangle$ sums these correlations over the whole lattice. It is found that $S(\pi, \pi)$ grows linearly with N at low T, indicating that the correlations extend over the whole lattice.

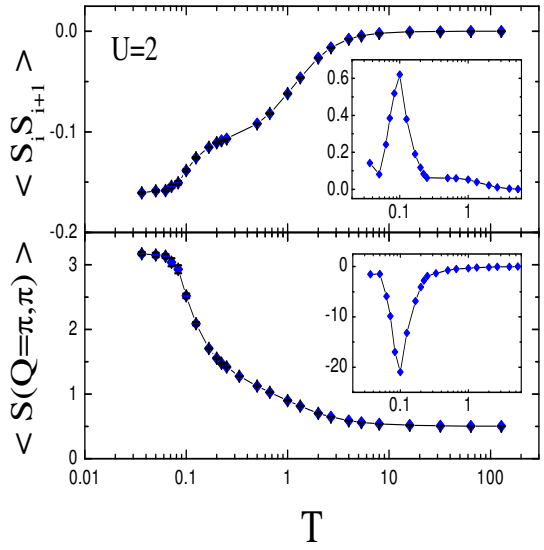

FIG. 18: The near neighbor spin correlations and magnetic structure factor of the half-filled Hubbard model at $U = 2t$.

Finally, in Fig. 4 we show the density of states at $\omega = 0$ for the half-filled Hubbard model

at different values of U. The suppression of $N(\omega = 0)$ at low T and large U is a signature of the presence of an insulating gap caused by the on-site repulsion.

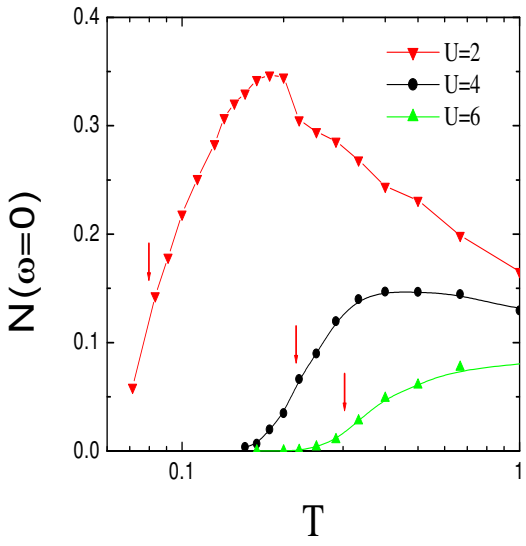

FIG. 19: The density of states at $N(\omega = 0)$. As T is lowered, a Mott-Hubbard gap opens up. The half-filled Hubbard model is insulating.

V. DQMC FOR THE ANDERSON-HUBBARD HAMILTONIAN

In the first three parts of this section we will present the results of Determinant Quantum Monte Carlo simulations of the Anderson-Hubbard Hamiltonian, that is, studies of the interplay of disordered one-body potential, two-body interactions, and a Zeeman field on magnetism, thermodynamics, and metal-insulator transitions. The final topic concerns the effect of interactions on the band insulating phase which arises from a periodic potential, as opposed to a random one. Journal references are given at the beginning of each subsection.

A. Interaction driven Anderson Insulator to Metal Transition

Journal Reference: "Conducting phase in the two-dimensional disordered Hubbard model", P.J.H. Denteneer, R.T. Scalettar, and N. Trivedi, Phys. Rev. Lett. **83**, 4610 (1999).

1. Introduction

As discussed in Section I, the central question motivated by experiments on silicon metal-oxide semiconductor field effect transistors is whether electron-electron interactions enhance the conductivity of a 2D disordered electron system, and possibly lead to a conducting phase and a metal–insulator transition. We can address this question by studying the *disordered Hubbard model*, which contains both relevant ingredients: interactions and disorder. While the Hubbard model does not include the long range nature of the Coulomb repulsion, studying the simpler model of screened interactions is an important first step in answering the central qualitative question posed above. We use the Determinant Quantum Monte Carlo simulation techniques introduced in Section IV, which enable us to avoid the limitations of perturbative approaches (while of course being confronted with others). We mention that recent studies using very different techniques from ours have indicated that interactions may enhance conductivity: two interacting particles instead of one in a random potential has a delocalizing effect[31], and weak Coulomb interactions were found to increase the conductance of spinless electrons in (small) strongly disordered systems[32].

The quantity of immediate interest when studying a possible metal–insulator transition is the *conductivity* and especially its T-dependence. By the fluctuation–dissipation theorem σ_{dc} is related to the zero-frequency limit of the current-current correlation function. A complication of the QMC simulations is that the correlation functions are obtained as a function of *imaginary* time. To avoid a numerical analytic continuation procedure to obtain frequency-dependent quantities, which would require Monte Carlo data of higher accuracy than produced in the present study, we employ an approximation that was used and tested before in studies of the superconductor–insulator transition in the attractive Hubbard model[44]. This approximation is valid when the temperature is smaller than an appropriate energy scale in the problem. Additional checks and applicability to the present problem are discussed below. The approximation allows $\sigma_{\rm dc}$ to be computed directly from the wavevector $\mathbf{q}$- and imaginary time τ-dependent current-current correlation function $\Lambda_{xx}(\mathbf{q},\tau)$:

$$\sigma_{\rm dc} = \frac{\beta^2}{\pi}\Lambda_{xx}(\mathbf{q}=0,\tau=\beta/2)\ . \tag{50}$$

Here $\beta = 1/T$, $\Lambda_{xx}(\mathbf{q},\tau) = \langle j_x(\mathbf{q},\tau)\, j_x(-\mathbf{q},0)\rangle$, and $j_x(\mathbf{q},\tau)$ the $\mathbf{q},\tau$-dependent current in the x-direction, is the Fourier transform of $j_x(\ell) = i\sum_\sigma t_{\ell+\hat{x},\ell}(c^\dagger_{\ell+\hat{x},\sigma}c_{\ell\sigma} - c^\dagger_{\ell\sigma}c_{\ell+\hat{x},\sigma})$. (See also Ref.[71]).

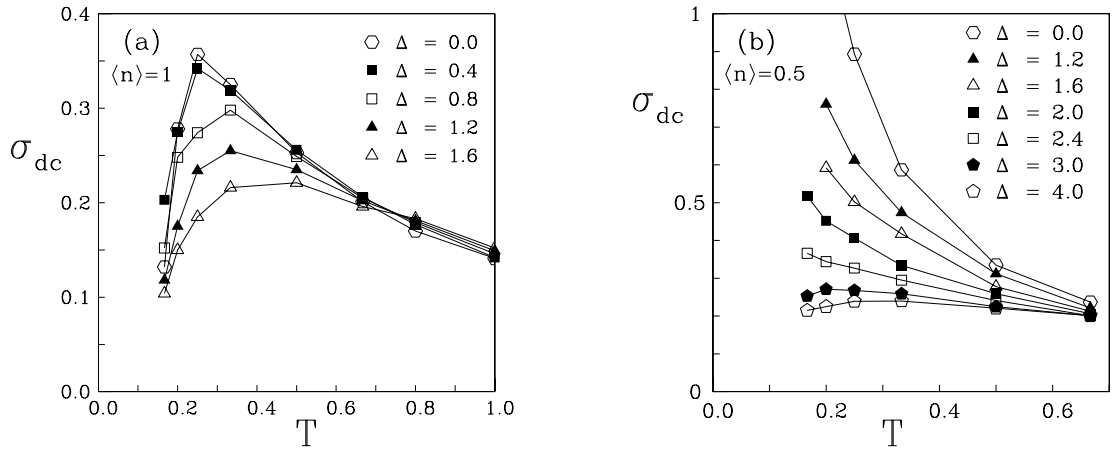

FIG. 20: Conductivity $\sigma_{\rm dc}$ as a function of temperature T for various values of disorder strength Δ at $U = 4$ for (a) half-filling ($\langle n\rangle = 1$) and (b) $\langle n\rangle = 0.5$. Calculations are performed on an 8×8 square lattice; data points are averages over 4 realizations for a given disorder strength.

2. Results/Discussion

As a test for our conductivity formula (Eq. 59) we first present results in Fig. 23(a) for $\sigma_{\rm dc}(T)$ at half-filling for $U = 4$ and various disorder strengths Δ. The behavior of the conductivity shows that as the temperature is lowered below a characteristic gap energy, the high T "metallic" behavior crosses over to the expected low T Mott insulating behavior for all Δ, thereby providing a reassuring check of the formula and of our numerics.

In Fig. 23(b), we show $\sigma_{\rm dc}(T)$ for a range of disorder strengths at density $\langle n\rangle = 0.5$ and $U = 4$. The figure displays a change from metallic behavior at low disorder to insulating behavior above a critical disorder strength, $\Delta_{\rm c} \simeq 2.7$. If this persists to $T = 0$ and in the thermodynamic limit, it would describe a ground state metal–insulator transition driven by disorder.

In order to obtain a more precise understanding of the role of interactions on the conductivity, we compare in Fig. 24 the results of Fig. 23(b) with the disordered *non-interacting* σ_0[72]. The comparison is made at strong enough disorder $\Delta = 2.0$ such that the localization length is less than the lattice size and the non-interacting system is therefore insulating with $d\sigma_0/dT > 0$ at low T. Interactions are found to have a profound effect on the conductivity: in the high-temperature "metallic" region, interactions slightly reduce σ compared to the non-interacting σ_0 behavior. On the other hand in the low-temperature "insulating" region of σ_0 the data shows that upon turning on the Hubbard interaction the behavior is completely changed with $d\sigma/dT < 0$, characteristic of metallic behavior. This is the regime of interest for the MIT.

In order to ascertain that the phase produced by repulsive interactions at low T is not an insulating phase with a localization length larger than the system size but a true metallic phase we have studied the conductivity response for varying lattice sizes. We find a markedly different size dependence for the $U = 0$ insulator and the $U = 4$ metal, resulting in a confirmation of the picture given above. For $U = 0$, the conductivity on a larger (12×12) system is *lower* than that on a smaller (8×8) system (see Fig. 24), consistent with insulating

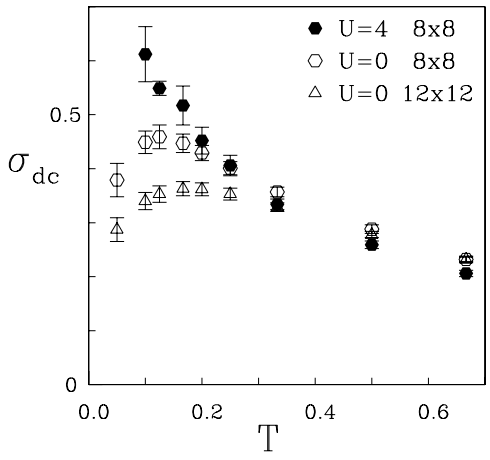

FIG. 21: Conductivity $\sigma_{\rm dc}$ as a function of temperature T comparing $U = 4$ and $U = 0$ at $\langle n \rangle = 0.5$ and disorder strength $\Delta = 2.0$. Data points are averages over many realizations for this disorder strength (see text). Error bars are determined by the disorder averaging and not the Monte Carlo simulation.

behavior in the thermodynamic limit, whereas for $U = 4$ the conductivity on the larger (8×8) system is *higher* than that on the smaller (4×4) system (data not shown), indicative of metallic behavior. Thus the enhancement of the conductivity by repulsive interactions becomes more pronounced with increased lattice size[73].

Concerning finite-size effects for the non-interacting system we note that at lower values of Δ, where the localization length exceeds the lattice size, σ_0 shows "metallic" behavior which is diminished upon turning on the interactions[74]. Based on our analysis above, we would predict that at low enough T and large enough lattice size, the conductivity curves for the non-interacting σ_0 and interacting σ cross with $\sigma > \sigma_0$ at sufficiently low T.

To obtain information on the spin dynamics of the electrons and because it is a quantity often discussed in connection with the localization transition, we also compute the spin susceptibility χ as a function of T (through $\chi(T) = \beta S_0(T)$ where S_0 is the magnetic structure factor at wavevector $\mathbf{q} = 0$). Fig. 25 shows two things: 1) $\chi(T)$ is enhanced by interactions with respect to the non-interacting case (at fixed disorder strength), and 2) starts to diverge when T is lowered, both on the metallic ($\Delta = 2$) and insulating ($\Delta = 4$) sides of the alleged transition. This is in agreement with experimental and theoretical work on phosphorus-doped silicon, where a (3D) MIT is known to occur and the behavior is explained by the existence of local moments[75], and also with diagrammatic work on 2D disordered, interacting systems[14].

To establish definitively the existence of a possible quantum phase transition in the disordered Hubbard model requires: (i) Extending the present data at $T = 0.1 = W/80$, where W is the non-interacting bandwidth, to lower T, which is however difficult because of the sign problem. (ii) A more detailed analysis of the scaling behavior in both linear dimension and some scaled temperature. (iii) A more accurate analytic continuation procedure to extract the conductivity. The condition for the validity of the approximate formula (Eq. XX) for $\sigma_{dc}(T)$, requires that T be less than an appropriate energy scale which is fulfilled within the two phases, but breaks down close to a quantum phase transition where the energy scale

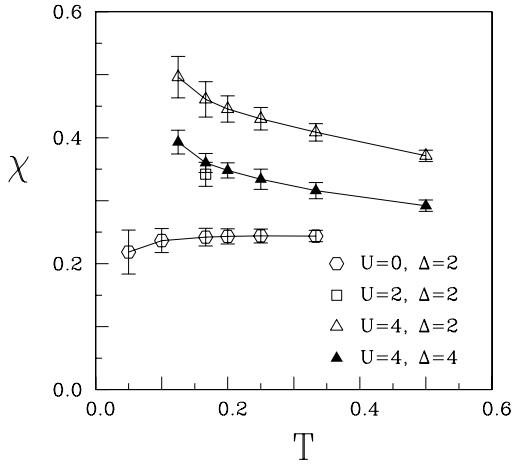

FIG. 22: Spin susceptibility χ as a function of temperature T at $\langle n \rangle = 0.5$ comparing interaction strengths $U = 0, 2, 4$ and disorder strengths $\Delta = 2, 4$. Calculations are performed on 8×8 square lattices; error bars are from disorder averages over up to 8 realizations.

vanishes.

Given the well-known difficulty of DQMC simulations resolving the issue of d-wave superconductivity in the clean Hubbard model because of the sign problem mentioned in (i) above, it is worth discussing briefly why more definitive results are obtainable in this study of the MIT. The most important reason concerns the higher temperature scale of the phenomenon: interactions enhance the conductivity and lead to metallic behavior in a temperature range (about 1/10 of the Fermi energy) here, similar to that of experiments. In the cuprates, although the transition temperatures are very high by the standards of othe superconductors, they are of the order of 1/100 of the Fermi energy, a factor of ten lower. Furthermore, the region of highest transition temperature is, very unfortunately, at a doping $\rho \approx 1 - \frac{1}{8}$ where the sign problem in the simulations is worst.

3. Conclusion/Summary

In summary, we have studied the temperature-dependent conductivity $\sigma(T)$ and spin susceptibility $\chi(T)$ of a model for two-dimensional electrons containing both disorder and interactions. We find that the Hubbard repulsion can enhance the conductivity and lead to a clear change in sign of $d\sigma/dT$. More significantly, from a finite size scaling analysis we demonstrate that repulsive interactions can drive the system from one phase to a different phase. We find that $\sigma(T)$ has the opposite behavior as a function of system size in the two phases indicating that the transition is from a localized insulating to an extended metallic phase. The $\chi(T)$ data further suggests the formation of an unusual metal, a non-Fermi liquid with local moments. While the simplicity of the model we study prevents any quantitative connection to recent experiments on Si-MOSFETs, there is nevertheless an interesting qualitative similarity between Fig. 23(b) and the experiments. Varying the disorder strength Δ at fixed carrier density $\langle n \rangle$, as in our calculations, can be thought of as equivalent to varying carrier density at fixed disorder strength, as in experiments, since in a metal–insulator tran-

sition one expects no qualitative difference between tuning the mobility edge through the Fermi energy (by varying Δ) and *vice-versa* (by varying $\langle n \rangle$). Our work then suggests that electron-electron interaction induced conductivity plays a key role in the 2D metal–insulator transition.

B. Zeeman Field

Journal Reference: "Interacting electrons in a two-dimensional disordered environment: Effect of a Zeeman magnetic field", P.J.H. Denteneer and R.T. Scalettar, Phys. Rev. Lett. **90**, 246401 (2003).

1. Introduction

A hundred years after the Nobel prize was awarded in 1902 for the discovery of the Zeeman effect and the subsequent explanation by Lorentz, applying a magnetic field continues to be a powerful means to elucidate puzzling phenomena in nature. One of the most recent examples is to the topic of these notes: the interplay of interactions and disorder in electronic systems and the pioneering experiments on the metal–insulator transition (MIT) in effectively two–dimensional low-density silicon metal-oxide-semiconductor field-effect transistors (MOSFETs) discussed earlier[16–18].

Contrary to the well-known effect of a magnetic field in weak-localization theory to disturb interference phenomena and hence *undo* localization and insulating behavior, the negative magnetoresistance effect[2], in the Si MOSFETs and similar heterostructures, the magnetic field is found to suppress the metallic behavior and therefore *promote* insulating behavior[20,76,77]. The effect is present for all orientations of the magnetic field relative to the 2D plane of the electrons. In particular, a Zeeman magnetic field, applied parallel to the 2D plane of electrons and therefore coupling only to the spin, and not the orbital motion of the electrons, has been used extensively. This puts into focus the important role played by the spin degree of freedom of the electron, and its polarization[78–81].

In this section, we continue our DQMC study of the Anderson-Hubbard Hamiltonian, but now include the effect of a Zeeman magnetic field, that is, an additional term in H of the form,

$$+B_{\parallel} \sum_{j\sigma} \sigma n_{j\sigma} \tag{51}$$

While the numerical evidence is mixed concerning the occurrence of a MIT due to interactions,[82–85] there is a consensus in favor of a Zeeman magnetic field tuned transition[84–87], as we shall describe in more detail below.

Our main focus continues to be on the conductivity, although now we explore its $B_{\parallel}$–dependence as well as its T–dependence. Another interesting quantity to study in conjunction with the magnetoconductivity is the degree of spin-polarization P of the electronic system:

$$P = \frac{n_{\downarrow} - n_{\uparrow}}{n_{\downarrow} + n_{\uparrow}} \ , \tag{52}$$

where $n_{\downarrow}, n_{\uparrow}$ are the average spin-densities of the corresponding number operators.

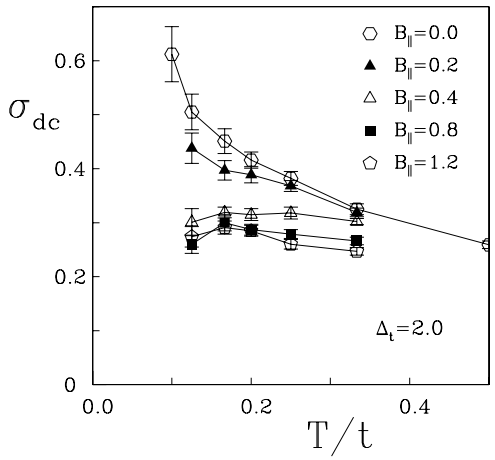

FIG. 23: Conductivity $\sigma_{\rm dc}$ (in units of $e^2/\hbar$) as a function of temperature T for various strengths of Zeeman magnetic field $B_\parallel$. As $B_\parallel$ increases, a transition from metallic to insulating behavior is seen in $\sigma_{\rm dc}$. Calculations are performed on 8×8 lattices for $U/t = 4$ at density $\langle n \rangle = 0.5$ with disorder strength $\Delta_t = 2.0$ (see text); error bars result from averaging over typically 16 quenched disorder realizations. $B_\parallel$ and Δ_t are given in units of t.

2. Results/Discussion

In order to study the effect of the Zeeman magnetic field $B_\parallel$ on the metallic behavior, we start from the case with density $\langle n \rangle = 0.5$ and disorder strength $\Delta_t = 2.0$ for which the model exhibits clear metallic behavior: $\sigma_{\rm dc}$ rising when lowering temperature T[88]. Fig. 26 shows that turning on $B_\parallel$ reduces the conductivity and suppresses the metallic behavior; at field strength $B_\parallel = 0.4$, $\sigma_{\rm dc}$ appears T-independent (within the error bars), and at larger field strengths shows a tendency to decrease upon lowering T. We do not expect $\sigma_{\rm dc}$ to go to zero, as for a real insulator, unless very low T and very large lattices (out of reach of our computational approach) are employed. Nevertheless, Fig. 26 shows the qualitative features of a magnetic-field-driven metal–insulator transition, similar to what is seen in experiment[20,76,77]. Previous numerical approaches using different techniques have also produced this effect[84–86].

Since the effect of $B_\parallel$ is to polarize the electronic system (with our sign choice in Eq. 60), $n_\downarrow$ is promoted at the expense of $n_\uparrow$), a large enough $B_\parallel$ will result in electrons with spin down only and, because of the nature of the Hubbard interaction, in a non-interacting system[89]. Therefore, in the limit of large 2D lattices and low temperature, the hopping disorder will force the conductivity to vanish. Our nonzero value of $\sigma_{\rm dc}$ at very large $B_\parallel$ is then a direct measure of the systematic errors due to finite size and non-zero T. In Fig. 27, we subtract out this value, focus more on fields close to $B_\parallel = 0.4$, and show the resulting $\delta\sigma_{\rm dc}$ vs. $B_\parallel$ for our lowest temperatures. A rather abrupt onset appears of $\delta\sigma_{\rm dc}$ below $B_\parallel \approx 0.5$, which is about the field value where the curves of $\sigma_{\rm dc}$ vs. T change from insulating to metallic (Fig. 1). Our data for a 2D system in Fig. 27 are consistent with a linear vanishing of $\delta\sigma_{\rm dc}$ as the (quantum) critical point is approached. At present, our results, while presenting compelling evidence for the transition itself, are clearly not precise enough to obtain critical exponents. Interestingly, a transition from insulator to metal upon increasing magnetic field, i.e. the known negative magnetoresistance effect, occurs in an amorphous three-dimensional

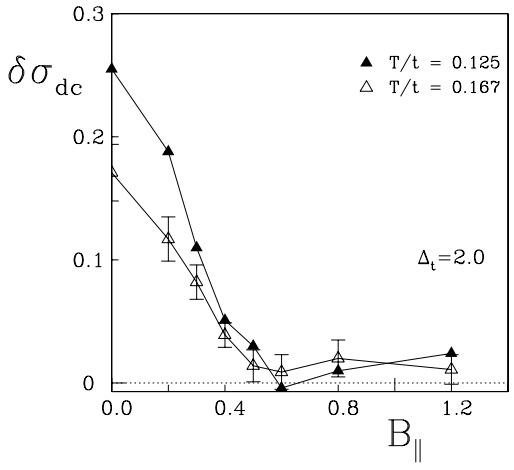

FIG. 24: Conductivity difference $\delta\sigma_{\rm dc} \equiv \sigma_{\rm dc}(B_\parallel, T) - \sigma_{\rm dc}(B_\parallel = 4, T)$, with conductivity at very high B-field subtracted, as a function of $B_\parallel$ for low temperature T. A sharp onset of conductivity is seen at a Zeeman field at which the slope of $\sigma_{\rm dc}(T)$ changes sign in Fig. 1. Computational details and units are as in Fig. 1; for clarity, only error bars on $T = t/6$-data are shown; those on $T = t/8$-data are typically sligthly larger (cf. Fig. 1).

Gd-Si alloy (showing a MIT at zero field), also with a linear vanishing of the conductivity[90]. While it is possible that these observations are unrelated, it is also conceivable that this is an indication of a, yet hidden, connection between the two transitions.

In Fig. 28, we show the *resistivity* ρ ($\equiv 1/\sigma_{\rm dc}$) as a function of $B_\parallel$ for low T. The crossing point (between $B_\parallel = 0.3$ and 0.4) demarks a critical field strength B_c which separates fields for which the resistivity decreases when lowering temperature (low-field metallic behavior) from fields for which ρ increases upon lowering T (high-field insulating behavior). It is especially noteworthy that the critical field strength (which can be roughly estimated to lie between 0.3 and 0.5 from Figs. 27 and 28) is clearly lower than the field for which full spin-polarization sets in. Indeed, in Fig. 29, we show how the spin polarization P, defined in (52), behaves as a function of $B_\parallel$ at the lowest temperature used: there is no reflection of the critical field strength in the behavior of the polarization and full spin-polarization only happens for $B_\parallel > 1.2$. This feature of our data is in excellent agreement with recent experiments performed on 2D electron- and hole-gases in GaAs and AlAs[80,81]. Since complete spin-polarization is equivalent to a non-interacting system, the separation of the two field strengths and the incomplete polarization at the MIT present evidence that the Zeeman field tuned MIT must be seen as a property of a fully interacting many-body system, at least in the 2D disordered Hubbard model.

Another interesting feature of Fig. 28 is what appears to be the saturation of resistivity at a field not much higher than B_c. Experiments also show this behavior, but only for AlAs, where the saturation is shown to coincide with full spin polarization[80]. We argue that the on-site nature of the interactions in the Hubbard model make the saturation happen at much reduced field strength compared to that of complete polarization: at our rather low total density the minority spin species will effectively be decoupled from the majority spin species and both spin species form non-interacting subsystems at a field where the minority spin has not disappeared completely. Increasing magnetic field further at constant total density

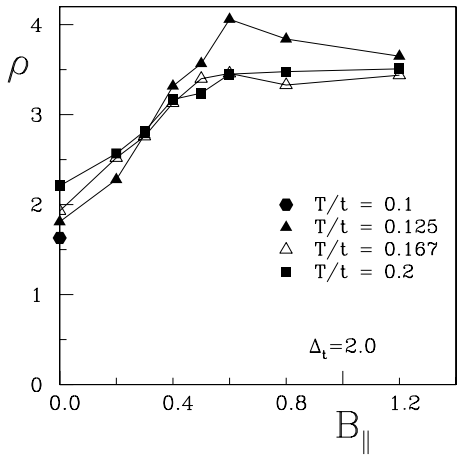

FIG. 25: Resistivity ρ as a function of $B_\parallel$ for various low T. The crossing point provides another estimate for the critical field strength. Computational details and units are as in Figs. 26 and 27; for clarity the error bars have been omitted, but can be estimated from Figs. 26 and 27.

will then not change the conducting properties anymore.

The notion of a predictable and straightforward effect of $B_\parallel$ is also concordant with the phenomenon that $\rho(B_\parallel)$ behaves qualitatively the same in the metallic and insulating phases[3], and therefore the same physical mechanism seems at play in both cases. Our results suggest as a likely candidate for this mechanism: the reduction of the effective interaction by spin polarization.

3. Conclusion/Summary

In summary, applying a Zeeman magnetic field in the 2D disordered Hubbard model reduces the effect of the Hubbard interaction and is able to bring about a transition from a metallic phase to an insulator at a critical field strength. We find this critical field is considerably less than the field required for full spin polarization, emphasizing that, for the disordered Hubbard model, the metal-insulator transition occurs in a region where a considerable degree of electronic correlation remains. This is in good qualitative agreement with experimental observations when a magnetic field is applied parallel to a 2D electron or hole gas in GaAs– and AlAs–based heterostructures[80,81]. For Si MOSFETs, the general phenomenon of suppression of the metallic behavior is in agreement, but the issue of the critical field being smaller than a saturating field is less clear[79]. In earlier work, we studied the T-dependence of $\sigma_{\rm dc}$ for various Δ_t without a B-field and showed that the Hubbard interaction enhances $\sigma_{\rm dc}$ and leads at low T to metallic behavior that can be made insulating by sufficiently strong disorder. Our present results concerning the effect of a magnetic field are consistent with that conclusion and therefore strengthen it: the rather strong interactions that caused the conducting phase at disorder strength $\Delta_t = 2.0$ (below the critical disorder strength of approximately 2.4 above which the system is insulating) without B-field are reduced by a B-field which is able to drive the system back to its insulating phase. The latter is also its natural state in the absence of interactions. We believe that this consistency

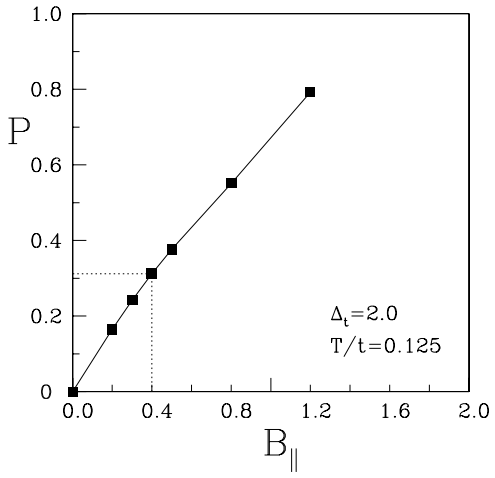

FIG. 26: Degree of spin polarization P (defined in (52) in text) as a function of $B_{\|}$ for fixed low $T = t/8$. The polarization shows little change through the metal-insulator transition and is close to 0.4 only at the critical field strength.

indicates that the disordered Hubbard model provides a coherent, qualitative picture of the phenomena in 2D electronic, disordered systems both in the presence and absence of a Zeeman magnetic field.

C. The Role of Particle-Hole Symmetry

Journal Reference: "Particle–Hole Symmetry and the "Effect of Disorder on the Mott–Hubbard Insulator", P.J.H. Denteneer, R.T. Scalettar, and N. Trivedi, Phys. Rev. Lett. **87**, 146401 (2003).

1. Introduction

In recent years, it has become increasingly clear that for non-interacting electrons the presence or absence of certain symmetries is crucial in determining the effect of disorder on both transport and thermodynamic properties, as well as critical properties of the localization transition.[91] Recent examples where symmetry considerations are important are given in the context of quantum wires[92] and disordered superconductors,[93,94] where chiral, time–reversal, and spin–rotation symmetries play an important role.

In the preceding sections, we studied bond-disordered Hamiltonians which retain the particle-hole symmetry of the clean Hubbard model. In this section, we examine the effect of different types of disorder, including those which break this symmetry, on both the dynamic and equilibrium thermodynamics in the vicinity of half-filling, electron density $\langle n \rangle = 1$. Our results suggest that the presence or absence of *particle–hole symmetry* determines the effect of randomness on the conductivity and the Mott gap.

In order to make the distinction between the different types of disorder clear, we write

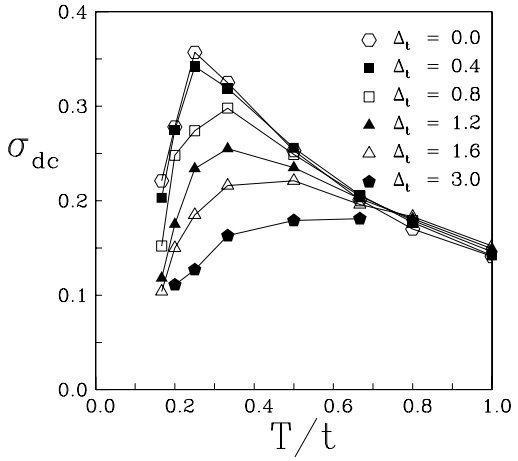

FIG. 27: The effect of particle–hole–symmetry preserving (near-neighbor) bond disorder in the half-filled Hubbard Hamiltonian is to decrease the conductivity $\sigma_{\rm dc}$. Data is for $U = 4t$ on a 8×8 square lattice; Δ_t measures the strength of the bond disorder.

down again the 2d Anderson-Hubbard Hamiltonian we consider,

$$H = -\sum_{\langle \mathbf{ij}\rangle,\sigma} t_{\mathbf{ij}} c^\dagger_{\mathbf{i}\sigma} c_{\mathbf{j}\sigma} - \sum_{\langle\langle \mathbf{ik}\rangle\rangle,\sigma} t'_{\mathbf{ik}} c^\dagger_{\mathbf{i}\sigma} c_{\mathbf{k}\sigma} + U \sum_{\mathbf{j}} (n_{\mathbf{j}\uparrow} - \frac{1}{2})(n_{\mathbf{j}\downarrow} - \frac{1}{2}) - \sum_{\mathbf{j},\sigma} \mu_{\mathbf{j}}\, n_{\mathbf{j}\sigma} \ . \tag{53}$$

Here $t_{\mathbf{ij}}$ is a bond–dependent hopping matrix element on near-neighbor sites $\langle \mathbf{ij}\rangle$, $t'_{\mathbf{ik}}$ is a bond–dependent hopping matrix element on next-near-neighbor sites $\langle\langle \mathbf{ik}\rangle\rangle$, U is an on–site repulsion, and $\mu_{\mathbf{j}}$ is a site-dependent chemical potential. We choose $P(t_{\mathbf{ij}}) = 1/\Delta_t$ for $t_{\mathbf{ij}} \in [t - \Delta_t/2, t + \Delta_t/2]$, and zero otherwise, with $t = 1$ to set our scale of energy. Similarly, $P(t'_{\mathbf{ik}}) = 1/\Delta'_t$ for $t'_{\mathbf{ik}} \in [t' - \Delta'_t/2, t' + \Delta'_t/2]$, and $P(\mu_{\mathbf{j}}) = 1/\Delta_\mu$ for $\mu_{\mathbf{j}} \in [-\Delta_\mu/2, +\Delta_\mu/2]$, so that the various Δ measure the disorder strength. We will focus on half–filling where the effects of interactions are most prominent, as evidenced by the formation of antiferromagnetic correlations and a Mott-Hubbard charge gap at low temperatures.

This Hamiltonian, Eq. 62, is particle–hole (ph) symmetric when $t'_{\mathbf{ik}} = \mu_{\mathbf{j}} = 0$. That is, under the transformation $c^\dagger_{\mathbf{i}\sigma} \rightarrow (-1)^{\mathbf{i}} c_{\mathbf{i}\sigma}$ the Hamiltonian is unchanged, and the system is precisely half–filled for all values of the parameters in H and also for all T. Therefore, while near-neighbor bond and local site disorder both introduce randomness into the system, they differ fundamentally in that site disorder breaks ph–symmetry.

In addition to the conductivity and spin polarization of the preceding sections, we also extract the *temperature-dependent* density of states at the chemical potential $N(\epsilon = 0)$[95] from the one-electron Green function as a function of imaginary time,

$$N(0) \simeq -\beta\, G\,(\mathbf{r} = 0,\, \tau = \beta/2)\,/\pi \ . \tag{54}$$

This quantity allows a more clear characterization of the transport and thermodynamic properties of the system. For $\sigma_{\rm dc}$ and $N(0)$, "Trotter" errors associated with the discretization of imaginary time β are considerably less than the fluctuations associated with monte carlo and disorder averaging.

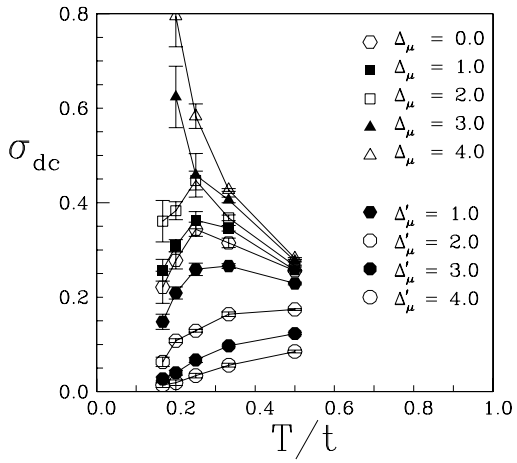

FIG. 28: Canonical site disorder (with strength Δ_μ) enhances the conductivity. Particle–hole symmetric site disorder (with strength Δ'_μ), as with bond disorder (Fig. 1), suppresses the conductivity. Other parameters are as in Fig. 1.

2. Results

First we discuss the transport properties: in Fig. 31, which includes some dtat previously shown in Fig. 24, we exhibit the effect of near-neighbor hopping (bond) disorder on the conductivity. For all disorder strengths Δ_t, at temperatures greater than a characteristic temperature T_* related to the Mott gap, the system shows metallic behavior with $\sigma_{\rm dc}$ increasing upon lowering T. The conductivity turns down sharply as the temperature drops below T_* and the system shows insulating behavior with $\sigma_{\rm dc}$ decreasing upon lowering T. In the case of zero randomness, the perfect nesting of the Fermi surface in 2d leads to antiferromagnetic long range order (AFLRO) in the ground state with an associated spin density wave gap for arbitrarily small U evolving to a Mott gap at larger U. Hopping disorder reduces AFLRO via the formation of singlets on bonds with large hopping $t_{\mathbf{ij}}$ and hence large coupling $J = t_{\mathbf{ij}}^2/U$ and ultimately destroys it beyond $\Delta_t \approx 1.6t$.[96] The fascinating result we have found is that insulating behavior in the conductivity nevertheless persists to much larger Δ_t. Moreover from the shift of the maximum in Fig. 31 we deduce that the mobility gap in fact increases with increasing Δ_t.

The situation is quite different in the case of site disorder, as shown in Fig. 32: at fixed temperature T, as site disorder Δ_μ is turned on, the conductivity increases, i.e. the Mott insulating state is weakened.[97] At weak disorder, the conductivity drops with decreasing T, reflecting again the presence of the Mott insulating phase. As the disorder strength becomes large enough to neglect U, one would expect a similar temperature dependence arising from Anderson insulating behavior. We believe that in all cases the conductivity will ultimately turn over and go to zero at low T, but we are limited in these simulations to temperatures $T > W/48$ because of the fermion sign problem. Nevertheless, the data for site disorder offer a dramatic contrast to that of bond disorder (Fig. 31) where randomness decreases the conductivity.

What is the underlying reason for the different effects of bond and site disorder on the conductivity? There are several obvious differences in the effect of bond and site disorder on local and even longer range spin and charge correlations. Site disorder enhances the

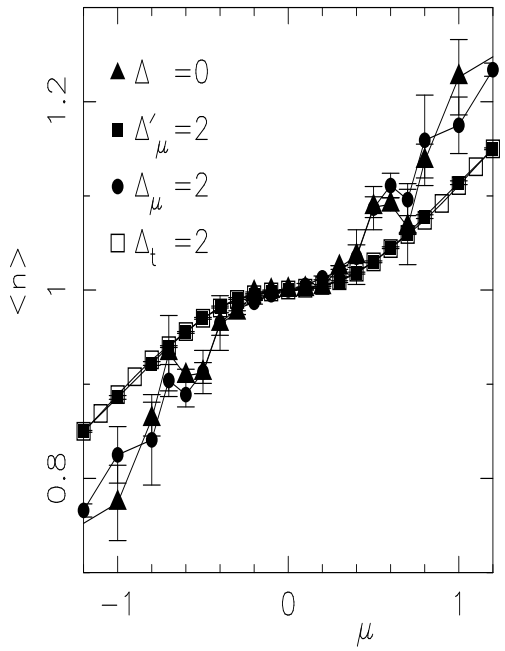

FIG. 29: The Mott gap is made more robust by the addition of bond disorder or particle-hole symmetric site disorder (open and filled squares) of strength $\Delta = 2t = U/2$, as indicated by the response of the density to changes in the chemical potential. For canonical site disorder (filled circle) the Mott gap is practically unaffected by this strength of randomness. [19] Calculations are for $T = t/8 = W/64$ on a 8×8 lattice.

amount of double occupancy on the lattice, since the energy cost U of double occupancy is compensated by differences in site energies. One explanation of why site disorder increases σ_{dc} is that the concomitant increase in empty sites leads to more mobility. This destruction of local moments ultimately also leads to the end of antiferromagnetic order. Surprisingly, we find in our simulations that bond disorder has a similar diminishing effect on local moments, suggesting that the difference in the behavior of the conductivity arises from a different origin.

We argue here that *particle–hole symmetry* is the unifying criterion which underlies and determines the effect of disorder. As emphasized above, site and bond disorder have rather similar effects on the double occupancy. Moreover, the consequences of this effect for $\sigma_{\rm dc}$ are expected to become visible only above a threshold value of disorder strength, whereas we observe effects on $\sigma_{\rm dc}$ already for weak disorder. Instead, the key distinction is in the presence or absence of ph–symmetry. In order to explore this conjecture more fully, we have studied two other types of disorder: site disorder that preserves ph–symmetry and bond disorder that breaks ph–symmetry (by including next-near-neighbor hopping).

Particle–hole symmetric site disorder is introduced by adding random chemical potentials to the Hubbard model which couple with opposite sign to the density of up and down electrons, i.e. choose $\mu_{\mathbf{j}} \equiv \mu_{\mathbf{j}\sigma} = \sigma\mu_{\mathbf{j}}$ in Eq. 62. This type of disorder represents a random (Zeeman) magnetic field. For $U = 0$ ph–symmetric site disorder has precisely the same effect as conventional site disorder, since moving in a given random chemical potential landscape or one obtained by reversing all the site energies is entirely equivalent. However the behavior of the conductivity at finite U is dramatically different. Fig. 32 shows that ph–symmetric site disorder (with strength Δ'_μ) has the *same* effect on $\sigma_{\rm dc}$ as bond disorder, i.e. conductivity decreases with increasing Δ'_μ.

To seek final confirmation of our conjecture, we have also explored the effect of next-near-neighbor (nnn) hopping and randomness therein. Such longer ranging hybridization breaks

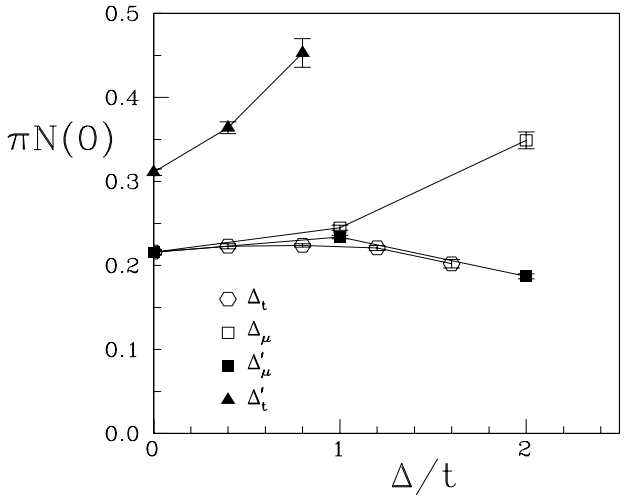

FIG. 30: Behavior of the density of states $\pi N(0)$ at the Fermi level and at fixed low temperature as a function of disorder strength Δ/t for various types of disorder. All data are for $T = t/6$, except data for randomness in next-near-neighbor hopping (disorder strength Δ_t') which are at temperature $T = t/5$ (the value $t' = 0$ is used). [19] Other parameters are as in Figs. 1 and 2.

ph–symmetry on a square lattice, since it connects sites on the same sublattice. We find that such disorder has the *same* effect as conventional site randomness, i.e. increases the conductivity at finite T. Thus in all four types of disorder, the behavior of the conductivity falls into the appropriate class based on the preservation or destruction of ph–symmetry, strengthening the evidence that it is this symmetry which is playing the crucial role in determining the effect of randomness on the transport properties.

We now turn to thermodynamic properties. The most direct measure of the Mott gap is from the compressibility, or from the behavior of density $\langle n \rangle$ as a function of chemical potential μ, as shown in Fig. 33. The range of μ where $\langle n \rangle$ is constant (and the system is incompressible) is a direct measure of the gap in the spectrum. Hopping and ph-symmetric site disorder clearly stabilize the plateau of the density at half–filling. On the other hand, conventional site disorder (with $\Delta_\mu = U/2$) has a compressibility which is indistinguishable (within the computational possibilities) from the clean system.

The density of states (DOS) at the Fermi level $N(0)$ gives valuable information on the effect of disorder on the Mott gap. In the pure system, QMC studies have shown that the DOS exhibits a clear Mott gap with $N(0) \to 0$ as T is lowered to zero. The nonzero values of $N(0)$ we obtain at nonzero T reflect the small residual slopes in the plateaus in the $\langle n \rangle$ vs. μ plot (cf. Fig. 33); at lower T, $N(0)$ approaches zero just as the plateaus become perfectly flat. The behavior of $N(0)$ at a fixed low T as a function of the strength of the various types of disorder is given in Fig. 4. $N(0)$ is rather insensitive to ph–symmetric disorder (Δ_t and Δ_μ') and is even reduced by it: the Mott gap persists. On the other hand, ph–symmetry breaking disorder (Δ_μ and Δ_t') clearly enhances $N(0)$, i.e. fills up the Mott gap.

Our results provide a clear numerical demonstration of the key role of particle–hole symmetry. The effects can also be understood qualitatively as follows: In the clean case, at $\langle n \rangle = 1$ and strong coupling, the DOS consists of an occupied lower Hubbard band (LHB)

and an unoccupied upper Hubbard band (UHB), separated by a charge gap of the order of U. In the case of ph–symmetric disorder, the effect of disorder on LHB and UHB is identical. Therefore the Fermi energy remains in the middle of the gap: this enables the insulating behavior and Mott gap to stay intact. A stabilized charge gap for ph–symmetric *site* disorder is evident since double occupation is strongly suppressed. For nn-hopping disorder a simple argument is less obvious, but the data in Fig. 33 clearly show that these two cases fall into the same class. When ph-symmetry is broken, the LHB and the UHB will be affected differently; different numbers of states will appear at either side of the gap. As a consequence, the Fermi energy ends up in one of the tails of the DOS, resulting in an enhanced $N(0)$ (cf. Fig. 34) and increased conductivity (Fig. 32). The fact that the states introduced by disorder are localized[98] will keep the system in an insulating state (cf. Fig. 32).

3. Conclusions

We have shown that particle–hole (ph) symmetry plays a decisive role in determining the effect of randomness on transport and thermodynamic properties of the half-filled Hubbard model. By exploring four different types of disorder, of which two preserve ph symmetry and two break it, we demonstrate that a classification by this symmetry allows us to understand the effect of disorder on $\sigma_{\rm dc}(T)$, the charge gap and the compressibility. The presence of ph symmetry is found to have a *protective* influence on the charge gap.

A related example where symmetry plays a crucial role in the effects of disorder is the case of localization in the superconducting phase, where the quasiparticles are described by a Bogoliubov–de Gennes Hamiltonian.[94] In this case, one can classify the system according to the presence or absence of time reversal and spin rotation symmetries, and it is found in one dimension that in the absence of spin rotation symmetry, the conductance decays algebraically with system size, while in the symmetric case it decays exponentially. Therefore, in this situation as well, the extra spin rotation symmetry leads to a strengthening of insulating behavior.

The question of the behavior of the half–filled fermion Hubbard model as disorder is added is furthermore reminiscent of similar issues in the ph-symmetric boson Hubbard model.[37] At generic densities, it is believed that a new 'Bose glass' phase arises to intervene in the original ground state phase diagram between superfluid and Mott insulating phases, but the situation at the ph-symmetric tip of the Mott lobe is uniquely different. Our work is a first step in the analysis of the nature of the behavior of the fermionic model.

D. Interaction driven Band Insulator to Metal Transition

Journal Reference: "Quantum Monte Carlo Study of an Interaction-Driven Band Insulator to Metal Transition", N. Paris, K. Bouadim, F. Hebert, G.G. Batrouni, and R.T. Scalettar, cond-mat/0607707.

Introduction

Thus far in these notes we have emphasized the role of interaction effects in disordered, tight-binding models such as the Hubbard Hamiltonian in driving a metallic transitions from an Anderson insulating states originating in the random potential. Actually, a somewhat more simple context in which to study the possibility of interaction driven insulator to metal transitions is to begin with a band insulating state, in which the insulating behavior is caused

by a periodic external potential as opposed to a random one[57–60,65]. Recently, this issue has been addressed within dynamical mean field theory (DMFT) and a number of interesting conclusions emerged[99]. However, because DMFT treats only a single site (retaining, however, all the dynamical fluctuations of the self-energy ignored in conventional, static mean field theory) it is important to undertake complementary work which is able to retain intersite fluctuations.

In this section, we investigate such band insulator-metal transitions with DQMC. The specific Hamiltonian we study is the "ionic Hubbard model":

$$H = -t\sum_{\langle lj\rangle\sigma}(c^\dagger_{j\sigma}c_{l\sigma} + c^\dagger_{l\sigma}c_{j\sigma}) + U\sum_l n_{l\uparrow}n_{l\downarrow} + \sum_l(\Delta(-1)^l - \mu)(n_{l\uparrow} + n_{l\downarrow}) \ . \tag{55}$$

Instead of a random chemical potential, the term $\Delta(-1)^l$ provides a staggered site energy. In the noninteracting limit, $U = 0$, the effect of Δ is to produces a dispersion relation, $E(k) = \pm\sqrt{\epsilon(k)^2 + \Delta^2}$ with $\epsilon(k) = -2t[\cos k_x + \cos k_y]$, which is gapped at half-filling. (See Ex. xx.) A considerable amount is know concerning this model in one dimension[100], but the existence of an interaction driven metallic phase at half-filling is still unresolved even in $d = 1$. Metal-insulator transitions in a related system with *randomly* located site energies with a bimodal distribution have also been studied within DMFT[101,102].

1. *Results*

We begin by showing the temperature dependence of the conductivity $\sigma_{\rm dc}$ for increasing values of the interaction strength for $\Delta = 0.5$. In Fig. 35 we see that the insulating behavior at $U = 0$ signalled by $d\sigma_{\rm dc}/dT > 0$ at low T is changed to metallic $d\sigma_{\rm dc}/dT < 0$ at low T when $U = 1$. A further increase of the correlations to $U = 2$ weakens the metallic behavior, and which is finally destroys completely in a transition to a Mott insulator at $U = 4$. When the band gap is larger ($\Delta = 1$), the screening of the one-body potential is not sufficiently strong for $U = 1$ to cause metallic behavior, as is shown by the corresponding data set in Fig. 1. Here, and throughout this paper unless otherwise mentioned, the lattice size used in the simulations is $N = 6 \times 6$ and the filling is $\rho = 1.0$ (half-filling).

In the single site ($t = 0$) limit, the ionic Hubbard model is a band insulator for $U < 2\Delta$ and a Mott insulator for $U > 2\Delta$. That is, at weak coupling and half-filling, the sites with lower energy $-\Delta$ are doubly occupied and those with higher energy $+\Delta$ are empty, with a gap to further addition of particle set by $2\Delta - U$. At strong coupling, both types of sites are singly occupied, with a gap to further addition of particles set by $U - 2\Delta$. correlations close the band gap At the single special value $U = 2\Delta$ correlations close the band gap[65,99]. Fig. 36, which presents results for $\sigma_{\rm dc}$ for $\Delta = 0.5$, shows that when t is nonzero, this single metallic point is expanded to a finite range of U values. Interestingly, however, the largest conductivity remains at $U = 2\Delta = 1$ as one might expect from the $t = 0$ analysis. The band-insulator to metal transiton occurs at $U_{c1} \approx 0.4t$, where the change in the order of the three curves indicates a transition from $\sigma_{\rm dc}$ decreasing as β increases to $\sigma_{\rm dc}$ increasing as β increases. The metal transiton to Mott insulator transition is at $U_{c2} \approx 2.5t$, where $\sigma_{\rm dc}$ once again decreases as β increases.

The use of DQMC to study the ionic Hubbard model allows us to examine the behavior of intersite correlations, among them the spin-spin correlations and their Fourier tranform $S(k)$. Fig. 37 shows results for the antiferromagnetic structure factor $S(\pi, \pi)$ as a function of U for $\beta = 10, 12, 16$. Comparing with Fig. 36 we see that the band insulating and metallic

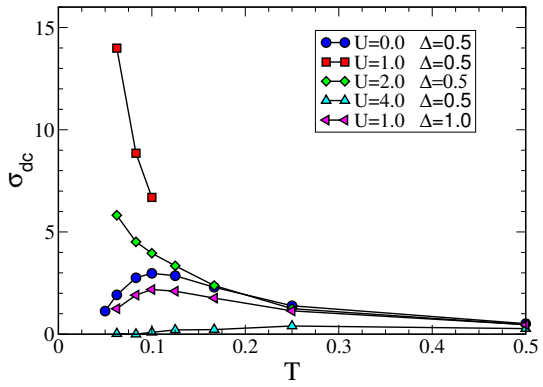

FIG. 31: The transitions, at half-filling, from a band insulator to metal to Mott insulator with increasing U are shown for periodic potential strength $\Delta = 0.5$. At U=0 the conductivity $\sigma_{\rm dc}$ goes to zero as T is lowered. However, for at intermediate $U = 1, 2$ the system is metallic. Mott insulating behavior sets in for $U = 4$. The lattice size is 6×6. When $\Delta = 1.0$, the band gap increases and $U = 1$ is no longer sufficiently large to screen the one body potential and drive the system metallic.

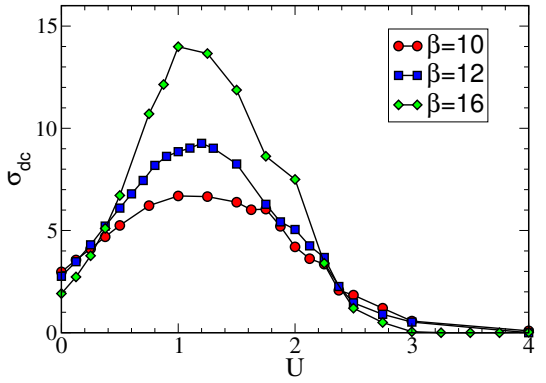

FIG. 32: The conductivity $\sigma_{\rm dc}$ at half-filling for $\Delta = 0.5$ is shown as a function of U for three different low temperatures, $\beta = 10, 12, 16$. The band-insulator to metal transition is signaled by the crossing of the curves at $U_{c1} \approx 0.4t$. At $U_{c2} \approx 2.5t$ the three curves cross again, indicating the Mott insulator transition.

phases are paramagnetic, but that the transition to Mott insulating behavior is accompanied by the onset of antiferromagnetic order.

One way in which the inclusion of such intersite correlations changes the physics in a fundamental way is when the periodic potential is absent, that is, at $\Delta = 0$. In DMFT in the paramagnetic phase, the Hubbard model is a metal at weak coupling[67,103]. However it is known that the $d = 2$ square lattice Hubbard model being studied here is an antiferromagnetic insulator at *all* U, even weak coupling. Fig. 38 presents results for the conductivity which confirms this. At all U values shown, $\sigma_{\rm dc}$ ultimately decreases as T is lowered. Indeed, we have verified that the value of T where $\sigma_{\rm dc}$ has its maximum correlates well with the temperature T_* at which antiferromagnetic correlations begin to rise rapidly. This temperature,

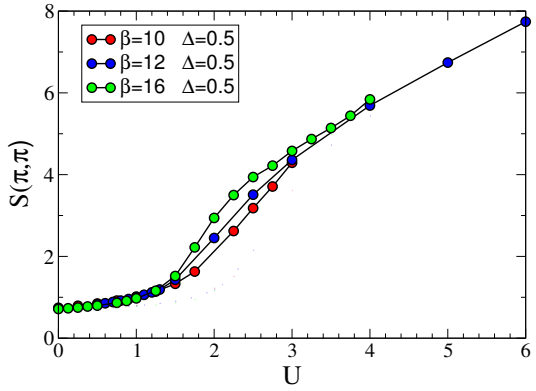

FIG. 33: The antiferromagnetic structure factor is shown at half-filling as a function of U for two different values of the periodic potential $\Delta = 0.5$ and inverse temperature $\beta = 10, 12, 16$.

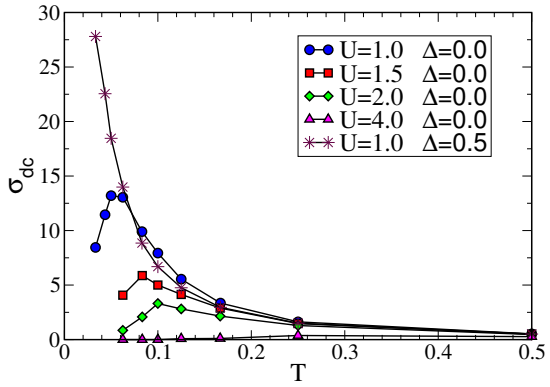

FIG. 34: The conductivity $\sigma_{\rm dc}$ is shown as a function of temperature at half-filling. When the periodic potential, and hence the non-interacting band gap, is absent ($\Delta = 0.0$) the square lattice Hubbard model is insulating for *all* U, due to nesting of the Fermi surface. We re-display data for $\delta = 0.5, U = 1$ from Figure 1 to emphasize the contrast between the metallic behavior there and the insulating behavior for all U when $\Delta = 0$.

like the Neél temperature in the $d = 3$ Hubbard model, is a non-monotonic function of U, falling to small values both at weak ($T_* \propto t \exp(a\sqrt{t/U})$ and at strong ($T_* \propto t^2/U$) coupling. To our knowledge, this is the first time the insulating nature of the square lattice Hubbard model at weak coupling has been shown from Quamtum Monte Carlo studies of $\sigma_{\rm dc}$. It is interesting to note that while all the $\Delta = 0$ curves share a common low temperature slope $d\sigma_{\rm dc}/dT > 0$, a distinction between the antiferromagnetic and Mott origins of insulating behavior is clearly evident. At small U, $\sigma_{\rm dc}$ attains a much larger value before turning over as T is lowered than in the strong coupling Mott regime.

While DQMC allows us to look at intersite correlations and the associated phenomena like antiferromagnetism and insulating behavior deriving therefrom, the method employs lattices of finite size, unlike DMFT which directly probes the thermodynamic limit. Thus, it is important to verify that the metallic phase we observe persists to larger lattices. In Fig. 39 we show results for $\sigma_{\rm dc}$ as a function of temperature in the metallic phase for lattices

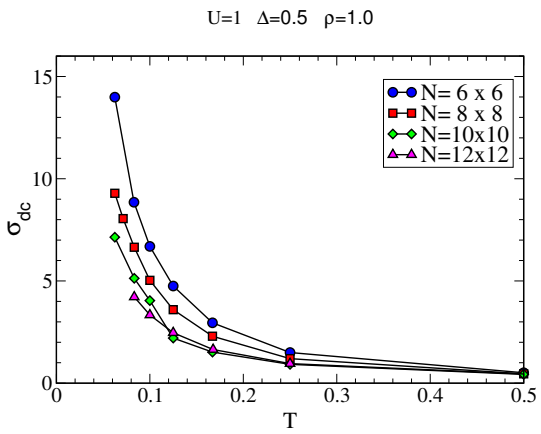

FIG. 35: The conductivity at half-filling is shown for different lattice sizes for $U = 1$, close to the point where the system is most metallic for periodic potential $\Delta = 0.5$. (See. Fig. 2.) Although $\sigma_{\rm dc}$ decreases with increasing lattice sizes, the signature of metallic behavior ($d\sigma_{\rm dc}/dT < 0$) is unchanged.

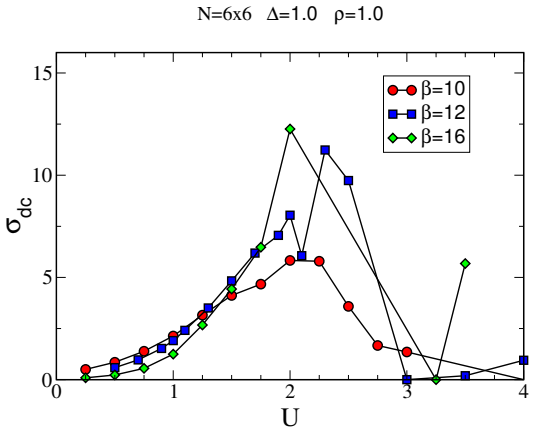

FIG. 36: The conductivity at $\rho = 1.0$ is shown as a function of U for $\Delta = 1.0$ and $\beta = 10, 12, 16$. The system is a band insulator up to $U \approx 1.5$ whereupon metallic behavior onsets.

up to 12×12. The rise in $\sigma_{\rm dc}$ with decreasing T is seen to occur for all the lattices studied. We comment that it is not surprising that we find the lattice size has a rather substantial influence on the conductivity for these parameter, since is known that such finite size effects are larger at weak coupling.

Fig. 40 shows the conductivity as a function of U for three different temperatures at $\Delta = 1.0$. There is now a much larger band-insulating phase at weak coupling, with a critical U for the metallic transition at $U_c \approx 1.5$. It is interesting that the conductivity again appears to peak at the value $U = 2\Delta$ where the $t = 0$ analysis suggests might be most amenable to the formation of a metal. Unfortunately, as U is increased into the metallic phase, the data become extremely noisy. This is a consequence of the sign problem.

Fig. 41 shows the average sign as a function of U for $\Delta = 1$. We see that it is not possible to do DQMC simulations at low T beyond $U = 2$ or so.

The evidence for metallic behavior at $\Delta = 1.0$ in Fig. 40 is a bit lost in the noise. In Fig. 42 we show the conductivity focussing on U values just inside the metallic rgion where the sign

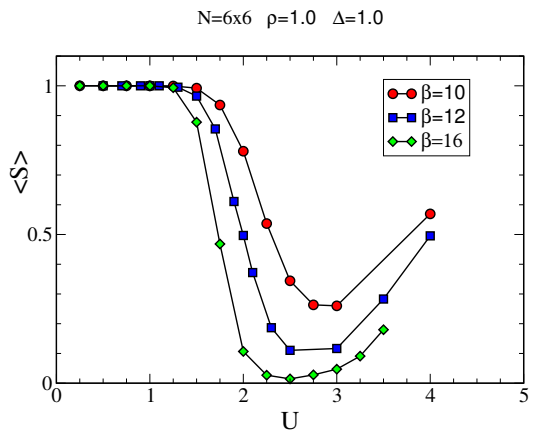

FIG. 37: The average sign in the DQMC simulations as a function of U. $\langle S \rangle$ rapidly becomes small as the metallic region is entered. It rises again in the Mott insulator.

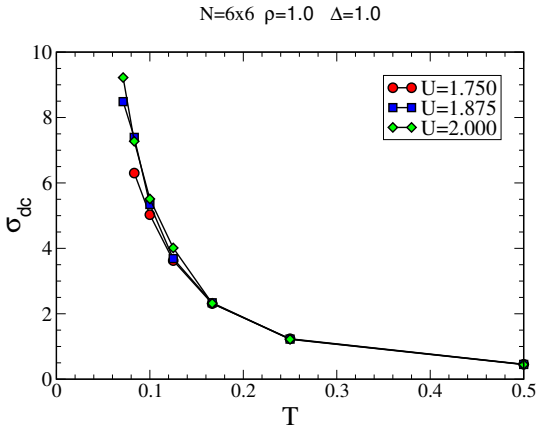

FIG. 38: The conductivity as a function of T for $U = 1.750, 1.875$, and 2.000. The system is clearly metallic.

problem is not yet so bad. The steady increase of $\sigma_{\rm dc}$ as T decreases shows convincingly that the system is a metal at these U values.

Conclusions

In this section, we have presented determinant Quantum Monte Carlo studies of the two-dimensional Hubbard Hamiltonian which demonstrate that interactions can drive a band insulator metallic. This work complements DMFT studies by including intersite antiferromagnetic correlations which qualitatively alter the ground state phase diagram.

We have focused most of our results on $\Delta = 0.5$. It would be interesting to attempt to construct the full phase diagram in the $\Delta/t - U/t$ plane for the $d = 2$ ionic Hubbard model, and compare with that obtained in DMFT[99]. As we have emphasized, the behavior along the $\Delta = 0$ axis is significantly different. At intermediate values of Δ, DMFT indicates the interesting result the metallic phase closes, with a direct band insulator to Mott insulator transition occurring beyond $\Delta/W \approx 1/8$. We would like to study this within DQMC.

Unfortunately, the sign problem, which becomes serious at intermediate $\Delta \approx t$, prevents us from exploring this full phase diagram at present.

However, one limit which we expect will be accessible, that is not have an insurmountable sign problem, is the case of large Δ, where we have very widely separated bands. Related studies of the boson-Hubbard model in a "superlattice" potential, which exhibit a band-insulator to superfluid transition[57–60,65], show the appearance of insulating phases at half-integer fillings. These 'charge-transfer' insulators occur as a result of Mott splitting of the widely separated bands[101]. It would be interesting to explore this possibility in the fermion case.

VI. CONCLUSIONS

In these notes and lectures we have tried to provide an introduction to the Anderson-Hubbard Hamiltonian and some of the physics arising from the combination of interactions and randomness. We have first seen how to understand the behavior of the clean model in the limit of no interactions, no kinetic energy, small clusters, and mean field theory before describing the determinant quantum monte carlo method and the results it gives.

One significant ommission concerning the physics of the Hubbard model is the idea of a 'Kondo resonance'. It turns out that as one progresses from weak to strong coupling, the spectral function of the Hubbard model does not smoothly evolve from a single blob to two upper and lower Hubbard bands. Instead, sometime in the course of changing the interaction strength a three peak structure is in evidence: The beginning of the formation of upper and lower Hubbard bands, but also a sharp peak at the Fermi energy. Actually, it was originally thought that such peaks only arise in variants of the Hubbard model which contain both localized and delocalized electrons. It is only relatively recently, with the introduction of dynamical mean field theory (DMFT), that it was realized this sharp peak occurs in the Hubbard model as well. This very important idea is at the heart of much of the current research into the Hubbard model and its experimental realizations. DMFT is also being applied to the study of the Anderson-Hubbard Hamiltonian and its variants, with fascinating results[104].

VII. APPENDIX 1: CREATION AND DESTRUCTION OPERATORS AND THE HUBBARD HAMILTONIAN

Creation and destruction operators,

$$\hat{a} = \sqrt{\frac{m\omega}{2\hbar}}\hat{x} + i\sqrt{\frac{1}{2m\omega\hbar}}\hat{p}$$
$$\hat{a}^\dagger = \sqrt{\frac{m\omega}{2\hbar}}\hat{x} - i\sqrt{\frac{1}{2m\omega\hbar}}\hat{p} \ , \tag{56}$$

are familiar from the treatment of the harmonic oscillator. They are the language in which tight-binding Hamiltonians like the Hubbard model are written, but differ in several respects. Perhaps most confusing is that the fermion operators in the Hubbard model are not introduced in terms of familiar position and momentum operators as are $\hat{a}, \hat{a}^\dagger$ above. Rather they stand on their own.

Also, instead of just one creation and one destruction operator, in the Hubbard model there is a set of such operators, which are distinguished by attaching indices $\mathbf{j}$ and σ. Thus we write $\hat{c}^\dagger_{\mathbf{j}\,\sigma}$ and $\hat{c}_{\mathbf{j}\,\sigma}$. The index $\mathbf{j}$ labels the spatial lattice site and the index σ labels the electron spin (up or down). As a consequence, the occupation number states are no longer characterized by a single number n, as for a single harmonic oscillator, but instead by a collection of occupation numbers $n_{\mathbf{j}\sigma}$. One writes such states as $|\, n_{\mathbf{1}\uparrow}\, n_{\mathbf{2}\uparrow}\, n_{\mathbf{3}\uparrow}\, \ldots\, n_{\mathbf{1}\downarrow}\, n_{\mathbf{2}\downarrow}\, n_{\mathbf{3}\downarrow}\, \ldots \,\rangle$

Finally, because these operators are meant to describe fermions, they obey *anticommutation* relations. (The anticommutator of two operators $\{\hat{A}, \hat{B}\}$ is defined to be $\hat{A}\hat{B} + \hat{B}\hat{A}$.)

$$\begin{aligned} \{\hat{c}_{\mathbf{j}\sigma}, \hat{c}^\dagger_{\mathbf{l}\sigma'}\} &= \delta_{\mathbf{j},\mathbf{l}}\delta_{\sigma,\sigma'} \\ \{\hat{c}^\dagger_{\mathbf{j}\sigma}, \hat{c}^\dagger_{\mathbf{l}\sigma'}\} &= 0 \\ \{\hat{c}_{\mathbf{j}\sigma}, \hat{c}_{\mathbf{l}\sigma'}\} &= 0. \end{aligned} \tag{57}$$

An immediate consequence of these anticommutation relations is the Pauli principle: the maximum occupation of a particular site with a given spin is 1.

Exercise A1: Show that the Pauli exclusion principle is a consequence of the anticommutation relation amongst the fermion creation operators by considering $\mathbf{j} = \mathbf{i}$ and showing that $\hat{c}^\dagger_{\mathbf{j}\sigma}|1\rangle = 0$. Here $|1\rangle$ is the state with one electron on site $\mathbf{j}$ and with spin σ.

Note that while a fermion creation operator annihilates a state which already has a fermion in it, its action on the empty state is $\hat{c}^\dagger|0\rangle = |1\rangle$, which looks just like the bosonic operator $\hat{a}^\dagger$. Besides the Pauli principle, the anticommutation relations also ensure that the particles are fermions, that is, their wave function changes sign when two electrons with different labels $\mathbf{j}$ are exchanged. To keep track of these signs, one needs to specify a convention for the relation between a state like $|\,1\,0\,1\,0\,0\,\ldots\rangle$ and the vacuum state $|\mathrm{vac}\rangle = |\,0\,0\,0\,0\,0\,\ldots\rangle$. The two possibilities, $|\,1\,0\,1\,0\,0\,\ldots\rangle = c^\dagger_{\mathbf{1}}c^\dagger_{\mathbf{3}}|\mathrm{vac}\rangle$ and $|\,1\,0\,1\,0\,0\,\ldots\rangle = c^\dagger_{\mathbf{3}}c^\dagger_{\mathbf{1}}|\mathrm{vac}\rangle$ differ by a sign. Either definition is fine, but in all subsequent manipulations whatever convention was chosen must be followed consistently.

Exercise A2: Suppose the indices labeling the fermion operators runs over eight possible values. Figure out the occupation number state which results from the following applications of the indicated creation and destruction operators. Choose as your convention that a given

occupation number state is formed by acting on the vacuum state with the lowest indices at the right of the string of creation operators. (This corresponds to the second of the two choices discussed above.)

$$\begin{aligned}
\hat{c}_5^\dagger\,\hat{c}_4^\dagger\,\hat{c}_2^\dagger\,|\mathrm{vac}\rangle &= ?\\
\hat{c}_2^\dagger\,\hat{c}_4^\dagger\,\hat{c}_5^\dagger\,|\mathrm{vac}\rangle &= ?\\
\hat{c}_4^\dagger\,\hat{c}_5^\dagger\,|\,1\,1\,0\,0\,0\,0\,0\,1\,\rangle &= ?\\
\hat{c}_4^\dagger\,\hat{c}_5^\dagger\,|\,1\,1\,0\,0\,1\,0\,0\,1\,\rangle &= ?\\
\hat{c}_1^\dagger\,\hat{c}_2\,|\,0\,1\,0\,0\,1\,0\,0\,1\,\rangle &= ?\\
\hat{c}_1^\dagger\,\hat{c}_4\,|\,0\,1\,0\,0\,1\,0\,0\,1\,\rangle &= ?\\
\hat{c}_1^\dagger\,\hat{c}_5\,|\,0\,1\,0\,0\,1\,0\,0\,1\,\rangle &= ?
\end{aligned} \tag{58}$$

Having introduced creation and annihilation operators, we can now write down the Hubbard Hamiltonian. Before doing so, let's think about how we might simply describe the motion and interactions of electrons in a solid.

First, we need to account for the fact that there is a regular array of nuclear positions in a solid, which for simplicity we consider to be fixed. (In other words, we will not worry about lattice vibrations.) This suggests that we begin with a lattice of atoms (sites) on which the electrons move. A single atom is already a very complex structure, with many different energy levels. The most simple 'atom' we can imagine would have a single energy level. Then, the Pauli principle would tell us that at most two electrons (one with spin up and one with spin down) can sit on this 'atom'.

In a solid where electrons can move around, the electrons interact via a screened Coulomb interaction. The biggest interaction will be for two electrons on the same atom. For simplicity, Hubbard stops just there, so that interactions are modeled by a term which is zero if the atom is empty of electrons or has only a single electron on it, but has the value U if the atom has two electrons. There is no interaction between electrons on different sites.

Our kinetic energy will consist of an expression which allows electrons to move from one site to its neighbors. The energy scale t which governs this 'hopping' will be determined by the overlap of two wavefunctions on the pair of atoms. Since wavefunctions die off exponentially, we can begin by allowing hopping only between the closest atoms in our lattice.

Now let's formalize this construction. We define $c_{\mathbf{j}\sigma}^\dagger$ to be the operator which creates an electron of spin σ on lattice site $\mathbf{j}$. (We will now drop all the 'hats' which I had been using to emphasize things were operators.) Similarly, $c_{\mathbf{j}\sigma}$ is the destruction operator, and $n_{\mathbf{j}\sigma} = c_{\mathbf{j}\sigma}^\dagger c_{\mathbf{j}\sigma}$ is the number operator.

The Hubbard Hamiltonian is then,

$$H = -t\sum_{\langle \mathbf{j},\mathbf{l}\rangle\sigma} c_{\mathbf{j}\sigma}^\dagger c_{\mathbf{l}\sigma} + U\sum_{\mathbf{j}} n_{\mathbf{j}\uparrow}n_{\mathbf{j}\downarrow} - \mu\sum_{\mathbf{j}}(n_{\mathbf{j}\uparrow}+n_{\mathbf{j}\downarrow}). \tag{59}$$

The first term is the kinetic energy: It describes the destruction of an electron of spin σ on site $\mathbf{l}$ and its creation on site $\mathbf{j}$ (or *vice-versa*). The symbol $\langle \mathbf{j},\mathbf{l}\rangle$ emphasizes that hopping is allowed only between two sites which are adjacent. The second term is the interaction energy. It goes through all the sites and adds an energy U if it finds that the site is doubly occupied. The final term is a chemical potential which controls the filling. (See Exercise x.) We refer to the situation where the filling is one electron per site as 'half-filling' since the

lattice contains half as many electrons as the maximum number (two per site). Studies of the Hubbard model often focus on the half-filled case because it exhibits a lot of interesting phenomena (Mott insulating behavior, anti-ferromagnetic order, etc.)

Exercise A3: Show that the Hubbard Hamiltonian commutes with the operators $N_\uparrow = \sum_{\mathbf{j}} n_{\mathbf{j}\uparrow}$ and $N_\downarrow = \sum_{\mathbf{j}} n_{\mathbf{j}\downarrow}$. It is useful to begin by considering the commutator of the kinetic energy on a single 'link' of the lattice connecting sites $\mathbf{i}$ and $\mathbf{j}$ with the total number of electrons on those two sites. That is, begin by computing,

$$[c^\dagger_{\mathbf{i}\sigma} c_{\mathbf{j}\sigma} + c^\dagger_{\mathbf{j}\sigma} c_{\mathbf{i}\sigma}, n_{\mathbf{i}\sigma} + n_{\mathbf{j}\sigma}] \tag{60}$$

After working through the algebra, can you think of an argument that this should be the case based on the structure of H, that is, based on how the creation and destruction operators appear together?

As discussed in Appendix 1, the Hubbard Hamiltonian commutes with the total spin up and spin down number operators, $N_\uparrow = \sum_{\mathbf{j}} n_{\mathbf{j}\uparrow}$ and $N_\downarrow = \sum_{\mathbf{j}} n_{\mathbf{j}\downarrow}$. Thus in finding the eigenstates, we can consider different sectors of $N_\uparrow$ and $N_\downarrow$ separately. As might be expected, in the non-interacting limit, from a solution in the single particle sector, $N_\uparrow = 1$ and $N_\downarrow = 0$ a solution of the many electron problem can be built.

Exercise A4: Suppose you have a one dimensional lattice of eight sites. Write down all the occupation number states in the sector $N_\uparrow = 1, N_\downarrow = 0$, Figure out what H does to each state. Use 'periodic boundary conditions' so that site eight is considered a neighbor of site one. Write down the matrix for H using this basis.

In Exercise 41, we encounter an NxN tridiagonal matrix with "a" along the diagonal and "b" above and below the diagonal, with periodic boundary conditions. The eigenvalues of such a matrix are $\lambda_k = a + 2b\cos k$ where k takes on the discrete values $k_n = 2\pi n/N$ and $n = 1, 2, 3, \ldots N$.

Exercise 42: For general N, what is the eigenvector corresponding to $n = N$ so that the momentum $k = 2\pi = 0$? What is the eigenvector corresponding to $n = N/2$ which has momentum $k = 2\pi$?

Using this result for the eigenvalues of a tridiagonal matrix, we see that the single particle, one-dimensional Hubbard Hamiltonian has energy levels $\epsilon_k = -2t\cos k$. One can view this as a simple 'energy band' of bandwidth $W = 4t$. This establishes a rough connection between the hopping parameter t in the Hubbard Hamiltonian and physical energy scales like the bandwidth W of a real material.

The eigenvalues of the Hubbard Hamiltonian at $U = 0$ in higher particle sectors are obtained by occupying these single particle levels according to the restrictions of the Pauli principle. It is amusing explicitly to re-do Exercise 2 in the $N_\uparrow = 2, N_\downarrow = 0$, computing the eigenvalues (perhaps numerically with a LAPACK routine- there are 28 states!), and verifying that they are indeed Pauli-restricted combinations of the eigenvalues obtained in the single particle case.

Let us now look at the non-interacting limit in a more formal way by transforming to momentum creation and destruction operators.

$$c^\dagger_{\mathbf{k}\sigma} = \frac{1}{\sqrt{N}} \sum_{\mathbf{l}} e^{i\mathbf{k}\cdot\mathbf{l}} c^\dagger_{\mathbf{l}\sigma}. \tag{61}$$

We can think about this process in analogy with the classical normal mode problem: We are defining new (momentum) creation operators as a linear combination of the old (position) ones. As we shall see in Exercises xx and xx, in the Hubbard model at $U = 0$ the different momentum modes decouple from each other and behave independently, just as for classical normal modes.

Notice that on a finite lattice the momentum $\mathbf{k}$ cannot be any real number but has discretized values. For a one-dimensional lattice of N sites, the periodic boundary condition $c^\dagger_{N+1} = c^\dagger_1$ yields $k_n = 2\pi n/N$. This is of course the same condition as when we considered the eigenvalues of the tri-diagonal matrix above. For a two-dimensional square or three dimensional cubic lattice, each component separately has such a discretization.

We know that the different Fourier functions are orthogonal. The analog for these discrete site and momentum variables is given in the following Exercise:

Exercise 43: Prove the following two 'orthogonality' relations:

$$\frac{1}{N}\sum_l e^{i(k_n-k_m)l} = \delta_{n,m} \tag{62}$$

$$\frac{1}{N}\sum_{k_n} e^{ik_n(l-j)} = \delta_{l,j} \tag{63}$$

Exercise 4: Use the orthogonality relations invert Eq. 2, that is, to prove,

$$c^\dagger_{\mathbf{l}\sigma} = \frac{1}{\sqrt{N}}\sum_{\mathbf{k}} e^{-i\mathbf{k}\cdot\mathbf{l}} c^\dagger_{\mathbf{k}\sigma}. \tag{64}$$

Here, of course, the sum over $\mathbf{k}$ means you sum over the discrete allowed momenta $\mathbf{k}_n$. With these relations in hand, we can show a lot of interesting things about the momentum space operators.

Exercise 5: Verify the anticommutation relations

$$\begin{aligned} \{c_{\mathbf{k}\sigma}, c^\dagger_{\mathbf{p}\sigma'}\} &= \delta_{\mathbf{k},\mathbf{p}}\delta_{\sigma,\sigma'} \\ \{c^\dagger_{\mathbf{k}\sigma}, c^\dagger_{\mathbf{p}\sigma'}\} &= 0 \\ \{c_{\mathbf{k}\sigma}, c_{\mathbf{p}\sigma'}\} &= 0. \end{aligned} \tag{65}$$

In other words, the anticommutation relations are "preserved" by this change in "basis" from site indices to momentum indices.

We can now write down the $U = 0$ Hubbard model in terms of these momentum space operators, and obtain more elegantly the same dispersion relation (energy band) as we obtained by considering the matrix of H in the one particle sector.

Exercise 6: Show that for $U = 0$ the one dimensional Hubbard model is,

$$H = \sum_{k\sigma} (\epsilon_k - \mu) c^\dagger_{k\sigma} c_{k\sigma} \tag{66}$$

where $\epsilon_k = -2t\cos k$. As part of this Exercise, you will show that the sum of all the number operators over different spatial sites and spin equals the sum of all the number operators over different momenta and spin.

It is important to realize that the result that an analysis of the one-particle sector gives us full information about the model for any particle number rests only on the fact that the interactions are turned off. It is not necessary that the hopping t between different sites be the same for all pairs of sites, or that it be limited to near neighbors, or that the chemical potential be the same on all sites. All that matters is that H be a quadratic form in the fermion creation and destruction operators. To emphasize: To solve any Hamiltonian H which takes the form $H = \sum_{\mathbf{i},\mathbf{j}} c^\dagger_{\mathbf{i}} \, h_{\mathbf{ij}} \, c_{\mathbf{j}}$ with h a (symmetric) matrix of real numbers, simply diagonalize h and allow the resulting energy levels to be filled in a way which satisfies the exclusion principle. We will see an important application of this theorem when we do mean field theory.

Exercise 7: Show that for $U = 0$ the two dimensional Hubbard model on a square lattice is

$$H = \sum_{\mathbf{k}\sigma} (\epsilon_{\mathbf{k}} - \mu) c^\dagger_{\mathbf{k}\sigma} c_{\mathbf{k}\sigma} \tag{67}$$

where $\epsilon_{\mathbf{k}} = -2t \, (\cos k_x + \cos k_y)$.

In real space, all the different (site occupation) states in the $U = 0$ model are mixed with each other. In momentum space the different states are decoupled: A fermion operator of a give $\mathbf{k}$ appears only together with operators of the same $\mathbf{k}$. This means that the different momentum modes can be treated independently, leading to the following result.

Exercise 8: Show that the partition function of the $U = 0$ Hubbard model is given by

$$Z = \prod_{\mathbf{k}} (1 + e^{-\beta(\epsilon_{\mathbf{k}} - \mu)}). \tag{68}$$

It is useful to remember that if a Hamiltonian is comprised of the sum of independent pieces then the partition function is the product of the associated partition functions. Can you prove this? The result is also true for classical systems.

Exercise 9: Compute the per site average occupation of the $U = 0$ Hubbard model and show it is given by,

$$\rho = \sum_{\mathbf{k}} (1 + e^{+\beta(\epsilon_{\mathbf{k}} - \mu)})^{-1}. \tag{69}$$

Note this takes the form of the sum of the occupations of different pieces, and that the Fermi function, $f_{\mathbf{k}} = 1/[1 + e^{\beta(\epsilon(k) - \mu)}]$, naturally arises. Show that when $\mu = 0$ the density $\rho = 1$ for any β if $\epsilon_{\mathbf{k}}$ is of the form derived for the $d = 1$ or $d = 2$ square lattice Hubbard model.

The allowed k values together with the dispersion relation determine the density of states $N(E)$ which counts the number of ways in which the system can have a given energy E. Formally, $N(E)$ is defined by

$$N(E) = \frac{1}{N} \sum_{\mathbf{k}} \delta(E - \epsilon_{\mathbf{k}}). \tag{70}$$

In the continuum limit (large number of sites) the sum over discrete momenta values is replaced by an integral according to the rule $\frac{1}{N} \sum_{\mathbf{k}} \rightarrow (2\pi)^{-d} \int d\mathbf{k}$, where d is the spatial dimension. As a simple example, suppose we are in one dimension with a relativistic

dispersion relation $\epsilon_k = ck$ for $k > 0$. We can get the density of states as follows:

$$N(E) = (2\pi)^{-1} \int dk \delta(E - ck) = (2\pi)^{-1} \int dk \frac{1}{c} \delta(E/c - k) = (2c\pi)^{-1}(1 - \theta(k)). \quad (71)$$

Here the function $1 - \theta(k)$ emphasizes that $k > 0$ is required. Likewise, for a quadratic dispersion relation $\epsilon_k = ak^2$

$$N(E) = (2\pi)^{-1} \int dk \delta(E - ak^2) = (2\pi)^{-1} \int dk \frac{1}{2ak} \delta(\sqrt{E/a} - k) = (4a\pi)^{-1} \sqrt{a/E}. \quad (72)$$

Exercise 13: Compute (analytically) the density of states $N(E)$ of one dimensional Hubbard model. Explain why $N(E)$ diverges at $E = \pm 2t$ in terms of a picture of the dispersion relation $E(k) = -2t \cos k$. Compute $N(E)$ numerically and compare to your analytic calculation.

VIII. APPENDIX 2: FORMAL FOUNDATION OF CLASSICAL MONTE CARLO

A. Introduction

The Monte Carlo method is often referred to as a 'computer experiment'. One might think of this as a way of conveying the fact that the output of simulations is not an equation, as in conventional theory. Instead, numbers appear on the computer screen in somewhat the same way that numbers appear on a measuring device in the laboratory. Thus there is the implication that somehow simulations are a bit of a 'black box' and that the use of the computer is hiding the underlying physics. The purpose of this note is partly to emphasize some of the mathematical rigor behind Monte Carlo: It is not a happy accident that the computer is generating configurations with the desired probability distribution! Indeed, the fundamental equations underlying simulations are the same as analytic theories, and one can view simulations as a way of solving the mathematics (differential equations) when it becomes too complicated for analytic techniques.

With all that said, it is still useful to pursue the 'Monte Carlo as experiment' point of view. Consider the process of making a measurement in the laboratory. Nature prepares a 'configuration' i of the system, and the experimentalist takes that configuration and records a value for some quantity of interest. To get better statistics (or perhaps inevitably because of finite measuring time) nature actually produces many configurations, and the experimentalist averages over the values obtained. It is useful to emphasize that no matter how long the experimentalist measures, the configurations she sees are an *incredibly* small subset of those that the system is capable of exploring.

Nature uses some very complex rules for time evolving the system from configuration to configuration, for example the many particle Newton or Schroedinger equations. These rules govern the states that the experimentalist sees, and hence the data she takes.

Here's one useful way to think about computer simulations: The goal of a computer simulation is to devise a method where the *computer* plays a similar role to that of *nature* for the experimentalist. That is, the computer generates configurations upon which we make measurements. This leaves us with the problem of devising instructions for the computer that replicate nature's way of generating configurations.

One approach to constructing a simulation would be actually coding up the microscopic equations governing the system's time evolution. Simulations of classical systems going under the name 'molecular dynamics' are actually done precisely this way. One computes the force F_n on each particle n, uses the force to compute the acceleration $a_n = F_n/m$, and then moves the velocity and position forward a small time interval dt with, $v_n \to v_n + a_n\,dt$; $x_n \to x_n + v_n\,dt$.

But in the spirit of statistical mechanics, we really don't care about the microscopic time evolution and the paths $x_n(t)$ and $v_n(t)$ the particles take in phase space. All we really need is to replicate the *probability* $P(\{x_n, v_n\})$ that nature uses to generate her configurations. If we can do that, we'll get the same answers as the experimentalist!

If we were doing classical statistical mechanics, the probability distribution that we would be attempting to emulate would be the Boltzmann distribution $P(\{x_n, v_n\}) = Z^{-1}e^{-\beta E(\{x_n,v_n\})}$. However, let's discuss Monte Carlo within the context of a general probability distribution. This will emphasize that Monte Carlo is by no means limited to Boltzmann statistics. To make the notation less unwieldy, we will also label our probabilities by a single index i which will be understood to represent particular values of all the degrees of freedom of the system we are studying (for example i could mean a collection of positions and velocities $\{x_n, v_n\}$). In the remainder of this note I will denote the inverse temperature by $\beta = 1/T$, and set Boltzmann's constant to unity.

As we shall see, to do Monte Carlo, we actually don't need to know p_i, but only ratios of p_j/p_i for two configurations. This is certainly an important point for statistical mechanics since $p_j/p_i = e^{-\beta(E_j - E_i)}$ is known, but the individual p_i involve the unknown partition function Z.

B. Transition Probabilities and Detailed Balance

Our goal is to figure out a rule T_{ji} to evolve the configuration i into the configuration j which will generate configurations with a desired probability. More precisely, our process will not be deterministic, but will involve random changes, so T_{ji} will be the probability to generate j from i.

Because probabilities are non-negative, and sum up to unity, the rule T_{ji} satisfies,

$$\begin{aligned} T_{ji} &\geq 0 \\ \sum_j T_{ji} &= 1. \end{aligned} \tag{73}$$

A matrix obeying these two restrictions is called a 'stochastic matrix'. Its eigenvalues obey $|\lambda| \leq 1$. Also, there is an eigenvector with eigenvalue $\lambda = 1$. These facts are simple to prove.

Consider the eigenvector equation,

$$\sum_i T_{ji} v_i = \lambda v_j. \tag{74}$$

Take absolute values of both sides of the equation and use the fact that $T_{ji} \geq 0$ and the triangle inequality.

$$\sum_i T_{ji} \, |v_i| \geq |\lambda| \, |v_j|. \tag{75}$$

Now sum both sides of the equation over j and use the fact that $\sum_j T_{ji} = 1$,

$$\sum_i |v_i| \geq |\lambda| \sum_j |v_j|. \tag{76}$$

We now see that $|\lambda| \leq 1$.

To show that a stochastic matrix has an eigenvalue of unity, consider the vector with all components the same, $v_j = 1$. Then, from the second line of Eq. 1,

$$\sum_j v_j T_{ji} = v_i. \tag{77}$$

So the constant vector is a left eigenvector of T of eigenvalue 1. Remember that the eigenvalues of a matrix are the same whether one considers left or right eigenvectors, but the eigenvectors themselves can be quite different unless the matrix is symmetric. This is important to keep in mind, because we will be showing that the right eigenvector of T is not the trivial constant vector. In fact, the right eigenvector of T is p_j.

That the eigenvalue $\lambda = 1$ is non-degenerate is a consequence of the Perron-Frobenius theorem.

Because T is our rule for generating one configuration from the next, we can view the generation of a long sequence of configurations in the Monte Carlo process[105] as the repeated application of the matrix T. We know that when we repeatedly apply a matrix to a vector, we project out the eigenvector of largest eigenvalue. As we have seen above, because T is stochastic, we will generate the eignevector of eigenvalue 1.

So we can now make our goal a little bit more precise: We want to figure out T obeying Eq. 1 whose eigenvector of eigenvalue one is the vector of desired probabilities p_i. Then, repeatedly applying T will give us p and we're done.

It is easy to show that if we construct T to obey 'detailed balance',

$$T_{ji}\, p_i = T_{ij}\, p_j \tag{78}$$

then p_i is an eigenvector of T of eigenvalue 1:

$$\sum_i T_{ji}\, p_i = \sum_i T_{ij}\, p_j = p_j \sum_i T_{ij} = p_j. \tag{79}$$

It is also easy to formulate T to obey detailed balance. The most famous prescription is due to Metropolis. The Metropolis algorithm says that one suggests a move from i to j and then accepts the move with probability one if j is more likely than i, that is, if $p_j/p_i > 1$. If j is less likely than i, accept j with probability p_j/p_i.

Exercise 1: Show that if you generate a random number r uniformly on $[0, 1]$ and accept the move when $r < p_j/p_i$, then the Metropolis algorithm is correctly implemented.

C. Summary of Why Monte Carlo Works

The argument presented above can be summarized as follows:

```
[a] Metropolis  ---> Detailed Balance ---> p is eigenvector of T of eigenvalue 1

[b] T is stochastic ---> max eigenvalue of T is 1

[a+b]  p is eigenvector of T of largest eigenvalue

[c]  repeated application of matrix results in eigenvector of largest eigenvalue

[a+b+c]  repeated application of T gives p, as desired.
```

D. Summary of Monte Carlo Procedure

(i.) Take an initial configuration i and propose a change to a new configuration j.
(ii) Accept the new configuration with probability $\min(1, p_j/p_i)$.
(iii) Measure quantities of interest.
(iv) Repeat the process many times.

There are of course many subtleties: What sort of procedure is followed to "suggest changes"? How many configurations do you need to generate and do you, as in some experiments, need to allow the system time to equilibrate? We will address some of these issues below.

E. Analogies Between Monte Carlo and Experiments

There are a number of useful analogies between Monte Carlo and experiment. Perhaps most importantly, when first encountering Monte Carlo it is natural to wonder how the relatively small sample of configurations that a computer generates could possibly replicate the behavior of physical systems which have incredibly huge numbers of states. A partial answer is provided by noting that the exact same question could be posed to any experimentalist, where, similarly, measurements are based on a very small subset of states which are generated by the time evolution during the course of the experiment.

Second, when one collects data in a Monte Carlo, one measures observables for each configuration generated and then does a simple average over all the configurations. There are no probabilities p_i put in the averaging. The reason, of course, is that the computer is putting the p_i in for you, by generating the configurations with their correct p_i. This is just as in an experiment. No experimentalist weights her measurements with the Boltzmann factor!

In addition to averages, error bars are generated in Monte Carlo just as in experiments. (See Sec. XI.)

One often has to wait a little while after starting a simulation to allow the system to equilibrate, much as the experimentalist will not start recording data until some time has passed following perturbing the system in some way.

F. A Subtlety Concerning T and Detailed Balance

If you think about it, the transition matrix T actually has two pieces in its construction. The first is the suggestion of a new state j, and the second is the decision (e.g. Metropolis) whether to accept j or not. It is the *combination* of these two factors which determines T and which must obey detailed balance. Examples of how the method of suggesting states might go awry are given in Exercises 7 and 12.

G. Some Exercises

1. The Heat Bath Algorithm

The Metropolis algorithm is not the only way to go.

Exercise 2: Show that the "heat bath" prescription

$$T_{ji} = p_j/(p_i + p_j) \tag{80}$$

obeys detailed balance.

Thus the starting point 'Metropolis' of [a] in Sec. III can be replaced by 'Heat Bath'.

2. When Do You Measure?

Exercise 3: Consider a system with two states and associated probabilities p_1, p_2. Suppose the observable A has the values A_1 and A_2 in the two states. What will you get for $\langle A \rangle$ if you measure A only when a move is accepted? What is the correct value for $\langle A \rangle$? When should you measure A to get the right answer? Argue qualitatively that, if $p_1 >> p_2$, the sequence of configurations generated gives a sensible answer when you put your measurement in the correct spot.

3. Explicitly Constructing the matrix T

Exercise 4: Consider a system with three states and associated probabilities p_1, p_2, p_3. Construct the 3x3 matrix for T assuming that if you are in a state i you suggest a change to one of the other two states with probability $\frac{1}{2}$ each, and then accept or reject with Metropolis. Verify that your T obeys Eq. 1 and that the vector $(p_1\ p_2\ p_3)$ is a right eigenvector of T of eigenvalue one. Verify the other two eigenvalues are less than one in absolute value.

Exercises 5 and 6 below emphasize that the rule T for generating states is not unique. The art of Monte Carlo is in finding the T which works best, that is, which moves you around in phase space most rapidly and generates the smallest error bars.

Exercise 5: Do Exercise 4 again, but use the heat bath algorithm.

Exercise 6: Again consider the same three state system as Exercise 4. Construct the 3x3 matrix for T assuming that if you are in a state i you suggest a new state (which could be the same as the one you are in) randomly, that is, with pick the new state to be 1 or 2 or 3, with probabilty $\frac{1}{3}$, and then do Metropolis. Verify that your T obeys Eq. 1 and that the vector $(p_1\ p_2\ p_3)$ is a right eigenvector of T of eigenvalue one. Verify the other two eigenvalues are less than one in absolute value. In which case is the next smallest eigenvalues closer to $|\lambda| = 1$, here, or in Ex. 5?

Exercise 7: Consider a system with an infinite number of states $E_i = \omega\, i$ for $i = 0, 1, 2, 3, \ldots$., and associated probabilities $p_i \propto e^{-\beta E_i}$. Construct the matrix for T assuming that your suggestion of a move from state i is to one of the two immediately adjacent states $j = i \pm 1$, with probability $\frac{1}{2}$. Verify $(p_1\ p_2\ p_3\ \ldots)$ is a right eigenvector of T. Be especially careful with the state $i = 0$ which has no state beneath it! Should you suggest state $j = 1$ all the time, since there is no $j = -1$? This is an example of the subtlety mentioned in Sec. VI.

4. Very Simple Monte Carlo Simulations

Exercise 8: Write a Monte Carlo code which computes $\langle E \rangle$ for the three state system of Exercise 4, using the T described in that exercise.

Exercise 9: Write a Monte Carlo code corresponding to the T of exercise 5.

Exercise 10: Write a Monte Carlo code corresponding to the T of exercise 6.

Exercise 11: Write a Monte Carlo simulation for an energy which has a continuous degree of freedom x with $E(x) = \frac{1}{2}kx^2$. Construct T by suggesting the new state $x' = x + \Delta(r - \frac{1}{2})$ where Δ is the 'step-size', and r is a random number uniformly distributed on (0,1). Use Metropolis to accept/reject x'. What is the correct value for $\langle E \rangle$? Show your code gets it, for any value of Δ. What values of Δ are best? See also Sec. XI below.

Exercise 12: Do Exercise 11 again, except this time construct T by suggesting the new state $x' = x + \Delta(r - \frac{1}{3})$, and then use Metropolis. Show you code gets the wrong value for $\langle E \rangle$. Show that your T violates detailed balance, even though you use Metropolis after the move suggestion.

5. Less Simple Monte Carlo Simulations

Many readers going through these notes have a particular (and presumably non-trivial) problem they wish to address with Monte Carlo. If, however, you do not, a standard Monte Carlo simulation to try is the two dimensional Ising model. Many books on simulations contain descriptions.[106–108]

6. Testing Monte Carlo Simulations

As with all codes, tests are essential. Here I will mention three very useful ones.

First, Monte Carlo simulation codes can often be tested on small lattices. That is, it is often possible to enumerate all the possible states of a small system (e.g. a 4x4 Ising lattice has 2^{16} configurations) and have the computer then generate the partition function and expectation values through an explicit enumeration of all the configurations.

Second, limits of the Hamiltonian in question are often soluble. At high and low temperatures, one often can figure out the values of the energy and other observables. Likewise, by turning off one or more terms in the Hamiltonian, it may become analytically soluble. Or, if you write your code so that the interactions are different in different directions, you can sometimes turn off one or more directions and reduce the dimensionality of the system to a point where analytic solutions are known.

Finally, while you will usually write your code so that it averages observable which should be equivalent by some symmetry, looking at the unaveraged values first is often useful: Many bugs in codes are fingered by measurements which should be equal by symmetry but are not.

My experience is that if your code checks out for the entire model on small lattices, and then individual pieces on different lattice sizes, and also the high and low T limits, then it is very likely correct.

H. Quantum Monte Carlo

The above discussion seems to rely very heavily on the fact that the system is classical. However, it turns out to be relatively easy to generalize classical Monte Carlo to Quantum Monte Carlo. All I will say here is that one takes the *operator* $e^{-\beta\hat{H}}$ and writes its trace as a path integral. This sum over paths involves a *classical* action, which then can be attacked with classical Monte Carlo. A nice discussion of this for the quantum harmonic oscillator is given by Creutz.[109] Another particularly interesting example is the mapping of the $d = 1$ Ising model in a transverse magnetic field onto the classical $d = 2$ Ising model.[110]

I. Relation to Molecular Dynamics

At the beginning of these notes, I mentioned that Molecular Dynamics (MD) as one way we might get a computer to emulate nature. Since the equations of MD keep the energy constant (to within time step errors), one way to view MD is as a Monte Carlo where the proposed move does not change the energy, and is therefore accepted with unit probability according to the Metropolis prescription. Thus MD and Monte Carlo should give the same result, under the condition that the MD energy is initialized at the same value $\langle E \rangle$ as the average energy which comes out of the Monte Carlo. This is the usual equivalence of the canonical and microcanonical ensembles in statistical mechanics.

In practice, one might want to do MD at a particular temperature T instead of at fixed E. One way to accomplish this is to evolve the positions and velocities x_n and v_n using the MD equations, but then periodically 'refresh' the velocities by replacing their current values with new ones drawn from the Gaussian distribution $e^{-m_n v_n^2/2T}$. Here m_n is the mass of the nth particle. We choose to 'refresh' the momenta, because usually the energy takes the form $E = \frac{1}{2}\sum_n m_n v_n^2 + V(\{x_n\})$. That is, the potential energy doesn't depend on the velocities. So the probability distribution for the velocities is Gaussian, and we know how to generate

Gaussian distributed random numbers. The positions usually invovle a more complicated V than Gaussian.

This sort of finite T molecular dynamics can be understood as a Monte Carlo with two types of moves. As remarked above, the conventional MD moves keep the energy constant and hence are always accepted. The momentum refreshment moves change the energy and hence are sometimes rejected according to the Metropolis prescription.

Exercise 13: Write a Molecular Dynamics code for $E = \frac{1}{2}kx^2 + \frac{1}{2}mv^2$. (That is, use $F = -kx$ and $a = F/m$ to update v.) Verify that you travel along an ellipse in phase space at constant energy, when dt is small. Here 'dt small' really means dt is much less than the period $2\pi\sqrt{m/k}$. Compute $\langle x^2 \rangle$ and $\langle p^2 \rangle$ and show you get the correct answers (which only depend on x_0 and v_0). Note that the Molecular Dynamics integration of equation of motion introduces time step errors. In the Euler method, the accumulation of these errors will lead to an exponential increase in E. The "leap-frog" method is much more robust.

Exercise 14: Include steps which refresh the momentum. Compute $\langle x^2 \rangle$ and $\langle p^2 \rangle$ and show you get the correct answers (which now do not depend on the initial conditions as in Ex. 13 but only on temperature T.)

J. Relation to the Langevin Equation

Monte Carlo can also be related to the Langevin Equation. Consider a system with an energy $E(x)$ which depends on the degree of freedom x. (For simplicity, let's just consider a single degree of freedom.) Suppose we define a procedure for updating x via

$$x' = x - \epsilon \frac{\partial E}{\partial x} + \sqrt{4\epsilon T}\, r \tag{81}$$

Here r is a Gaussian random number, $p(r) = e^{-r^2}/\sqrt{\pi}$, and T is the temperature. We will now show that this equation satisfies detailed balance with $p(x) \propto e^{-\beta E(x)}$.

The Langevin Equation amounts to a prescription T for getting a new state x' from an original state x. Given x' and x, the value of T is given by the probability of throwing the appropriate random number which will take you from x to x'.

$$T(x', x) = \frac{1}{\sqrt{\pi}} e^{-r^2} \tag{82}$$

$$r = \frac{1}{\sqrt{4\epsilon T}} (x' - x + \epsilon \frac{\partial E}{\partial x}) \tag{83}$$

Therefore, introducing the notation $dx = x' - x$,

$$T(x', x) = \frac{1}{\sqrt{\pi}} e^{-(dx + \epsilon \frac{\partial E}{\partial x})^2/(4\epsilon T)} \tag{84}$$

Likewise,

$$T(x, x') = \frac{1}{\sqrt{\pi}} e^{-(-dx + \epsilon \frac{\partial E}{\partial x})^2/(4\epsilon T)} \tag{85}$$

Note that actually the gradient of the energy n Eq. 13 should now be evaluated at x', but because ϵ is small, dx will be small and x' close to x. Since the gradient is already multiplied by ϵ the difference is higher order and we drop it.

Putting this together,

$$\frac{T(x',x)}{T(x,x')} = e^{-\frac{\partial E}{\partial x}dx/T} = e^{-dE/T} = e^{-(E(x')-E(x))/T} \tag{86}$$

$$T(x,x')e^{-E(x')/T} = T(x',x)e^{-E(x)/T}, \tag{87}$$

where again we have dropped terms which are higher than linear order in ϵ. Eq. 15 completes the demonstration that the Langevin equation obeys detailed balance. Hence by our general theorems concerning Monte Carlo, it will generate configurations of the system according to the Boltzmann distribution.

A final comment: You will notice that the prefactors of the random force and the force which depends on E in the Langevin equation are not independent. This is an example of the fluctuation-dissipation theorem.

Exercise 15: In proving detailed balance we threw away higher order terms in ϵ. Consider the energy $E(x) = \frac{1}{2}kx^2$ and go through the Langevin analysis retaining terms to all orders in ϵ. Show that detailed balance is obeyed with a k shifted by order ϵ. Will $\langle x^2 \rangle$ be overestimated or underestimated?

Exercise 16: Write a computer code to implement the Langevin equation for $E(x) = \frac{1}{2}kx^2$. Verify your results from Exercise 15.

K. Error Analysis in Monte Carlo

This final section is intended to review error analysis in Monte Carlo, and illustrate it with the very simple example of a simulation of $E(x) = \frac{1}{2}kx^2$.

1. Introduction and Definitions

We begin with the definitions,

$$\langle x \rangle = \frac{1}{N}\sum_{i=1}^{N} x_i \tag{88}$$

$$\langle x^2 \rangle = \frac{1}{N}\sum_{i=1}^{N} x_i^2 \tag{89}$$

$$\sigma = \sqrt{\frac{\langle x^2 \rangle - \langle x \rangle^2}{N-1}}. \tag{90}$$

Here x_i is the ith measured value of x, and N is the number of measurements. The definitions of $\langle x \rangle$ and $\langle x^2 \rangle$ are unambiguous. The entire content of this note is to clarify the proper denominator of the definition of σ. Specifically, the formula for σ assumes that the N measurements are all independent. Since successive values of x are generated from each

FIG. 39: First 1000 steps in Monte Carlo time history of x for three different step sizes $\Delta = 1, 10, 200$. (Acceptance rates=0.70, 0.35, 0.02).

FIG. 40: Autocorrelation functions for the complete data sets (400,000 steps) as in figure 1. (Step sizes $\Delta = 1, 10, 200$, Acceptance rates=0.70, 0.35, 0.02).

other, this is never true. The x values are more and more related the less time one waits between measurements.

To quantify the correlations among successive x values, we define the autocorrelation function,

$$c(l) = \frac{1}{N-l} \sum_{i=1}^{N-l} y_i y_{i+l} \tag{91}$$

Here $y(i) = x(i) - \langle x \rangle$ measures the fluctuation of x about its average value. $c(l)$ measures whether those fluctuations are related for x values l measurements apart. Saying x_i and x_{i+l} are independent means whether x_{i+l} is above or below $\langle x \rangle$ (the sign of y_{i+l}) is unrelated to the sign of y_i. If that is the case, $c(l) = 0$ (to within errors). Clearly $c(0)$ is never zero. In fact, $c(0) = \sigma^2$. It is conventional to redefine $c(0) \to c(0)/\sigma^2$ so that $c(0) = 1$.

2. Time Histories

Let's begin by looking at actual time histories of x. I chose $k = 1$ and $T = 2$ so that $\langle x^2 \rangle = 2$. The step size for suggested changes in x is Δ. I measure every Monte Carlo step and ran for $N = 400000$ sweeps. Here of course since $\langle x \rangle = 0$, $y_i = x_i$. The Monte Carlo time histories are given in Figure 1. That the data are correlated is immediately evident. If a value of x_i is positive, its successors tend to be positive and similarly if it is negative. The dependence on the step size Δ is easy to interpret.
If Δ is small you do not suggest much of a change, and successive values of x are highly correlated. Likewise, if Δ is large, most suggested Monte Carlo moves take you out of the part of phase space of low energy and are rejected. (This results in the long flat regions of the evolution of x.)

3. Correlation Functions

The plots of $c(l)$ resulting from the same data are given in Figure 2. We see that $c(l)$ has a characteristic decaying exponential form. We define the correlation time τ to be the point when $c(l = \tau) = e^{-1}$ and say that measurements of x are independent when l exceeds τ. (Strictly speaking, we want c to go to zero, but $c(\tau) = e^{-1}$ is an acceptable criterion.) Notice you can almost guess the values of τ given by Figure 2 directly from the time histories of Figure 1.

As mentioned earlier, in generating the above results I measured x every Monte Carlo step. What happens if one instead measures only every mth step? Define $c_m(l)$ to be the correlation function when measurements are only every mth Monte Carlo step. It is easy to convince yourself that $c_m(l) = c_1(ml)$, so the correlation function rescales in a trivially fashion. The point is that if one choose $m > \tau$, then the measurements all become independent.

• *So one way to ensure the value for the error bar σ is correct is to make sure measurements are separated by a waiting time $m > \tau$.*

This approach has the advantage that one does not waste time making measurements when the measurements are not independent.

4. Rebinning Data

An alternate (and equivalent) approach to getting the correct σ is by "rebinning" the data. Take a file containing the complete time history of a measurement, for example the data for x which is partially shown in Figure 1. Choose a "bin size" M, and average the data for x over each of the $L = N/M$ bins (remember $N =$ total number of measurements) to create L "binned measurements" m_j.

$$m_j = \frac{1}{M} \sum_{i=M*(j-1)+1}^{M*j} x_i. \tag{92}$$

Treat these L values for m as your independent measurements. As seen in Equation 5, the values for m are already averages over M values of x. Define averages and error bars as in Equation 1, with L replacing N in the normalizations $1/N$ and $1/\sqrt{N-1}$. The average $\langle x \rangle$ is independent of M since all one is doing is reordering a linear sum. The average $\langle x^2 \rangle$ is however altered, and hence so is the error bar σ. Figure 3 shows values for σ as a function of the number of x values in each bin, M.

What is the interpretation of Figure 3? Consider $M = 1$. In this case only one value of x is put in each bin, so that in calculating σ it is assumed all x are independent. The error bar σ thus obtained is too small. As M becomes larger, more x values are put in each bin, the number of bins (independent measurements) decreases, and σ increases. Eventually σ goes to an asymptotic value which gives the correct error bar.

FIG. 41: Error bars for different bin sizes M. Data is that of Figures 1,2: step sizes $\Delta = 1, 10, 200$. (Acceptance rates=0.70, 0.35, 0.02).

Why does σ not increase indefinitely as M increases? You might expect it to, since the denominator $\sqrt{L-1}$ is getting smaller and smaller. The answer is that as more measurements are put in each bin, the different bins fluctuate less and less. The numerator which measures these fluctuations decreases in exact compensation to the denominator. (However, to reiterate, initially for M small when you put more measurements in the bins the new values are not independent and so the numerator does *not* decrease.)

• *So a second way to ensure the value for the error bar σ is correct is to consider different binnings of the data, and use the value obtained asymptotically as each bin contains a lot of data.*

How do we see this result is consistent with the correlation function analysis? There are two checks. The first is to see that the value for M at which σ starts to flatten out should be roughly the same as the value of τ for which $c(l)$ gets small. Second, one can compare the values of σ_1 at $M = 1$, where one assumes all the x are independent, with the asymptotic value σ_∞. The claim is that these should be related by $\sigma_\infty = \sqrt{\tau}\sigma_1$. You can see this is roughly true: For $\Delta = 1$ we get $\sigma_1 = 0.0022$ and $\sigma_\infty = 0.030$ from Figure 3. If you assume all the measurements are independent, you underestimate σ by more than an order of magnitude. Meanwhile, from figure 2, $\tau \approx 85$, and hence $\sqrt{\tau}$ similarly reflects this order of magnitude correction factor.

5. Acceptance Rate

The acceptance rate provides a rough guide to the choice of a good step size. If the acceptance rate is too much greater than 0.5, then one is likely in the limit of Figures (1–3)a where the correlation time is unnecessarily large due to small suggested moves. Likewise, if the acceptance rate is too much less than 0.50, then one is likely in the limit of Figures (1–3)c where the correlation time is unnecessarily large due to multiple rejections.

6. A "Cheap" Approach

I recommended a "cheapo" approach to error bars, which was to bin the data from your run into 10 bins. ($M = N/10$.) This strategy assumes that you were doing a reasonably long run, so that $N/10 > \tau$. My thinking is that if this is violated, you are in more serious trouble than just getting the wrong error bars: you will have less than 10 independent measurements (and perhaps have not even properly equilibrated) so it is likely your expectation values themselves are wrong. For the particular example we are doing, the reported values from my simplistic approach for $\langle x^2 \rangle$ and σ were $1.973 \pm 0.051, 1.993 \pm 0.010, 1.995 \pm 0.039$ for $\Delta = 1, 10, 200$ respectively. These error bars should be the same as the asymptotic values of σ in Figure 3.

7. Final Comments

Does it matter which measurement you look at? I have looked entirely at x_i in doing this analysis. Would it matter if I had examined x_i^2 or some other measurement? For this simple problem I don't think so. In more complicated simulations it may be important to calculate correlation times separately for measurements of "local" quantities (observables for degrees of freedom that are close together spatially) and "global" quantities (observables for degrees of freedom that are far apart spatially). The spatial separation of the different degrees of freedom in an observable can affect the autocorrelation time. In particular, observables containing quantities which are widely spaced generally have longer correlation times.

More generally, the size of the system you are simulating (and hence the spatial separations of the degreees of freedom) can greatly affect the correlation time, especially in the vicinity of a phase transition. Just as physical quantities like the specific heat, susceptibility etc can diverge at a critical point, the correlation time can diverge too as the system size increases near a critical point. This of course makes Monte Carlo very difficult. There is a big literature on solving this problem.

IX. APPENDIX 3: DETERMINANT QUANTUM MONTE CARLO

A. A Useful Analogy: Multidimensional Gaussian Integration

The equations involved in determinant QMC bear many similarities with multidimensional Gaussian integrals. Reviewing these identities will help provide an intuitive feel for the formulae of determinant QMC, within a familiar context.

The generalization of the one dimensional Gaussian integral,

$$\int_{-\infty}^{+\infty} dx\, e^{-ax^2} = \frac{\sqrt{\pi}}{a}, \tag{93}$$

to many dimensions is,

$$Z = \int_{-\infty}^{+\infty}\int_{-\infty}^{+\infty}\ldots\int_{-\infty}^{+\infty} dx_1 dx_2 \ldots dx_N\ e^{-\vec{x}\,A\,\vec{x}^{\,T}} = \frac{\pi^{n/2}}{\sqrt{\det A}}. \tag{94}$$

Here $\vec{x}$ is an N dimensional vector of real numbers and A is a real, symmetric, N dimensional matrix. I have used the notation Z for the integral to emphasize that it would be the partition function for a set of classical variables whose action is given by the quadratic form $\vec{x}A\,\vec{x}^{\,T}$.

We also know how to do these integrals when the integrand includes factors of x_i.

$$\langle x_i x_j\rangle = Z^{-1}\int_{-\infty}^{+\infty}\int_{-\infty}^{+\infty}\ldots\int_{-\infty}^{+\infty} dx_1 dx_2 \ldots dx_N\ x_i x_j\ e^{-\vec{x}\,A\,\vec{x}^{\,T}} = \frac{1}{2}[A^{-1}]_{ij} \tag{95}$$

Again, the notation $\langle x_i x_j\rangle$ emphasizes a possible statistical mechanical interpretation of the ratio of integrals.

Further factors of x_i in the integrand generate expressions like,

$$\begin{aligned}\langle x_i x_j x_k x_l\rangle &= Z^{-1}\int_{-\infty}^{+\infty}\int_{-\infty}^{+\infty}\ldots\int_{-\infty}^{+\infty} dx_1 dx_2 \ldots dx_N x_i x_j x_k x_l e^{-\vec{x}A\vec{x}^{\,T}} \\ &= \frac{1}{4}([A^{-1}]_{ij}[A^{-1}]_{kl} + [A^{-1}]_{ik}[A^{-1}]_{jl} + [A^{-1}]_{il}[A^{-1}]_{jk}).\end{aligned} \tag{96}$$

These are similar in form to 'Wick's Theorem', which tells us that contractions of products of many fermion operators can be expressed as sums of products of contractions taken two operators at a time, in all possible permutations.

While it is possible to do these integrals with arbitrary polynomials as part of the integrand, they cannot be done when a quartic term appears in the exponential. We shall see shortly the analogies of these various statements for traces over fermion Hamiltonians.

B. Basic Formalism of Determinant QMC

In solving the Hubbard model we want to evaluate expressions like

$$\begin{aligned}\langle\hat{A}\rangle &= Z^{-1}\,\mathrm{Tr}\,[\hat{A}e^{-\beta\hat{H}}] \\ Z &= \mathrm{Tr}\,e^{-\beta\hat{H}}\end{aligned} \tag{97}$$

The "Tr" is a trace over the 4^N dimensional Hilbert space, where N is the number of sites.

In analogy with multidimensional Gaussian integration, we can do such traces if they are over *quadratic* forms of fermion operators. Suppose

$$\hat{H} = \tag{98}$$

Here h is an NxN matrix. The identity is,

$$Z = \mathrm{Tr}\, e^{-\beta \hat{H}} = \det[I + e^{-\beta h}]. \tag{99}$$

Note that while the original "Tr" is over a quantum mechanical 4^N dimensional Hilbert space, the "det" is a usual determinant of NxN matrices. "I" is the N dimensional identity matrix and "h" is the matrix of *numbers* entering the definition of $\hat{H}$. It is worth emphasizing that because we are taking the trace over the full 4^N dimensional Hilbert space, we are including states of all occupation numbers. The determinant QMC method, as formulated here, works in the grand canonical ensemble. Particle density is controlled by changing the chemical potential.

It is trivial to check that Eq. 20 holds for a single fermion degree of freedom, with Hamiltonian $\hat{H} = \epsilon\, c^\dagger c$. There are two states in the Hilbert space and

$$Z = \langle\, 0 \,|\, e^{-\beta\, \epsilon\, c^\dagger c} \,|\, 0 \rangle + \langle\, 1 \,|\, e^{-\beta\, \epsilon\, c^\dagger c} \,|\, 1 \,\rangle = 1 + e^{-\beta\, \epsilon}. \tag{100}$$

More generally (e.g. for more than one fermion degree of freedom) Eq. 20 can be verified by going to the basis where h is diagonal. The equations can also be derived by employing the techniques of Grassman integration.

There is a more general identity. If one has a *set* of quadratic Hamiltonians $l = 1, 2, \ldots L$

$$\hat{H}(l) = \tag{101}$$

then,

$$Z = \mathrm{Tr}\,[e^{-\Delta\tau \hat{H}(1)} e^{-\Delta\tau \hat{H}(2)} \cdots e^{-\Delta\tau \hat{H}(L)}] = \det[\, I + e^{-\Delta\tau h(1)} e^{-\Delta\tau h(2)} \cdots e^{-\Delta\tau h(L)}]. \tag{102}$$

Here I have changed the prefactor in the exponential from β to $\Delta\tau$ for reasons which will soon be clear. It is also true that,

$$\begin{aligned} G_{ij} = \langle c_{i\sigma} c^\dagger_{j\sigma} \rangle &= Z^{-1}\, \mathrm{Tr}\,[c_{\,i\sigma} c^\dagger_{j\sigma}\; e^{-\Delta\tau H(1)} e^{-\Delta\tau H(2)} \cdots e^{-\Delta\tau H(L)}\,] \\ &= [\, I + e^{-\Delta\tau h(1)} e^{-\Delta\tau h(2)} \cdots e^{-\Delta\tau h(L)}\,]^{-1}_{ij}. \end{aligned} \tag{103}$$

The "fermions Greens function" is just an appropriate matrix element of the inverse of the NxN matrix whose determinant gives the partition function.

The above formulae describe how to perform traces over quadratic forms of fermion degrees of freedom. Unfortunately, the Hubbard Hamiltonian has an interaction term $U n_{i\uparrow} n_{i\downarrow} = U c^\dagger_{i\uparrow} c_{i\uparrow} c^\dagger_{i\downarrow} c_{i\downarrow}$ which is quartic in the fermion operators. To handle such terms, we employ the (discrete) Hubbard–Stratonovich transformation,

$$e^{-U\Delta\tau (n_\uparrow - \frac{1}{2})(n_\downarrow - \frac{1}{2})} = \frac{1}{2} e^{-\frac{U\Delta\tau}{4}} \sum_s e^{\,\lambda\, s\, (n_\uparrow - n_\downarrow)} \tag{104}$$

Here $\cosh\lambda = e^{U\Delta\tau/2}$, and s is an Ising variable which can take on the two values $S = \pm 1$. This identity can be verified by explicitly enumerating the 4 possible choices for $n_\uparrow, n_\downarrow$.

Now we divide $\beta = L\Delta\tau$ and employ the Trotter decomposition. This allows us to isolate different pieces of the Hamiltonian. We write $\hat{H} = \hat{K} + \hat{V}$ where $\hat{K}$ contains all the one–body pieces and $\hat{V}$ the on–site Hubbard interaction. Then,

$$Z = \mathrm{Tr}\, e^{-\beta\hat{H}} = \mathrm{Tr}\,[e^{-\Delta\tau\hat{H}}]^L \approx \mathrm{Tr}\,[\, e^{-\Delta\tau\hat{K}}\, e^{-\Delta\tau\hat{V}}\, e^{-\Delta\tau\hat{K}}\, e^{-\Delta\tau\hat{V}} \cdots]. \tag{105}$$

The final expression is only approximate since $\hat{K}$ and $\hat{V}$ do not commute. However, the approximation becomes better and better as L increases ($\Delta\tau$ decreases). As mentioned before, the errors should be pretty small if $t\,U\,(\Delta\tau)^2 \approx 1/10$.

The $e^{-\Delta\tau\hat{K}}$ are quadratic in the fermion operators. For each factor of the L terms $e^{-\Delta\tau\hat{V}}$ above, we introduce N Hubbard–Stratonovich fields, one for each of the spatial sites where we have an on–site interaction to decouple. The Hubbard–Stratonovich field $s(i,l)$ therefore has two indices, space i and imaginary–time l. Now the $e^{-\Delta\tau\hat{V}(l)}$ are also quadratic in the fermion operators. We put an argument l on $\hat{V}$ to emphasize that while the $\hat{K}$ are all identical, the $\hat{V}(l)$ contain different Hubbard–Stratonovich fields on the different imaginary time slices.

Applying Eqs. 22-23 allows the analytic evaluation of the trace,

$$Z = \sum_{s(il)} \mathrm{det}M_\uparrow\ \mathrm{det}M_\downarrow, \tag{106}$$

with,

$$M_\sigma = I + e^{-k}e^{-v_\sigma(1)}e^{-k}e^{-v_\sigma(2)}\cdots e^{-k}e^{-v_\sigma(L)}. \tag{107}$$

We get a determinant for each of the two spin species. The quantum partition function has now been expressed to a *classical* monte carlo problem: We need to sum over the possible configurations of the real, classical, variables $s(i,l)$ with the "Boltzmann weight" which is the product of the two fermion determinants. Note that as in world-line QMC, the classical variable to be summed over has an additional index l labeling imaginary time.

Eqs. 2-4 can now be understood as coming from applying the general operator identity of Eqs. 22-23 to our specific problem of evaluating Eq. 26, with the interaction operators $\hat{V}$ made into quadratic forms by using Eq. 25.

The algorithm, as stated, scales in CPU time as N^4L. The reason is that re–evaluating the determinant of M' takes N^3 operations, and we must do that NL times to sweep through all the Hubbard–Stratonovich variables (if, as is typically done, we change just one at a time). This scaling can be reduced to N^3L. (In what follows I will drop the spin indices.) The idea is to write $M' = M + dM$ and the ratio of determinants as,

$$\mathrm{det}M'/\mathrm{detM} = \mathrm{det}(M^{-1}\,M') = \mathrm{det}(M^{-1}\,(M + dM)) = \mathrm{det}(I + G\,dM), \tag{108}$$

with the definition $G = M^{-1}$. It turns out that dM is very simple because when a Hubbard–Stratonovich field is flipped, a single diagonal entry in $v(l)$ changes. Because dM is sparse, the evaluation of $\mathrm{det}(I + G\,dM)$ takes a cpu time independent of N and L! In fact, a little bit of thought will convince you that Eq. 6 arises from Eq. 31 and the form for dM.

However, we need to know $G = M^{-1}$ for this calculation, and once the Hubbard-Stratonovich field change is made, one needs to update G. This updating G does not take N^3 iterations, as one might expect of a matrix inversion, but can be done in only N^2 operations, again as a result of the simplicity of the change dM. The relevant identity which relates the new $G' = (M + dM)^{-1}$ to the old $G = M^{-1}$ is an application of the "Sherman–Morrison" formula given, for example, in Press's 'Numerical Recipes'. If you work through the Sherman-Morrison formula, as applied to our problem, you end up with Eqs. 7-8.

A final comment concerns the need for 'wrapping' Eq. 9. The use of Eq. 31 to derive Eq. 6, and the Serman-Morrison formula to derive Eqs. 7-8 require that the imaginary time slice of the Hubbard-Stratonovich variable being updated be at the end of the product in Eq. 28. The process of wrapping moves the appropriate interaction matrix to the end of the product through a cyclic permutation. That is,

$$\left[e^{-k}e^{-v_\sigma(L)}\right]\left[I + e^{-k}e^{-v_\sigma(1)}e^{-k}e^{-v_\sigma(2)}\cdots e^{-k}e^{-v_\sigma(L)}\right]^{-1}\left[e^{-k}e^{-v_\sigma(L)}\right]^{-1} \tag{109}$$

$$= \left[I + e^{-k}e^{-v_\sigma(L)}e^{-k}e^{-v_\sigma(1)}\cdots e^{-k}e^{-v_\sigma(L-1)}\right]^{-1} \tag{110}$$

C. Subtleties and "Tricks of the Trade"

While the above formulae allow you to write a "bare–bones" determinant QMC algorithm, there are a number of refinements which are important.
(1.) It is possible to measure correlation functions with non–zero imaginary time separation, but this requires considerably more work. Analytic continuation of such correlations is required to get the dynamical response. That is quite difficult.
(2.) The product of matrices required in constructing M and hence $G = M^{-1}$ (see Eq. 5 and Eq. 28) is numerically unstable at low temperatures and strong couplings. That is, the product has a very high ratio of largest to smallest eigenvalue. Special "stabilization" is required to do the matrix manipulations. While these add to the complexity of the code, they however have no content in the sense that all the above equations are valid, it is just a question of how best to multiply matrices on a machine of finite precision.
(3.) The determinants of the matrices can go negative. This is called the "fermion sign problem." The sign problem does not occur for certain special cases. For example, if U is negative (the "attractive" Hubbard model), the individual determinants can go negative, but the matrices are always equal and hence the determinant appears as a perfect square. This is a consequence of the fact that the appropriate Hubbard–Stratonovich transformation couples S to the charge $n_\uparrow + n_\downarrow$ as opposed to the spin as given in Eq. 25 for the repulsive model. If U is positive but the chemical potential $\mu = U/2$ ("half–filling") one is also okay. The matrices are not identical in this case, but the determinants are nevertheless related by a positive factor, that is, they again have the same sign, so their product is always positive. Some types of randomness are also acceptable. It is okay for the hoppings t and interactions U to depend on the link or site. These statements are demonstrated by various particle–hole transformations on the Hamiltonian.
(4.) Alternate Hubbard–Stratonovich transformations are possible. One can couple more symmetrically to the spin, that is not single out the z component Or, one can couple to pair creation operators. So far, all such alternatives give a worse sign problem than the transformation Eq. 25. These more complicated transformations are needed to do 'Hund's rule terms' in multi-orbital Hubbard models.
(5.) Very similar "ground state" determinant simulations exist which work at $T = 0$ and in the canonical ensemble.

D. What Determinant QMC Simulations Can Do

The state of the art of determinant QMC simulations, in the absence of a sign problem, are studies of several hundred electrons down to temperatures of $\beta t = 10 - 20$. In terms of temperature and bandwidth, this means T of roughly $1/100$ of the bandwidth $W = 8t$ of the 2-d Hubbard model. This is plenty cold enough to see well developed magnetic correlations.

For typical parameters, $t = 1, U = 4$ one chooses $\Delta\tau = 1/8$ so these beta values correspond to roughly $L = 100$, and the simulation involves approximately 10^4 Hubbard–Stratonovich variables.

In cases where one has a sign problem, βt is limited to 4–5. This is, unfortunately, not low enough in temperature to make conclusive statements about certain important problems, perhaps most prominently the question of the existence of long range $d-$wave superconducting correlations in the Hubbard model away from half-filling.

E. Concluding Remarks

Determinant QMC is a powerful method for simulating interacting electron Hamiltonians in more than one dimension. One can easily study problems with several hundred particles, an order of magnitude greater than with exact diagonalization, and often large enough to make compelling finite size scaling analysis. The sign problem is a very significant limitation, however. For the repulsive Hubbard model, one can go to temperatures on the order of $W/30$ where W is the bandwidth. For special cases like the attractive Hubbard model or the repulsive model at half-filling, there is no sign problem, and the ground state properties can be obtained.

Algorithm development in determinant QMC currently focusses on applications to DMFT, where the Hubbard-Stratonovich field is allowed to fluctuate only in imaginary time. A number of questions are being actively explored in this field: How does one incorporate more complex (e.g. Hund's rules) interactions into simulation which include multiple orbitals? Can one re-introduce some degree of spatial fluctuations?

X. APPENDIX 4: SUPPLEMENTARY MATERIAL

A. Particle-Hole Symmetry

The Hubbard Hamiltonian has a fascinating 'particle-hole' symmetry which allows us to relate its properties for different values of the parameters. Particle-Hole symmetry also plays an important role in quantum monte carlo simulations. Consider the introduction of new operators which exchange the role of creation and destruction:

$$d^\dagger_{\mathbf{i}\sigma} \quad = (-1)^{\mathbf{i}} c_{\mathbf{i}\sigma} \tag{111}$$

The meaning of the $(-1)^{\mathbf{i}}$ will be explained further below.

Exercise 59: Verify that the number operator for the d particles equals one minus the number operator for c particles: $d^\dagger_{\mathbf{i}\sigma} d_{\mathbf{i}\sigma} = 1 - c^\dagger_{\mathbf{i}\sigma} c_{\mathbf{i}\sigma}$. What happens to the interaction term in the Hubbard model $U(n_\uparrow - \frac{1}{2})(n_\downarrow - \frac{1}{2})$ under the particle-hole transformation?

Before seeing what happens to the kinetic energy term under a particle-hole transformation, we introduce the idea of a bipartite lattice. A bipartitie lattice is one which can be divided into two sublattices A and B in such a way that a site in A has neighbors which are all members of B and *vice-versa*. The $(-1)^{\mathbf{i}}$ factor in the particle-hole transformation takes the value -1 on one sublattice and $+1$ on the other.

Exercise 60: Is a one dimensional chain a bipartite lattice? How about a two-dimensional square lattice?

Exercise 61: Is the triangular lattice bipartite? What about the honeycomb lattice?

The following Exercise determines what happens to the kinetic energy term when the particle-hole transformation is performed.

Exercise 62: Verify that the kinetic energy is unchanged under a particle-hole transformation. That is, it takes exactly the same form in terms of the d operators as it did in terms of the c operators. Where does the bipartite nature of the lattice come enter? What role do the $(-1)^{\mathbf{i}}$ factors play?

What have we learned? Exercises 58 and 61 tell us that the Hubbard model, when the interaction term is written in the particle-hole symmetric form, is invariant under particle-hole transformations when $\mu = 0$. The condition $\mu = 0$ is necessary since the number operators which μ multiplies are not invariant but go into one minus themselves. Actually, a more precise statement is that the Hubbard model with a given μ maps into the Hubbard model with the sign of the chemical potential reversed, that is, with μ replaced by $-\mu$. In fact, this implies that the whole phase diagram of the Hubbard model on a bipartite lattice is symmetric about half-filling, as the following Exercises suggest.

Exercise 63: Show that the density of the Hubbard model on a bipartite lattice obeys the relation $\rho(\mu) = 2 - \rho(-\mu)$ by starting with $\rho = \langle n_\uparrow + n_\downarrow \rangle$ and making a particle-hole transformation.

Exercise 64: Show that the local moment of the Hubbard model on a bipartite lattice obeys the relation $\langle m^2 \rangle(\mu) = \langle m^2 \rangle(-\mu)$.

Exercise 65: Look back at you pictures of the density of states $N(E)$ obtained in Exercises 27-30 and explain their behavior when reflected about $E = 0$ in terms of particle-hole symmetry.

B. Relation between the attractive and Repulsive Hubbard Models

It is also interesting to consider what happens when a particle-hole transformation is performed only on one of the spin species.

Exercise 66:

Show that if we perform the transformation,

$$\begin{aligned} d_{\mathbf{i}\uparrow} &= c_{\mathbf{i}\uparrow} \\ d_{\mathbf{i}\downarrow} &= (-1)^{\mathbf{i}} c^{\dagger}_{\mathbf{i}\downarrow} \end{aligned}$$

the sign of the interaction term reverses, while the kinetic energy remains unchanges.

The Hubbard model with $-U$ is called the attractive Hubbard model because a negative value of U represents an attraction between spin up and psin down electrons on the same site. By considering various operators one can show that magnetic order in the $+U$ Hubbard model is related to superconducting and charge order in the $-U$ Hubbard model, so that an understanding of the phases of one model immediately implies considerable information about the other.

Exercise 67: Show that under a particle-hole transformation of just the down spin species, the following operator mappings occur. (Ignore constants.)

$$\begin{aligned} m_{z,\mathbf{i}} = n_{\mathbf{i}\uparrow} - n_{\mathbf{i}\downarrow} \leftrightarrow n_{\mathbf{i}} = n_{\mathbf{i}\uparrow} + n_{\mathbf{i}\downarrow} \\ m_{+,\mathbf{i}} = c^{\dagger}_{\mathbf{i}\uparrow} c_{\mathbf{i}\downarrow} \leftrightarrow c^{\dagger}_{\mathbf{i}\uparrow} c^{\dagger}_{\mathbf{i}\downarrow} \\ m_{-,\mathbf{i}} = c^{\dagger}_{\mathbf{i}\downarrow} c_{\mathbf{i}\uparrow} \leftrightarrow c_{\mathbf{i}\downarrow} c_{\mathbf{i}\uparrow} \end{aligned}$$

The physical content of these results is that spin correlations along the z axis are interchanged with charge correlations, and spin correlations along the x and y axes (which are compinations of m_+ and m_-) are interchanged with pairing correlations.

C. Alternates to Determinant QMC

1. World Line Quantum Monte Carlo

A discussion of the path integral formulation of quantum mechanics, starting with the harmonic oscillator and then moving to quantum spins, bosons, and fermions, with an emphasis on Quantum Monte Carlo, can be found at: http://leopard.ucdavis.edu/rts/resproj6.html by hitting the 'World-Line Quantum Monte Carlo" link (number 88).

A shorter discussion which starts immediately with the Heisenberg model can be found at: http://leopard.ucdavis.edu/rts/boulder.html by hitting the 'Lecture II (pdf file) link.

2. Dynamical Mean Field Theory

One of the reasons for the continued interest in the Hubbard model is because of a recently developed approach known as 'dynamical mean field theory' (DMFT). This new technique has allowed for very interesting solutions of the Hubbard model itself, and also, more importantly, has provided a framework for the inclusion of Hubbard-type interactions into density functional theory. A 'popular' introduction to DMFT is available in: while a much more complete technical review is in: "Strongly Correlated Materials: Insights From Dynamical Mean-Field Theory," Physics Today, March, 2004. A. Georges, G. Kotliar, W. Krauth, and M. Rozenberg, Rev. Mod. Phys. **68**, 13 (1996).

Note on Bibliography: This list of references is not intended to acknowledge all the papers in the field. Rather it is somewhat idiosyncratic, reflecting mainly papers that connected directly to the material of section V. However, in many cases, these papers themselves contain a more formal review of the literature for those who desire it.

---

[1] "Monte Carlo calculations of coupled boson-fermion systems. I," R. Blankenbecler, D.J. Scalapino, and R.L. Sugar, Phys. Rev. **D24**, 2278 (1981).

[2] "Disordered Electronic Systems," P.A. Lee and T.V. Ramakrishnan, Rev. Mod. Phys, **57**, 287 (1985); "The Anderson-Mott transition," D. Belitz and T.R. Kirkpatrick, Rev. Mod. Phys, **66**, 261 (1994).

[3] "Metallic behavior and related phenomena in two dimensions," E. Abrahams, S. V. Kravchenko, and M. P. Sarachik, Rev. Mod. Phys. **73**, 251 (2001); "Metal-insulator transition in two dimensional electron systems," S.V. Kravchenko and M.P. Sarachik, Rep. Prog. Phys. **67**, 1 (2004).

[4] "Lecture Notes on Electron Correlation and Magnetism," P. Fazekas, World Scientific Series in Modern Condensed Matter Physics, Vol. 5, (1999).

[5] E.Y. Loh, Jr., J.E. Gubernatis, D.J. Scalapino, R.L. Sugar, S.R. White, and R.T. Scalettar, in *Interacting Electrons in Reduced Dimensions*, ed. by D. Baeriswyl and D.K. Campbell, Plenum, New York (1989).

[6] "A Numerical Study of the Two-D Hubbard Model with Repulsive Coulomb Interaction," S.R. White, D.J. Scalapino, R.L. Sugar, E.Y. Loh, Jr., J.E. Gubernatis, and R.T. Scalettar, Phys. Rev. **B40**, 506 (1989).

[7] E.Y. Loh, Jr. and J.E. Gubernatis, in *Electronic Phase Transitions*, ed. by W. Hanke and Yu. V. Kopaev, North-Holland, Amsterdam (1992).

[8] www.ccmr.cornell.edu/ cyrus/book/muramatsu.ps.gz (This includes also a discussion of the 'world-line' method for the Hubbard Hamiltonian.)

[9] "Scaling Theory of Localization– Absence of Quantum Diffusion in 2 Dimensions," E. Abrahams, P.W. Anderson, D.C. Licciardello, and T.V. Ramakrishnan, Phys. Rev. Lett. **42**, 673 (1979).

[10] "Inverse participation ratio in 2+ epsilon dimensions," F. Wegner, Z. Phys. B **36**, 209 (1980).

[11] "Interaction between diffusion modes in localization theory," Zh. Eksp. Teor. Fiz. **79**, 1120 (1980). K.B. Efetov, A.I. Larkin, and D.E. Khmelnitskii, Sov. Phys. JETP **52**, 568 (1980).

[12] "Disordered Electronic Systems," P.A. Lee and T.V. Ramakrishnan, Rev. Mod. Phys. **57**, 287 (1985).

[13] "Weak localization and Coulomb interaction in disordered systems," A.M. Finkelstein, Zeit. fur Physik **B56** 189 (1984).

[14] "Interaction-driven metal-insulator transitions in disordered fermion systems," C. Castellani, C. Di Castro, P. A. Lee, and M. Ma, Phys. Rev. B **30**, 527 (1984).

[15] "The Anderson-Mott transition," D. Belitz and T. R. Kirkpatrick, Rev. Mod. Phys. **66**, 261 (1994).

[16] "Possible metal-insulator transition at B=0 in two dimensions," S. V. Kravchenko, G. V. Kravchenko, J. E. Furneaux, V. M. Pudalov, and M. D'Iorio, Phys. Rev. B **50**, 8039 (1994).

[17] "Scaling of an anomalous metal-insulator transition in a two-dimensional system in silicon at B=0," S. V. Kravchenko, W. E. Mason, G. E. Bowker, J. E. Furneaux, V. M. Pudalov, and M. D'Iorio, Phys. Rev. B **51**, 7038 (1995).

[18] "Electric Field Scaling at a B = 0 Metal-Insulator Transition in Two Dimensions," S. V. Kravchenko, D. Simonian, M. P. Sarachik, W. Mason, and J. E. Furneaux, Phys. Rev. Lett. **77**, 4938 (1996).

[19] "Metal-Insulator Transition in Two Dimensions: Effects of Disorder and Magnetic Field," D. Popović, A. B. Fowler, and S. Washburn, Phys. Rev. Lett. **79**, 1543 (1997).
[20] "Reflection symmetry at a B=0 metal-insulator transition in two dimensions ," D. Simonian, S. V. Kravchenko, and M. P. Sarachik, Phys. Rev. B **55**, R13421 (1997).
[21] "The Metallic-like Conductivity of a Two-Dimensional Hole System," Y. Hanien, U. Meirav, D. Shahar, C. C. Li, D. C. Tsui, and Hadas Shtrikman, Phys. Rev. Lett. **80**, 1288 (1998).
[22] "Metal-Insulator Transition at B = 0 in a Dilute Two Dimensional GaAs-AlGaAs Hole Gas," M. Y. Simmons, A. R. Hamilton, M. Pepper, E. H. Linfield, P. D. Rose, D. A. Ritchie, A. K. Savchenko and T. G. Griffiths, Phys. Rev. Lett. **80**, 1292 (1998).
[23] "Scaling Theory of Two-Dimensional Metal-Insulator Transitions," V. Dobrosavljević, E. Abrahams, E. Miranda, and S. Chakravarty, Phys. Rev. Lett. **79**, 455 (1997).
[24] "Metallic phase and metal-insulator transition in two-dimensional electronic systems," C. Castellani, C. Di Castro, and P. A. Lee, Phys. Rev. B **57**, R9381 (1998).
[25] "Interactions and scaling in a disordered two-dimensional metal," S. Chakravarty, L. Yin, and E. Abrahams, Phys. Rev. B **58**, R559 (1998).
[26] "Wigner glass, spin liquids and the metal-insulator transition," S. Chakravarty, S. Kivelson, C. Nayak, and K. Voelker, Phil. Mag. **B79**, 859 (1999).
[27] "Superconductivity in a two-dimensional electron gas," P. Phillips, Y. Wan, I. Martin, S. Knysh, and D. Dalidovich, Nature **395**, 253 (1998).
[28] "Possible triplet superconductivity in MOSFETs," D. Belitz and T. R. Kirkpatrick, Phys. Rev. B **58**, 8214 (1998).
[29] "Theory of Metal-Insulator Transitions in Gated Semiconductors," B. L. Altshuler and D. Maslov, Phys. Rev. Lett. **82**, 145 (1999).
[30] "A few electrons per ion scenario for the B=0 metal-insulator transition in two dimensions," T. M. Klapwijk and S. Das Sarma, preprint cond-mat/9810349.
[31] "Coherent Propagation of Two Interacting Particles in a Random Potential," D. L. Shepelyansky, Phys. Rev. Lett. **73**, 2607 (1994).
[32] "Do Interactions Increase or Reduce the Conductance of Disordered Electrons? It Depends!," T. Vojta, F. Epperlein, and M. Schreiber, Phys. Rev. Lett. **81**, 4212 (1998)]; "Delocalized Coulomb phase in two dimensions," X. Waintal, G. Benenti, and J.-L. Pichard, Europhys. Lett. **49**, 466 (2000).
[33] "Consistent description of high-Tc superconductors with the three-band Hubbard model," G. Dopf, A. Muramatsu, and W. Hanke, Phys. Rev. Lett. **68**, 353 (1992).
[34] "Two-dimensional Hubbard model-metal insulator transition studied by Monte Carlo calculation," N. Furukawa and M. Imada, J. Phys. Soc. Japan **61**, 3331 (1992).
[35] "Numerical simulation of the 1D and 2D Hubbard models: Fermi liquid behavior and its breakdown," S. Sorella, E. Tosatti, S. Baroni, R. Car, and M. Parinello, Int. J. Mod. Phys. **B1**, 993 (1988).
[36] "Two Dimensional Hubbard Model: Numerical Simulation Study," J.E. Hirsch, Phys. Rev. **B31**, 4403 (1985).
[37] "Boson Localization and the Superfluid–Insulator Transition," M.P.A. Fisher, P.B. Weichman, G. Grinstein, and D.S. Fisher, Phys. Rev. **B40**, 546 (1989).
[38] "Onset of superconductivity in the two-dimensional limit," D.B. Haviland, Y.Liu, and A.M. Goldman, Phys. Rev. Lett. **62** 2180, (1989).
[39] "Tunneling Study of Superconductivity near the Metal-Insulator Transition," R.C. Dynes *etal*, Phys. Rev. Lett. **53**, 2437 (1984); 'Destruction of Superconductivity in Quenched Condensed Two Dimensional Films," A.E. White, R.C. Dynes, and J.P. Garno, Phys. Rev. **B33**, 3549 (1986).
[40] "Magnetic Field Tuned Superconductor–Insulator Transition in Two Dimensional Films," A.F. Hebard and M.A. Paalanen, Phys. Rev. Lett. **65**, 927 (1990); and "Global phase coherence in two-dimensional granular superconductors," B.G. Orr, H.M. Jaeger, A.M. Goldman and C.G.

Kuper, Phys. Rev. Lett. **56**, 378 (1986).
[41] "Electron tunneling determination of the order-parameter amplitude at the superconductor-insulator transition in 2D," J.M. Valles, R.C. Dynes, and J.P. Garno, Phys. Rev. Lett. **69**, 3567 (1992).
[42] "Superconducting-insulating transition in two-dimensional a-MoGe thin films," A. Yazdani and A. Kapitulnik, Phys. Rev. Lett. **74**, 3037 (1995).
[43] "Pairing and Spin Gap in the Normal State of Short Coherence Length Superconductors," M. Randeria, N. Trivedi, A. Moreo, and R.T. Scalettar, Phys. Rev. Lett. **69**, 2001 (1992).
[44] "Superconductor–Insulator Transition in a Disordered Electronic System," N. Trivedi, R.T. Scalettar, and M. Randeria, Phys. Rev. **B54**, 3756 (1996).
[45] "Localization: Theory and Experiment," B. Kramer and A. MacKinnon, Rep. Prog. Phys. **56**, 1469 (1993).
[46] "Localization Transitions in Non-Hermitian Quantum Mechanics", N. Hatano and D.R. Nelson, Phys. Rev. Lett. **77**, 570 (1996); "Vortex pinning and non-Hermitian quantum mechanics," Phys. Rev. B **56**, 8651 (1997).
[47] "Statistics of complex levels of random matrices for decaying systems, " F. Haake, F. Izrailev, N. Lehmann, D. Saher, and H.J. Sommers, Zeit. Phys. B **88**, 359 (1992).
[48] "Spectrum of Large Random Asymmetric Matrices", H.J. Sommers, A. Crisanti, H. Sompolinsky, and Y. Stein, Phys. Rev. Lett. **60**, 1895 (1988).
[49] "Random Matrix Model of QCD at Finite Density and the Nature of the Quenched Limit," M.A. Stephanov, Phys. Rev. Lett. **76**, 4472 (1996).
[50] "Nonhermitian Random Matrix Models," R.A. Janik, M.A. Nowak, G. Papp, and I. Zahed, Nucl. Phys. B **501**, 603 (1997) and "Macroscopic Universality: Why QCD in Matter is Subtle," Phys. Rev. Lett. **77**, 4876 (1996).
[51] "Two-level system with noise: Blue's function approach," E. Gudowska-Nowak, G. Papp and J. Brickmann, J. Chem. Phys **220**, 125 (1997).
[52] TITLE, Y.V. Fyodorov, B.A. Khoruzhenkom and H.J. Sommers, Phys. Lett. A **226** 46 (1997).
[53] TITLE M.A. Halasz, A.D. Jackson, and J.J.M. Verbaarschot, Phys. Rev. D **56**, 5140 (1997).
[54] J. Feinberg and A. Zee, Nucl. Phys. B **504**, 579 (1997).
[55] J. Feinberg and A. Zee, Nucl. Phys. B **501**, 643 (1997).
[56] B. Zickel, unpublished.
[57] "Cold Bosonic Atoms in Optical Lattices," D. Jaksch, C. Bruder, J.I. Cirac, C.W. Gardiner, and P. Zoller, Phys. Rev. Lett. **81**, 3108 (1998).
[58] "Phase diagram for ultracold bosons in optical lattices and superlattices," P. Buonsante and A. Vezzani, Phys. Rev. A **70**, 033608 (2004).
[59] "Fractional-filling loophole insulator domains for ultracold bosons in optical superlattices," P. Buonsante, V. Penna, and A. Vezzani, Phys. Rev. A **70**, 061603 (2004).
[60] "Cell strong-coupling perturbative approach to the phase diagram of ultracold bosons in optical superlattices," P. Buonsante, A. Vezzani, Phys. Rev. A **72**, 013614 (2005).
[61] J.B. Sokoloff, Phys. Rep. **126**, 189 (1985).
[62] Y. Last, Proc. of XIth Int. Congress of Math. Phys. 366, 1994); S. Jitomirskaya, *ibid*, 373.
[63] V.W. Scarola and S. Das Sarma, cond-mat/0506415.
[64] N. Trefethen and M. Embree, "Spectra and Pseudospectra - the behavior of nonnormal matrices and operators", Princeton University Press.
[65] V.G. Rousseau, D.P. Arovas, M. Rigol, F. Hébert, G.G. Batrouni, and R.T. Scalettar, cond-mat/0601681.
[66] "Constrained Path Quantum Monte Carlo Method for Fermion Ground States", S. Zhang, J. Carlson, and J. E. Gubernatis Phys. Rev. Lett. 74, 3652 (1995); "Constrained path Monte Carlo method for fermion ground states", S. Zhang, J. Carlson, and J. E. Gubernatis Phys. Rev. B 55, 7464 (1997).
[67] "Dynamical mean-field theory of strongly correlated fermion systems and the limit of infinite

dimensions," A. Georges, G. Kotliar, W. Krauth, and M. Rozenberg, Rev. Mod. Phys. **68**, 13 (1996).

[68] "Investigation of correlated electron systems using the limit of high dimensions," D. Vollhardt, in *Correlated Electron Systems*, edited by V. J. Emery (World Scientific, Singapore) 57 (1993).

[69] "Quantum Cluster Theories," Th. Maier, M. Jarrell, Th. Pruschke, and M. Hettler, Rev. Mod. Phys. **77**, 1027 (2005).

[70] "Monte Carlo Method for Magnetic Impurities in Metals, " J.E. Hirsch and R.M. Fye, Phys. Rev. Lett. **56**, 2521 (1986).

[71] "Insulator, metal, or superconductor: The criteria," D. J. Scalapino, S. R. White, and S. C. Zhang, Phys. Rev. B **47**, 7995 (1993).

[72] We also consider lower temperatures and average over larger numbers of disorder realizations: for the higher temperatures generally 4 realizations are sufficient, for the lowest temperatures the fluctuations are larger and up to 20 (72) realizations are used for $U = 4$ ($U = 0$).

[73] For a related enhancement of the superfluid density by interactions in a disordered Bose system, see "Superfluid-insulator transition in disordered boson systems," W. Krauth, N. Trivedi, and D. M. Ceperley, Phys. Rev. Lett. **67**, 2307 (1991).

[74] For $\Delta = 1.2$ and $\beta = 5$, $\sigma_{\rm dc} = 0.88(1), 0.76(1)$ for $U = 0, 4$, respectively. For $\Delta = 2.0$ and $\beta = 6$, $\sigma_{\rm dc} = 0.45(2), 0.49(3), 0.52(4)$ for $U = 0, 2, 4$, respectively. Numbers between brackets represent the error bar in the last digit shown.

[75] "Spin Dynamics of Nearly Localized Electrons," M. A. Paalanen, S. Sachdev, R. N. Bhatt, and A. E. Ruckenstein, Phys. Rev. Lett. **57**, 2061 (1986).

[76] "Spin Degree of Freedom in a Two-Dimensional Electron Liquid," T. Okamoto, K. Hosoya, S. Kawaji, and A. Yagi, Phys. Rev. Lett. **82**, 3875 (1999).

[77] "Parallel Magnetic Field Induced Transition in Transport in the Dilute Two-Dimensional Hole System in GaAs," J. Yoon, C. C. Li, D. Shahar, D. C. Tsui, and M. Shayegan, Phys. Rev. Lett. **84**, 4421 (2000).

[78] "Metal-Insulator Transition in a 2D Electron Gas: Equivalence of Two Approaches for Determining the Critical Point," A. A. Shashkin, S. V. Kravchenko, and T. M. Klapwijk, Phys. Rev. Lett. **87**, 266402 (2000).

[79] "Effects of a Parallel Magnetic Field on the Metal-Insulator Transition in a Dilute Two-Dimensional Electron System," K. V. Eng, X. G. Feng, D. Popović, and S. Washburn, Phys. Rev. Lett. **88**, 136402 (2002).

[80] E. Tutuc, E. P. De Poortere, S. J. Papadakis, and M. Shayegan, cond-mat/0204259 and Physica E **13**, 748 (2002).

[81] E. P. De Poortere, E. Tutuc, Y. P. Shkolnikov, K. Vakili, and M. Shayegan, cond-mat/0208437

[82] "Ground-state properties of the two-dimensional disordered Hubbard model," G. Caldara, B. Srinivasan, and D. L. Shepelyansky, Phys. Rev. B **62**, 10680 (2000).

[83] R. Kotlyar and S. Das Sarma, Phys. Rev. Lett. **86**, 2388 (2001).

[84] F. Selva and J.-L. Pichard, Europhys. Lett. **55**, 518 (2001).

[85] "Parallel magnetoconductance of interacting electrons in a two-dimensional disordered system," R. Berkovits and J. W. Kantelhardt, Phys. Rev. B **65**, 125308 (2002).

[86] "The effect of parallel magnetic field on the Boltzmann conductivity and the Hall coefficient of a disordered two-dimensional Fermi liquid," I. F. Herbut, Phys. Rev. B **63**, 113102 (2001).

[87] "nteraction corrections at intermediate temperatures: Magnetoresistance in a parallel field," G. Zala, B. N. Narozhny, and I. L. Aleiner, Phys. Rev. B **65**, 020201 (2002).

[88] "Conducting phase in the two-dimensional disordered Hubbard model," P. J. H. Denteneer, R. T. Scalettar, and N. T. Trivedi, Phys. Rev. Lett. **83**, 4610 (1999).

[89] This point of view of the effect of $B_\parallel$ in the experiments is substantiated in: "Fate of the extended states in a vanishing magnetic field: The role of spins in strongly interacting two-dimensional electron systems," M. R. Sakr, M. Rahimi, and S. V. Kravchenko, Phys. Rev. B **65**, 041303 (2002).

[90] W. Teizer, F. Hellman, and R. C. Dynes, Solid State Comm. **114**, 81 (2000);

[91] F. J. Wegner, Z. Phys. B **35**, 207 (1979), R. Gade and F. J. Wegner, Nucl. Phys. B **360**, 213 (1991).

[92] P. W. Brouwer, C. Mudry, and A. Furusaki, cond-mat/0009198.

[93] "Quasiparticle localization in superconductors with spin-orbit scattering," T. Senthil and M. P. A. Fisher, Phys. Rev. B **61**, 9690 (2000).

[94] "Localization and Delocalization in Dirty Superconducting Wires," P. W. Brouwer, A. Furusaki, I. A. Gruzberg, and C. Mudry, Phys. Rev. Lett. **85**, 1064 (2000), and cited references.

[95] "Deviations from Fermi-Liquid Behavior above Tc in 2D Short Coherence Length Superconductors," N. Trivedi and M. Randeria, Phys. Rev. Lett. **75**, 312 (1995). As in the case of Equation 2, this expression for the density of states is valid at temperatures below characteristic frequency scales of structures in $N(\omega)$.

[96] "Magnetic correlations in the two-dimensional Anderson-Hubbard model," M. Ulmke and R. T. Scalettar, Phys. Rev. B **55**, 4149 (1997), M. Ulmke, P. J. H. Denteneer, R. T. Scalettar, and G. T. Zimanyi, Europhys. Lett. **42**, 655 (1998).

[97] We have verified that beyond a certain large site disorder ($\Delta_\mu \geq 4t$) $\sigma_{\rm dc}$ decreases again.

[98] "Collapse of the charge gap in random Mott insulators," Y. Otsuka, Y. Morita, and Y. Hatsugai, Phys. Rev. B **58**, 15314 (1998).

[99] A. Garg, H.R. Krishnamurthy, and M. Randeria, cond-mat/0511351.

[100] J. Hubbard and J.B. Torrance, Phys. Rev. Lett. **47**, 1750 (1981); T. Egami, S. Ishihara and M. Tachiki, Science **261**, 130 (1994); "Macroscopic polarization as a geometric quantum phase: Many-body formulation," G. Ortiz and R. Martin, Phys. Rev. B **49**, 14202 (1994); "Many-Body Effects on Polarization and Dynamical Charges in a Partly Covalent Polar Insulator," R. Resta and S. Sorella, Phys. Rev. Lett. **74**, 4738 (1995) and "Electron Localization in the Insulating State," Phys. Rev. Lett. **82**, 370 (1999); "From Band Insulator to Mott Insulator in One Dimension," M. Fabrizio, A.O. Gogolin, and A.A. Nersesyan, Phys. Rev. Lett. **83**, 2014 (1999); T. Wilkens and R.M. Martin, Phys. Rev. B **63**, 235108 (2001); and "Exact Bond Ordered Ground State for the Transition between the Band and the Mott Insulator," C.D. Batista and A.A. Aligia, Phys. Rev. Lett. **92**, 246405 (2004).

[101] "Ferromagnetism and Metal-Insulator Transition in the Disordered Hubbard Model," K. Byczuk, M. Ulmke, and D. Vollhardt, Phys. Rev. Lett. **90**, 196403 (2003).

[102] "Mott-Hubbard metal-insulator transition at noninteger filling," K. Byczuk, W. Hofstetter, and D. Vollhardt, Phys. Rev. B **69**, 045112 (2004).

[103] "Anomalous normal-state properties of high-T_c superconductors: intrinsic properties of strongly correlated electron systems?", Th. Pruschke, M. Jarrell, and J.K. Freericks, Adv. Phys. **44**, 187 (1995).

[104] Anderson-Hubbard with DMFT.

[105] There is one slightly confusing point here. From the description provided, one might think that in a Monte Carlo simulation one stores a vector p_i and applies T to it. This is completely impractical because the number of one configurations i of the system is incredibly huge and we could never allocate enough memory to hold p_i. Instead, we generally store only one configuration i at a time, and T_{ji} gives us a probabilistic rule to get the (single) configuration j from i. The probability p_i appears through the average of all the single configurations over a long simulation.

[106] "Computational Physics," R.H. Landau and M.J. Páez, Wiley, 1997.

[107] "Computational Physics," N. Giordano, Prentice-Hall, 1997.

[108] "Statistical Mechanics of Phase Transitions," J. Yeomans, Oxford, 1992.

[109] M. Creutz and J. Freedman, Annals of Phys. **132**, 427 (1981).

[110] See, for exmaple, Sec. 3 of the article nato2.pdf available at http://leopard.physics.ucdavis.edu/rts/nato.html